The University of Adelaide
Department of Physics and Mathematical Physics

A STUDY OF STIMULATED BRILLOUIN SCATTERING AND ITS APPLICATION TO PHASE CONJUGATE OSCILLATORS

by

Martin O'Connor
B.Sc.(Honours) *Adelaide*, Grad. Dip. Bus. *Uni. S.A.*

Thesis submitted for the degree of

Doctor of Philosophy

in

The University of Adelaide

August, 1997

Abstract

A study of Stimulated Brillouin Scattering (SBS) and its use for correcting phase aberrations in laser oscillators is presented.

Chapter One includes a short description of Optical Phase Conjugation (OPC) and Stimulated Brillouin Scattering (SBS), and presents the research objectives of the thesis. Chapter Two details the transient theory of SBS incorporating a focusing geometry, random noise seed, and the effects of pump depletion and finite phonon lifetime.

In Chapter Three, the first experimental chapter, the phase conjugate properties of SBS are studied using a pulsed Nd:YAG laser with available energies up to 750mJ, under different operating conditions. Both long and short coherence length pumping regimes as well as different focusing geometries are investigated. For long coherence length pumping, intensity fluctuations in the SBS return beam are identified for particular focusing conditions. A region is found where no intensity fluctuations are observed. For short coherence length pumping, competing effects such as optical breakdown are studied in order to compare with results reported previously. The main emphasis of this chapter is the study of phase conjugate SBS performance with short coherence length pumping. The experiments presented in this chapter are essential for the characterization of the SBS process when incorporated within a laser oscillator. Phase conjugation of intracavity phase aberrations using an SBS oscillator is the subject of the following chapter.

In Chapter Four, phase conjugation of a Nd:YAG laser oscillator using SBS is investigated both theoretically and experimentally. A simple model is used to determine general characteristics of a resonator with an intracavity SBS cell. A series of resonator designs and modifications are presented. Time-resolved intracavity SBS reflectivity, as well as other laser beam parameters, are used to characterize the process under different experimental conditions. The final design presented incorporates an intracavity etalon in order to control the longitudinal mode content of the start-up cavity.

Finally, conclusions drawn from the work performed in this thesis are presented in Chapter Five.

This work contains no material which has been accepted for the award of any other degree or diploma in any university or other institution and, to the best of my knowledge and belief, contains no material previously published or written by another person, except where due reference has been made in the text.

I give consent to this copy of my thesis, when deposited in the University Library, being available for loan and photocopying.

Signed: (Martin O'Connor)

Date: 29 AUGUST 1997

Acknowledgments

Thanks must go to many people who have given me advice and support throughout the course of my research.

I thank my supervisor Jesper Munch. He is a very thorough researcher and was a continual supply of theories and suggestions to resolve difficulties which arose during this project. I was able to join an enthusiastic group just starting out and helped transform a number of empty rooms into modern laboratories which were always a hive of activity.

Great thanks must go to Vladimir Devrelis, Shahram Afsharvahid and Changjiang Wei who were always there to bounce an idea on and would always have good suggestions. They have contributed a great deal to this research work both in suggestions and in lending a hand in the lab. Thankyou also, to ARC and DSTO who have financially supported this project.

Finally and most importantly, to my parents and two sisters, who have supported me not only throughout the duration of this research project but also during my undergraduate studies. I owe a great deal to them for the advice and encouragement they have given to me over the last four years. Also, to Susan, who toward the end of this research project was there to support and motivate me, as well as contribute greatly to the preparation of this thesis.

Contents

Chapter 1

Introduction to Optical Phase Conjugation using Stimulated Brillouin Scattering

1.1 Introduction

This chapter firstly describes the Optical Phase Conjugation (OPC) technique and its aberration correcting properties. Then, a brief introduction to the nonlinear optical process stimulated Brillouin scattering (SBS) and some of its phase conjugate properties are presented. Finally, the motivation for SBS research and the scope of this work are summarized.

1.2 Optical Phase Conjugation

Optical phase conjugation (OPC) is a technique that usually incorporates nonlinear optical effects[1] to reverse both the propagation direction and the phase of each plane

[1] Holography which is a linear process can also perform optical phase conjugation.

wave in an arbitrary beam of light. Static holography was the earliest technique used to produce a phase conjugate wave [1,2]. The following development in the area of dynamic holography was based on the recognition that a grating (hologram) could be 'written' (in an appropriate material) by interfering two beams derived from the same laser followed by 'reading' the hologram using a third wave. This work was first developed by Gerritsen (1967) [3], Woerdman (1970) [4], Amodei (1971) [5], and Stepanov et al (1971) [6]. OPC using nonlinear optical processes (NOPC) was discovered in the USSR in 1971 at both the Physical Institute of the USSR Academy of Science (with stimulated scattering (SS)) and the Institute of Physics of the Belorussian Academy of Science (with four-wave interaction) [23]. OPC via SS was first reported by Zel'dovich *et al* 1972 [7]. Other research articles contributing to the initial development of OPC via SS were Nosach et al (1972) [8], Bel'dyugin et al (1976) [9], Zel'dovich and Shkunov (1977) [10], Kochemasov and Nikolaev (1977) [11], and Sokolovskaya et al (1977) [12]. OPC via degenerate four-wave mixing was then demonstrated by Yariv and Pepper (1977) [13] and, independently, by Bloom and Bjorklund (1977) [14]. AuYeung et al (1979) [15] proposed and demonstrated successful oscillation in laser resonators where one of the conventional mirrors was substituted by a phase conjugate mirror. In the 1980's and 1990's there has been a great deal of experimental and theoretical work performed with NOPC. There exist several comprehensive reviews of NOPC in the form of texts [16-19], previous reviews [20-23], special journal issues [24-26], and other related review articles [27-29].

The optical phase conjugate process can be regarded as acting like a mirror with 'time reversal' transformation properties, since a reflected light beam retraces its original path. Figure 1.1 illustrates the important difference between an OPC mirror and a conventional mirror reflection. A conventional plane mirror (Figure 1.1(a)) changes the sign of the k-vector component normal to the mirror surface while leaving the tangential component unchanged. An incoming light ray can thus be redirected arbitrarily by suitably tilting the mirror. On the other hand, the OPC mirror (Figure

1.1(b)) causes an inversion of the k-vector component normal to the mirror surface, so that the incident ray exactly returns upon itself, independent of the orientation of the conjugator.

By far the most important technological and scientific applications of these OPC mirrors involves the correction of propagation due to aberrations in practical optical systems. Figure 1.2 illustrates the aberration correcting properties of OPC mirrors compared with conventional mirrors. In Figure 1.2(a), a phase distorting medium (eg. a laser amplifier or the atmosphere) imparts a phase advance to part of a uniform plane wave. The conventional mirror reflection maintains the phase advance. Therefore, if the medium phase variations change slowly compared with the propagation of light, an additional phase advance is imparted to the plane wave on propagating back through the distortion. This is in contrast to Figure 1.2(b), where the OPC mirror exactly reverses the phase and direction of the incident wave. Therefore, the phase distortions imposed on the return aberrated wave cancel out the changes of the wavefront incurred during the first pass.

Although useful for an introductory description, the simple ray pictures in Figures 1.1 & 1.2 do not completely specify the conjugation process. In addition to reversing each k vector, an OPC mirror complex-conjugates the overall multiplicative electric field amplitude associated with each plane wave in the beam.

This remarkable property indicates that, through optical phase conjugation, a high-quality optical beam can be double passed through a poor quality optical system with no loss in beam quality, or output power.

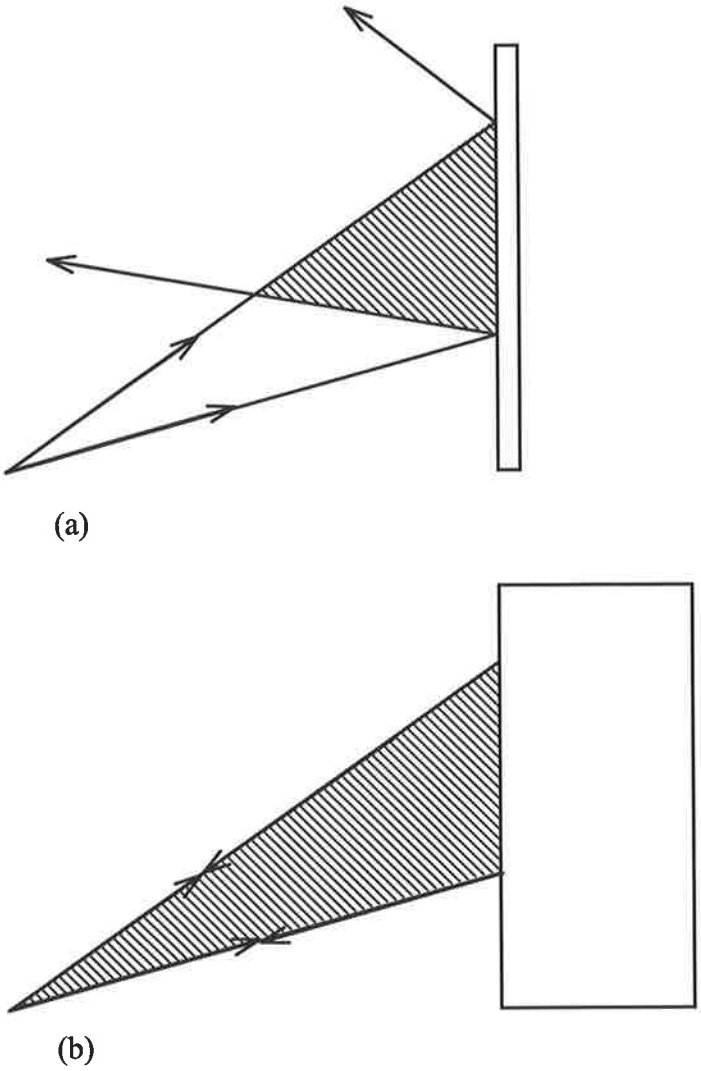

Figure 1.1 (a) Conventional mirror, (b) Phase-conjugate mirror

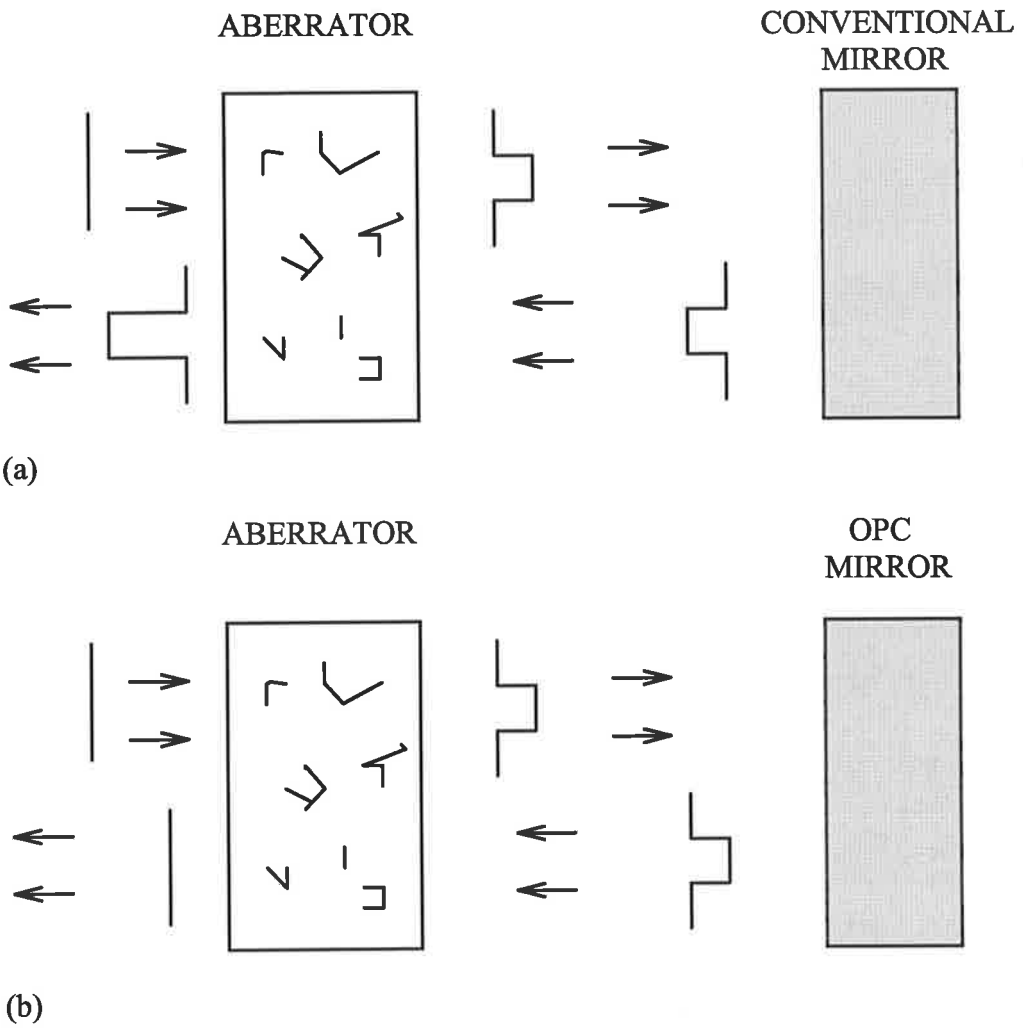

Figure 1.2 Phase correcting properties of a phase conjugate mirror. (a) Conventional mirror reflection, (b) OPC mirror reflection.

1.2.1 Aberration Correction Properties of a Phase-Conjugate Wave

In this section, a mathematical description of the aberration correcting nature of the conjugation process is presented. Consider a monochromatic wave propagating through a composite medium whose electric permittivity (dielectric constant) is given by $\varepsilon(\mathrm{r})$. The real quantity $\varepsilon(\mathrm{r})$ represents the presence in the beam of passive linear (non-absorbing) components, such as lenses, wedges, or the presence of distorting media such as a turbulent atmosphere. The scalar near-forward $(+z)$ propagating beam is taken as:

$$\mathrm{E}_1(\mathrm{r},\mathrm{t}) = \left(\frac{1}{2}\right) A_1(\mathrm{r}) \exp\left[-i(\omega\,\mathrm{t} - \mathrm{kz})\right] + c.c. \tag{1.1}$$

In the limit of slow spatial and temporal variations (slowly varying envelope approximation - SVEA), Equation 1.1 obeys Maxwell's scalar wave equation for paraxial waves:

$$\nabla^2 A_1 + \left[\omega^2 \mu\varepsilon(\mathrm{r}) - \mathrm{k}^2\right] A_1 + 2i\,\mathrm{k}\left(\frac{\partial A_1}{\partial\,\mathrm{z}}\right) = 0 \tag{1.2}$$

Let us next, as a purely mathematical operation, consider the complex conjugate of Equation 1.2 (with $\varepsilon(\mathrm{r}) = \varepsilon^*(\mathrm{r})$):

$$\nabla^2 A_1^* + \left[\omega^2 \mu\varepsilon(\mathrm{r}) - \mathrm{k}^2\right] A_1^* - 2i\,\mathrm{k}\left(\frac{\partial A_1^*}{\partial\,\mathrm{z}}\right) = 0 \tag{1.3}$$

Equation 1.3 is also the same wave equation applied to a wave propagating in the $-z$ direction of the form:

$$\mathrm{E}_2(\mathrm{r},\mathrm{t}) = \left(\frac{1}{2}\right) A_2(\mathrm{r}) \exp\left[-i(\omega\,\mathrm{t} + \mathrm{kz})\right] + c.c.\,, \tag{1.4}$$

provided we put:

$$E_2(r,t) = a\,E_1(r,-t)$$
$$A_2(r) = aA_1^*(r) \qquad (1.5)$$

where 'a' is a constant indicating the reflectivity of the process. Thus a backward-going wave A_2 whose complex amplitude is the complex conjugate of A_1 (within an arbitrary multiplicative constant) satisfies the same wave equation obeyed by A_1. This means that if, after traversing a distorting medium with beam E_1 we can generate a beam E_2 that is the phase conjugate of E_1 (within a multiplcative constant), then E_2 will propagate backwards and its amplitude A_2 will remain the complex conjugate of A_1. Therefore, its wave fronts will always coincide with those of E_1.

1.2.2 Applications of Optical Phase Conjugation

The aberration correcting properties of OPC have been used for a wide variety of applications.

One application of OPC is for the correction of aberrations encountered in imaging through turbulent atmospheres or via conventional imperfect optical imaging devices. The latter was first demonstrated using conventional holography by Goodman *et al* [30]. The reader is referred to a number of comprehensive texts and review articles [16-29] for further developments in this area.

Time dependent aberrations encountered in lasers for the generation or amplification of coherent light can be compensated with OPC. A phase conjugate mirror (PCM) can be employed to improve the final beam quality of a master oscillator - power amplifier (MOPA) system [8,31-42]. Nosach et al [8] first demonstrated a MOPA configuration using a ruby oscillator / amplifier laser system. The beam divergence of the amplifier

output was significantly reduced from 2.5mrad to 0.15mrad. Current 'state-of-the-art' MOPA systems produce near diffraction limited laser beams with 25-30J pulse energies in 14ns pulse widths with an average power of >150W and a peak power of 2GW [41]. However, at the beginning of this research work, questions regarding the phase fidelity of the SBS process still existed. A study of SBS phase fidelity forms a large part of Chapter 3 in this thesis.

Alternatively, the PCM may be incorporated into a laser oscillator for correction of intracavity aberrations. A small number of selected articles have been referenced here in order to provide an overview of past experimental and theoretical developments in this area [15,43-55]. The general aim in these devices is to develop a simple, compact oscillator with high average power that utilizes OPC to correct for the aberrations of the active material and the intracavity optical components. A more detailed discussion of phase conjugate oscillators using SBS is given in Section 4.1, and is a major component of this thesis.

There has been considerable research performed on pulse compression with OPC via degenerate four-wave mixing [56,57], stimulated Raman scattering [58-60], and stimulated Brillouin scattering [61-64]. Applications which depend on very good beam quality and very high peak powers, such as laser fusion and photolithography [65,66] directly benefit from improved pulse compression with OPC. Laser beam combination [67-72] is another application which has been the subject of numerous research studies. Information on many other OPC applications can be found in a number of different texts and review articles [16-29]. These applications are not topics of this thesis.

1.3 Introduction to Stimulated Brillouin Scattering

There are many non-linear processess that produce a phase conjugate wave. They include Stimulated Scattering (Brillouin, Raman, Rayleigh and temperature), Four-wave mixing (degenerate, non-degenerate), and photorefractive processes. In each case, a phase grating is created in the non-linear medium and a real-time phase correction is performed. A complete description of all these processes is beyond the scope of this thesis. Stimulated Brillouin scattering is by far the simplest technique for producing a phase conjugate beam. The work in this thesis utilizes SBS to obtain a phase conjugate wave. Therefore, only this technique will be described. The reader is referred to References 16-29, & 73 for further information on the other techniques.

Whilst a detailed analysis of SBS will be given in the following chapter, a brief introduction to some of the properties of SBS will be summarized here.

Stimulated Brillouin scattering was first demonstrated in 1964 [74] by Chiao et al, a few years after the advent of lasers[2]. However, as previously discussed, a useful real-time phase conjugate beam was not recognized until 1972 [7].

In the simplest SBS geometry, a laser beam is focused into a cell containing the non-linear material as shown in Figure 1.3. The electric field associated with the input laser beam drives the creation of an acoustic phase grating near the focal point in the medium[3]. The input laser beam then backscatters from this grating. A threshold power exists where the gain of the non-linear backscattering process increases exponentially. This threshold power is dependent on the properties of the input laser beam and on the properties of the non-linear material being used.

---

[2] The scattering of a light wave from an acoustic wave was first demonstrated in 1922 by Brillouin [75].
[3] A detailed mathematical description and physical interpretation of the SBS process can be found in Chapter 2.

Figure 1.3 Photograph of an experimental configuration for the focusing lens and SBS cell (Generator-SBS Configuration).

Above this threshold power, the lens and SBS cell combination represent an OPC mirror, as described previously, with a maximum reflectivity up to ~90%. There have been many experimental measurements of this result in the literature, however only one recent review article will be referenced here [22]. The peak powers that occur at the focal waist are necessarily very high for SBS threshold to be reached. As a result, gases and liquids are the most commonly used SBS materials due to their self-healing properties. These OPC mirrors can replace conventional mirrors in optical laser systems and can aid optical designers in achieving diffraction limited operation by compensating for the thermal and other phase aberrations that exist in most optical laser systems.

The ability to produce a phase conjugate wave is measured by the phase fidelity of the return wavefront. Phase fidelity describes how well the phase of the Stokes return wavefront matches that of the input laser wavefront. If the Stokes return is an exact copy of the input then the phase fidelity = 1. In practice, maximum phase fidelities of 0.9 are obtainable when using input laser pulse energies well above the SBS threshold. Again, there have been many demonstrations of this result in the literature but only one recent review article will be referenced here [22].

1.4 The Scope of this Work

1.4.1 Experimental Justification

When this work was started there were no commercial laser systems that used SBS technology. The last decade has seen a large number of research groups trying to bridge the gap between pure research in SBS and the development of commercial products. Since SBS corrects thermal aberrations it becomes especially useful in higher energy laser systems. In the U.S.A., there are many laboratories that have made extremely

good use of SBS in laser systems with pulse energies of tens of Joules (Lawrence Livermore National Labs. [41,66], TRW [77], and Hughes Research Labs. [38,72,78]). At such high pulse energies, SBS phase conjugation stands alone as the method of choice. Russian companies and institutes have also used their extensive expertise with SBS in Master Oscillator Power Amplifier (MOPA) systems to produce very high energy, phase conjugate laser pulses [79]. Most recently (in 1994), a major laser manufacturer in the U.S. has produced a moderate to low power MOPA SBS laser system which is currently on the market.

Diode pumped systems and 'state of the art' cooling systems, that reduce the thermal loading in active lasing materials have not removed the need of SBS, but have meant that using SBS for aberration correction has become more important in even higher laser power systems.

One of the most important issues that SBS addresses, which is one of the main features of current phase conjugate laser systems, is its simple and versatile operation. If conventional solid-state lasers require variations in power and pulse repetition frequency, good beam quality can be maintained only by re-aligning and re-optimizing the system. SBS laser systems offer variable laser operating conditions while maintaining beam quality without complicated re-alignment.

Some of the remaining issues for the present SBS technology that require further study and explanation are

- temporal fluctuations in the Stokes beam which have been observed under various operating conditions.
- poor SBS performance with short coherence length pumping, and
- competing phenomena such as optical breakdown and bubble formation.

Added to this is the lack of full understanding on the mechanisms involved in incorporating an SBS cell into an oscillator configuration. Using an SBS mirror in an oscillator configuration has been demonstrated to be an effective way of generating high output laser powers from a simple and compact device [15,43-55]. Although the operating mechanism of SBS oscillators has been considerably developed recently [51,83], there are continued problems in obtaining reliable, high average power laser pulses from these devices.

1.4.2 Research Objectives

Chapter 3:

Temporal intensity fluctuations in SBS backscattered beams and temporal variations in SBS reflectivity and phase fidelity have been reported in recent literature [80-82]. The objective of the work in this chapter is to understand the origins of these fluctuations and how to control them. The final result being the identification of operating regimes for the simple focussed beam SBS process which gives high reflectivity and high fidelity, with no fluctuations in the Stokes return beam. Another aim of this work is to study alternative SBS geometries which, although adding complexity, eliminate the observed fluctuations.

The main emphasis of this chapter involves the experimental study of SBS reflectivity and phase fidelity with a short coherence length pump. The aim of this work is to increase understanding of the parameters which govern short coherence length SBS and extend the operational range of SBS-OPC devices. Specifically, the goal is to study and characterize any phenomena which compete with SBS (for example:optical breakdown). As will be demonstrated, the investigation of SBS under a short coherence length pumping regime provides a natural and logical step toward the SBS oscillator study described in Chapter 4.

Chapter 4:

The purpose of this chapter is to investigate the application of SBS to phase conjugate oscillators, and to develop a simple, compact laser oscillator with an intracavity phase conjugating mirror.

The particular objective is to achieve an SBS oscillator design which provides a short coherence length, diffraction limited output beam with reliable operation and which can be used in higher power MOPA SBS systems.

Chapter 5:

The last chapter brings together the summaries of the previous chapters and presents some overall conclusions of the research work presented.

References

[1] H. Kogelnik, '*Holographic image projection through inhomogeneous media*', Bell Syst. Tech. J. **44**, 2451 (1965).

[2] E. N. Leith, J. Upatnieks, '*Holographic imaging through diffusing media*', J. Opt. Soc. Am. **56**, 523 (1966).

[3] H. J. Gerritsen, '*Non-linear effects in image formation*', Appl. Phys. Lett. **10**, 237 (1967).

[4] J. P. Woerdman, '*Formation of a transient free-carrier hologram in Si*', Opt. Commun. **2**, No 5, 212 (1970).

[5] J. M. Amodei, RCA Rev. **32**, 185 (1971).

[6] V. I. Stepanov, E. I. Ivarkin, and A. S. Rubanov, '*Recording two-dimensional and three-dimensional dynamic holograms in bleachable substances*', Sov. Phys.-Dokl.-Tech. Phys. **16**, 46 (1971).

[7] B. Ya. Zeldovich, V. I. Popovichev, V. V. Ragul'skii and F. S. Faizullov, '*Connection between the wave fronts of the reflected and exciting light in stimulated Mandel'shtram-Brillouin scattering*', Sov. Phys. JETP Lett. **15**, 109 (1972).

[8] O. Yu. Nosach, V. I. Popovichev, V. V. Ragul'shy, and F. S. Faizullov, '*Cancelation of phase distortions in an amplifying medium with a Brillouin mirror*' Sov. Phys. JETP Lett. **16**, 435 (1972).

[9] I. M. Bel'dyugin, M. G. Galushkin, E. M. Zemskov, and V. I. Mandrosov. '*Complex conjugation of fields in stimulated Brillouin scattering*' Sov. J. Quant. Electron. **6**, 1349 (1976).

[10] B. Ya. Zel'dovich, and V. V. Shkunov, '*Wavefront reproduction in stimulated Raman scattering*', Sov. J. Quant. Electron. **7**, 610 (1977).

[11] G. G. Kochemasov, and V. D. Nikolaev, '*Reproduction of the spatial amplitude and phase distributions of a pump beam in stimulated Brillouin scattering*', Sov. J. Quant. Electron. **7**, 60 (1977).

[12] A. I. Sokolovskaya, G. L. Brekhovskykh, A. D. Kudryavtseva, '*Wavefront reconstruction of light beams in stimulated Raman scattering*', Sov. Phys. - Dokl. **22**, 156 (1977).

[13] A. Yariv, and D. M. Pepper, '*Amplified reflection, phase conjugation, and oscillation in degenerate four-wave mixing*', Opt. Commun. **21**, 49, (1977).

[14] D. M. Bloom, and G. C. Bjorklund, '*Conjugate wave-front generation and image reconstruction by four-wave mixing*', Appl. Phys. Lett. **31**, 592 (1977).

[15] J. AuYeung, D. Fekete, D. M. Pepper, and A. Yariv, '*A theoretical and experimental investigation of the modes of optical resonators with phase-conjugate mirrors*', IEEE J. Quantum Electron. **QE-15**, 1180 (1979).

[16] R. A. Fisher (ed.), '*Optical Phase Conjugation*', New York: Academic Press, (1983).

[17] D. M. Pepper, '*Nonlinear optical phase conjugation*', Laser Handbook 4, M.L. Stitch and M. Bass (eds.), North Holland, Amsterdam, 333-486 (1985).

[18] B. Ya. Zel'dovich, N. F. Pilipetsky, V. V. Shkunov, '*Principles of Phase Conjugation*', T. Tamir (ed.), Berlin: Springer, (1985).

[19] N. G. Basov (ed.), '*Phase conjugation of laser emission*', in Proc. Lebedev Phys. Inst., Acad. Sci. USSR **172**, New York: Nova (1988).

[20] A. Yariv, '*Phase conjugate optics and real-time holography*', IEEE J. Quantum Electron., **QE-14**, 650 (1978); IEEE J. Quantum Electron. **QE-15**, 256 (1979); IEEE J. Quantum Electron. **QE-15**, 523 (1979).

[21] D. M. Pepper, '*Nonlinear optical phase conjugation*', Opt. Eng. **21**, 156-183 (1982).

[22] D. M. Pepper, D. A. Rockwell, and G. J. Dunning, '*Nonlinear optical phase conjugation*', IEEE Circuits and Devices, 21-48 (1991).

[23] G. A. Pasmanik, '*Optical phase conjugation in the USSR*', Optics and Photonics News, April, 22-27 (1992).

[24] D. M. Pepper (ed.), '*Special issue on Nonlinear Optical Phase Conjugation*', Opt. Eng. **21**, 155-283 (1982).

[25] R. A. Fisher (ed.), '*Special Issue on Optical Phase Conjugation*', J. Opt. Soc. Am. **73**, 524 (1983).

[26] D. M. Pepper (ed.), '*Special Issue on Nonlinear Optical Phase Conjugation*', IEEE J. Quantum Electron. **QE-25**, No 3, 312 (1989).

[27] C. R. Giuliano, '*Applications of optical phase conjugation*', Physics Today, **34**, 27 (1981).

[28] V. V. Shkunov and B. Ya. Zel'dovich, '*Optical phase conjugation*', Scientific American **253**, 54 (1985).

[29] D. M. Pepper, '*Applications of optical phase conjugation*', Scientific American **254**, 74 (1986); Scientific American **254**, 118 (1986).

[30] J. W. Goodman, W. H. Huntley, D. W. Jackson, and M. Lehman, '*Wavefront recontruction imaging through random media*', Appl. Phys. Lett. **8**, 311 (1966).

[31] Y. A. Anan'ev, '*Possibility of dynamic correction of wavefronts*', Sov. J. Quant. Electron. **4**, 929 (1975).

[32] V. Wang, '*Nonlinear optical phase conjugation for laser systems*', Opt. Eng. **17**, 267 (1978).

[33] N. Basov, and I. Zubarev, '*Powerful laser systems with phase conjugation by SMBS mirror*', Appl. Phys. **20**, 261 (1979).

[34] E. N. Ragozin, and M. E. Plotkin, '*Multiple use of wavefront reversal in laser systems*', Sov. J. Quant. Electron. **10**, 915 (1980).

[35] D. T. Hon, '*High brightness Nd:YAG laser using SBS phase conjugation*', J. Opt. Soc. Am. **70**, 635 (1980)

[36] M. J. Damzen, and M. H. R. Hutchinson, J. Opt. Soc. Am. **152**, 120 (1984).

[37] D. A. Rockwell, '*A review of phase conjugate lasers*', IEEE J. Quantum Electron. **24**, 1124 (1988).

[38] J-L. Aryal, J. Montel, and J-P. Huignard, *'Master oscillator-amplifier Nd:YAG laser with a SBS phase conjugate mirror*', SPIE **1500**, 81 (1991).

[39] M. S. Mangir, and D. A. Rockwell, '*4.5-J Brillouin phase-conjugate mirror producing excellent near- and far-field fidelity*', J. Opt. Soc. Am. B **10**, No 8, 1396 (1993).

[40] D. A. Rockwell, M. S. Mangir, and J. J. Ottusch, '*Energy scaling of phase-conjugate lasers and Brillouin conjugators*', Int. J. Nonlin. Opt. Phys. **2**, No 1, 131 (1993).

[41] C. B. Dane, L. E. Zapata, W. A. Neuman, M. A. Norton, and L. A. Hackel, '*Design and operation of a 150W near diffraction-limited laser amplifier with SBS wavefront correction*', IEEE J. Quantum Electron. **31**, No 1, 148 (1995).

[42] H. J. Eichler, A. Haase, and R. Menzel, '*100-Watt average output power 1.2 diffraction limited beam from pulsed neodymium single-rod amplifier with SBS phase conjugation*', IEEE J. Quantum Electron. **31**, No 8, 1265 (1995).

[43] P. A. Belanger, A. Hardy, and A. E. Seigman, '*Resonant modes of optical cavities with phase conjugate mirrors: Higher order modes*', Appl. Opt. **19**, 479 (1980).

[44] P. A. Belanger, A. Hardy, and A. E. Seigman, '*Resonant modes of optical cavities with phase conjugate mirrors*', Appl. Opt. **19**, 602 (1980).

[45] S. A. Lesnik, M. S. Soskin, and A. I. Khizhnyak, '*Laser with a stimulated-Brillouin-scattering complex-conjugate mirror*', Sov. Phys. Tech. Phys. **24**, No 10, 1249 (1980).

[46] N. N. LL'ichev, A. A. Malyutin, and P. P. Pashinin, '*Laser with diffraction-limited divergence and Q-switching by stimulated Brillouin scattering*', Sov. J. Quantum Electron. **12**, No 9, 1161 (1982).

[47] I. M. Bel'dyugin, B. Ya. Zeldovich, M. V. Zolotarev, and V. V. Shkunov, '*Lasers with wavefront-reversing mirrors (review)*', Sov. J. Quantum Electron. **15**, No 12, 1583 (1985).

[48] V. S. Arakelyan, and G. E. Rylov, '*Laser with a wavefront-reversing mirror and Q-switching by stimulated Brillouin scattering*', Sov. J. Quantum Electron. **15**, No 3, 433 (1985).

[49] A. A. Denisov, and O.L. Kulikov, '*Laser with a T-shaped resonator and a stimulated Brillouin scattering mirror*', Sov. J. Quantum Electron. **20**, No 6, 655 (1990).

[50] H.J. Eichler, R. Menzel, and D. Schumann, '*10-W single-rod Nd:YAG laser with stimulated Brillouin scattering Q-switching mirror*', Appl. Opt. **31**, No 24, 5038 (1992).

[51] H. J. Eichler, Chen, Jun, A. Kummrow, R. Menzel, and D. Schumann, '*Nd:YAG-Laser with SBS Q-switching mirror and repetition rate up to 50Hz*', Int. J. Nonlin. Opt. Phys. **2**, No 1, 187 (1993).

[52] A. Agnesi, and G. C. Reali, '*Passive and self-Q-switching of phase-conjugation Nd:YAG laser oscillators*', Opt. Commun. **89**, 41 (1992).

[53] S. Chandra, R. C. Fukuda, R. Utano, '*Sidearm stimulated scattering phase-conjugated laser resonator*', Opt. Lett. **10**, No 7, 356 (1985).

[54] P. P. Pashinin, E. I. Shklovsky, and V. S. Sidorin, '*Characteristics of a SBS self-Injection locked laser*', Laser Physics **1**, No 2, 160 (1991).

[55] R. A. Lamb, M. J. Damzen, '*Q-switching of a Nd:YAG phase conjugate laser using external stimulated Brillouin scattering*', AME1, 92 (1993).

[56] D. M. Pepper, D. Fekete, and A. Yariv, '*Observation of amplified phase conjugate reflection and optical parametric oscillation by degenerate four-wave mixing in a transparent medium*,' Appl. Phys. Lett. **33**, 41 (1978).

[57] H. Vanherzeele, and J. L. Van Eck, '*Pulse compression by intracavity degenerate four-wave mixing*', Appl. Opt. **20**, 524 (1981).

[58] J. R. Murray, J. Goldhar, D. Eimerl, and A. Szoke, '*Raman pulse compression of excimer lasers for application to Laser Fusion*', IEEE J. Quantum Electron. **QE-15**, 342 (1979).

[59] J. J. Ewing, R. A. Haas, J. C. Swingle, E. V. George, and W. F. Krupke, '*Optical pulse compression systems for laser fusion*', IEEE J. Quantum Electron. **QE-15**, 368 (1979).

[60] R. R. Jacobs, J. Goldhar, D. Eimerl, S. B. Brown, and J. R. Murray, Appl. Phys. Lett. **37**, 268 (1980).

[61] D. T. Hon, '*Pulse Compression by Stimulated Brillouin Scattering*', Opt. Lett. **5**, No 12, 516 (1980).

[62] M. J. Damzen, and M. H. R. Hutchinson, '*High-efficiency laser pulse compression by stimulated Brillouin scattering*', Opt. Lett. **8**, No 6, 313 (1983).

[63] M. J. Damzen, and M. H. R. Hutchinson, '*Pulse compression in a phase conjugating Brillouin cavity*', Opt. Lett. **9**, No 7, 282 (1984).

[64] C. B. Dane, L. A. Hackel, and W. A. Neuman, '*High energy pulse compression*', IEEE J. Quantum Electron. **30**, 1907 (1994).

[65] L. A. Hackel, C. B. Dane, M. R. Herman and L. E. Zapata, '*Phase Conjugated Lasers Applied to commercial X-ray Lithography*', Second International School and Topical Meeting on Applications of Non-linear Optics, Prague (1993).

[66] L. A. Hackel, J. L. Miller, and C. B. Dane, '*Phase conjugation in a high power regenerative laser amplifier system*', Int. J. Nonlin. Opt. Phys. **2**, No 1, 171 (1993).

[67] D. A. Rockwell, and C. R. Giuliano, '*Coherent coupling of laser gain media using phase conjugation*', Opt. Lett. **11**, No 3, 147 (1986).

[68] M. Valley, G. Lombardi, and R Aprahamian, '*Beam combination by stimulated Brillouin scattering*', J. Opt. Soc. Am. **3**, No 10, 1492 (1986).

[69] R. H. Moyer, M. Valley, and M. C. Cimolino, '*Beam combination through stimulated Brillouin scattering*', J. Opt. Soc. Am. B **5**, No 12, 2473 (1988).

[70] R. H. Moyer, '*Beam combination with stimulated Brillouin scattering: a review*', SPIE **1000**, 25 (1988).

[71] D. L. Carroll, R. Johnson, S. J. Pfeifer, and R. H. Moyer, '*Experimental investigations of stimulated Brillouin scattering beam combination*', J. Opt. Soc. Am. B **9**, No 12, 2214 (1992).

[72] D. S. Sumida, D. C. Jones, and D. A. Rockwell, '*An 8.2J phase-conjugate solid state laser coherently combining eight parallel amplifiers*', IEEE J. Quantum Electron. **30**, No 11, 2617 (1994).

[73] W. Kaiser and M. Maier, '*Stimulated Rayleigh, Brillouin and Raman spectroscopy*', in Laser Handbook, vol 2, F. T. Arecchi and E. O. Schulz-Dubois, eds. Amsterdam, North-Holland, ch E2, 1078 (1972).

[74] R. Y. Chiao, C. H. Townes and B. P. Stoicheff, '*Stimulated Brillouin Scattering and Coherent Generation of Intense Hypersonic Waves*', Phys. Rev. Lett. **12**, 592 (1964).

[75] L. Brillouin, '*Diffusion de la luminere et des rayons par un corps trasparent homogene*', Ann. Physique **17**, 88 (1922).

[76] C. B. Dane, W. A. Neuman, and L. A. Hackel, '*Pulse-shape dependence of stimulated Brillouin scattering phase conjugation fidelity for high input energies*', Opt. Lett. **17**, No 18, 1271 (1992).

[77] R. St. Pierre, H. Injeyan, R. Hilyard, M. Weber, J. Berg, M. Wickham, C. Hoefer, L. Harpols, and J. Machan, '*High brightness diode pumped solid-state laser development*', in Conf. Lasers and Electro-Opt., OSA Tech. Dig. Series **11**, 274 (1993).

[78] D. A. Rockwell, M. S. Mangir, and J. J. Ottusch, '*Energy scaling of phase-conjugate solid-state lasers*', SPIE **1627**, 56 (1992).

[79] V. N. Alekseev, V. V. Golubev, D. I. Dmitriev, A. N. Zhilin, V. V. Lyubimov, A. A. Mak, V. I. Reshetnokov, V. S. Sirazetdinov, and A. D. Starikov, '*Investigation of wavefront reversal in a phosphate glass laser amplifier with a 12cm output aperture*', Sov. J. Quant. Electron. **17**, 455 (1987).

[80] E. M. Dianov, A. Ya. Karasik, A. V. Lutchnikov, and A. N. Pilipetskii, '*Saturation effects at backward-stimulated scattering in the single-mode regime of interaction*', Optical and Quantum Electron. **21**, 381 (1989).

[81] A. L. Gaeta, and R. W. Boyd, '*Stochastic dynamics of stimulated Brillouin scattering in an optical fibre*', Phys. Rev. A **44**, 3205 (1991).

[82] M. S. Mangir, J. J. Ottusch, D. C. Jones, and D. A. Rockwell, '*Time-resolved measurements of stimulated Brillouin scattering phase jumps*', Phys. Rev. Lett. **68**, No 11, 1702 (1992).

[83] R. Menzel et al, IQEC Technical Digest FE6, Sydney, 259 (1996).

Chapter 2

Stimulated Brillouin Scattering

2.1 Introduction

Stimulated Brillouin Scattering (SBS) is the inelastic interaction between light and sound, and is the most common self-starting phase conjugation technique. It can be described by the 3rd-order term of the polarization ($\vec{P}$) induced in the medium by the applied optical field (with electric field - $\vec{E}$). It is associated with the χ_3 coefficient of the electric susceptibility of the material,

$$P = \varepsilon_o\left(\chi E + \chi_2 E^2 + \chi_3 E^3 + \ldots..\right)$$
$$\mapsto P_{NL}$$

where ε_o is the permittivity of free space and P_{NL} is the nonlinear polarization.

SBS is initiated by spontaneous Brillouin scattering of light from the background phonon field of the medium created by thermal noise fluctuations. This phonon field consists of a periodic pressure variation, and thus a refractive index variation in the medium. The applied incident laser pump then interferes with the Stokes scattered light

to increase the amplitude of the phonon field. This in turn exponentially increases the gain of the stimulated scattering process in the backward direction.

In the following analysis, a brief description of electrostriction, the phonon field driving force, is given. Then an analytical derivation of the coupled wave equations that describe the incident and reflected light fields, and the acoustic field for SBS is presented. The transient stimulated Brillouin scattering theory presented in this chapter incorporates a focusing geometry, random noise seed, and the effects of pump depletion and finite phonon lifetime. Numerical transient SBS theory has been used to study the effect of noise and the time-resolved amplitude of the phonon field in many recent articles [1-7]. This transient theory was developed as a collaboration with Vladimir Devrelis and Shahram Afsharvahid for use in these experiments [9,10].

2.2 Electrostriction

Before the backscattered field can be generated, the driving force from which stimulated Brillouin scattering can take place must first be described. Electrostriction is the force that compresses an optical material in the presence of an electric field.

From a microscopic viewpoint, molecules in the region of an applied electric field ($\vec{E}$), develop a dipole moment ($\vec{p} = \alpha \vec{E}$), where α is the molecular polarizability. The force acting on each molecule is related to the energy stored by its polarization and is given by:

$$\vec{F} = -\vec{\nabla} U = \left(\frac{1}{2}\right) \alpha \vec{\nabla} \left(E^2\right) \tag{2.1}$$

From this relation it can be seen that the molecules are pulled into the regions of high electric field strength. This movement of molecules leads to a density variation (ΔQ)

within the material. Due to this variation there is a corresponding change to the dielectric constant (ε). Using the first law of thermodynamics, an expression for the contribution to the pressure (p_{el}) on the material that is due to electrostriction can be obtained:

$$p_{el} = -\gamma_e \left(\frac{E^2}{8\pi} \right) \tag{2.2}$$

where $\gamma_e = Q_o \frac{\partial \varepsilon}{\partial Q}$ is known as the electrostrictive constant, and Q_o is the mean density of the medium. If we assume that the medium is charge-neutral, then spatial variations of the square of the electric field efficiently drive the sound wave by electrostriction.

2.3 Growth of the Backscattered Field

Spontaneous Brillouin scattering results from the scattering of the incident radiation off the sound waves that are present in thermal equilibrium. For a high power incident laser pump, the spontaneously scattered light can become very intense. The incident and scattered optical fields interfere to give density and pressure variations by means of electrostriction. The incident laser pump can then scatter from this refractive index variation. The scattered light will experience a small Doppler frequency shift due to the propagation of the sound wave, but will add constructively with the Stokes field that created the phonon field over the effective coherence length of the interaction. In this way, the incident laser pump and the backscattered Stokes return continue interfering to reinforce the growth of the phonon field in the medium.

A schematic of the phonon-photon interaction is shown in Figure 2.1. To conserve energy and momentum, the wave-vector and angular frequency of the incident laser

pump $\vec{k}_P, \omega_P$ and the Stokes wave-vector and angular frequency $\vec{k}_S, \omega_S$ must satisfy the conditions:

$$\begin{aligned} \omega_B &= \omega_P - \omega_S \\ \vec{k}_B &= \vec{k}_P - \vec{k}_S \end{aligned} \tag{2.3}$$

where $\omega_B, \vec{k}_B$ are the angular frequency and wave-vector corresponding to the Brillouin acoustic wave. The sound frequency is typically of the order of 0.1-100 GHz, which is much less than the optical frequency. This validates the approximation of the Bragg condition (when $|k_P| = |k_S|$):

$$|k_B| = 2n|k_P|\sin\left(\frac{\theta}{2}\right) \tag{2.4}$$

where 'θ' is the scattering angle, and 'n' is the refractive index. Therefore, the frequency shift is given by:

$$\nu_B = \frac{\omega_B}{2\pi} = \frac{2n\nu_P \upsilon_B}{c}\sin\left(\frac{\theta}{2}\right) \tag{2.5}$$

where ν_P is the laser pump frequency, and υ_B is the acoustic velocity.

The maximum frequency shift (ν_B) occurs when $\theta = \pi$ (i.e. backscattering (see Figure 2.2)). To conserve momentum in this case, a new phonon is created in addition to the one participating in the interaction.

A description of the growth of the scattered wave involves the non-linear coupling between acoustic and optical fields in the medium. Consider two monochromatic laser beams overlapping in a transparent dielectric medium, with one beam having a Stokes

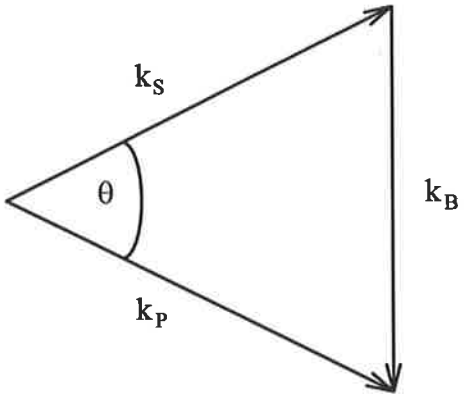

Figure 2.1 Vector diagram of Brillouin scattering.

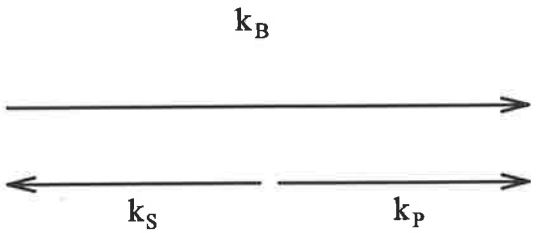

Figure 2.2 Vector diagram for Stokes scattering in the backward direction.

frequency shift relative to the other. The total optical field within the Brillouin medium can be represented as $\vec{E}(z,t) = \vec{E}_P(z,t) + \vec{E}_S(z,t)$, where:

$$\vec{E}_P(z,t) = \frac{1}{2} A_P \exp\left[i(\omega_P t + k_P z)\right] + c.c.$$
$$\vec{E}_S(z,t) = \frac{1}{2} A_S \exp\left[i(\omega_S t - k_S z)\right] + c.c. \qquad (2.6)$$

Similarly, the acoustic field can be described in the form:

$$\vec{Q}(z,t) = Q_o + \Delta Q(z,t)$$
$$\vec{Q}(z,t) = Q_o + \left[\frac{1}{2} Q \exp\left[i(\omega_B t + k_B z)\right] + c.c.\right] \qquad (2.7)$$

where $|k_B| = 2|k_P|$, and Q_o denotes the mean density of the medium.

Each field has a phase which can effect the gain of the Brillouin process. The gain is maximized when $\phi_P - \phi_S - \phi_B = \frac{\pi}{2}$. To incorporate phase pulling, the amplitudes of the fields inside the medium can be redefined as:

$$A_P = A_P e^{-i\phi_P}, A_S = A_S e^{-i\phi_S}, Q = Q e^{-i\phi_B} \qquad (2.8)$$

It should be noted here that the phase relationship between the three interacting fields can, alternatively, be represented by defining the input pump (A_P) as $\rightarrow A_P + i\phi_P$ where the real part represents the amplitude and the imaginary part represents the phase. This technique gives rise to three coupled equations which contain '$\pm i$' factors [2-4].

The density perturbation (ΔQ) will obey the Navier-Stokes wave equation. The acoustic wave will suffer damping in the form of the medium viscosity and will also be driven by the electrostrictive force provided by the time varying electric fields of the light waves. Spatial variations for the acoustic field have been neglected (using SVE

Approximation) since the acoustic wave does not propagate far on the time scale of the scattering ($\upsilon_B << c$). The optical field in the medium is described by Maxwell's wave equations with the non-linear Polarization ($\vec{P}_{NL}$), acting as the source term. Therefore, after some simplification, a set of coupled equations can be obtained:

$$\left.\begin{aligned}
\left(\frac{\partial}{\partial z}-\frac{n}{c}\frac{\partial}{\partial t}\right)A_P &= -g_2\sin\left(\phi_P-\phi_S-\phi_B\right)A_S Q \\
\left(\frac{\partial}{\partial z}+\frac{n}{c}\frac{\partial}{\partial t}\right)A_S &= g_2\sin\left(\phi_S-\phi_P+\phi_B\right)A_P Q \\
\left(\frac{\partial}{\partial t}+\frac{1}{2\tau_B}\right)Q &= g_1\sin\left(\phi_S-\phi_P+\phi_B\right)A_P A_S + f_1
\end{aligned}\right\} \qquad (2.9)$$

and

$$\left.\begin{aligned}
\left(\frac{\partial}{\partial z}-\frac{n}{c}\frac{\partial}{\partial t}\right)\phi_P &= -g_2\cos\left(\phi_P-\phi_S-\phi_B\right)\frac{A_S}{A_P}Q \\
\left(\frac{\partial}{\partial z}+\frac{n}{c}\frac{\partial}{\partial t}\right)\phi_S &= g_2\cos\left(\phi_S-\phi_P+\phi_B\right)\frac{A_P}{A_S}Q \\
\left(\frac{\partial}{\partial t}\right)\phi_B &= g_1\cos\left(\phi_S-\phi_P+\phi_B\right)\frac{A_P A_S}{Q}+f_2
\end{aligned}\right\} \qquad (2.10)$$

where τ_B is the phonon lifetime, related to the spontaneous Brillouin linewidth $\Gamma = \frac{1}{2\tau_B}$, and g_1, g_2 are the electric and acoustic field coupling coefficients. Langevin noise sources f_1, f_2 have been added to the phonon amplitude and phonon phase equations. They have Gaussian statistics and describe the thermal fluctuations in the density of the medium leading to spontaneous Brillouin scattering [3,5]. Also, it should be noted that optical absorption was chosen not to be included in the equations above to simplify this analysis.

Figure 2.3 shows the schematic of the geometry used for the transient SBS analysis. The reduction in beam cross-sectional area, and hence in intensity, can be described using simple Gaussian Beam optics [8]. The radius of a propagating Gaussian beam is given by:

$$w(z) = w_o\left[1+\frac{(L+d-z-f)^2}{\lambda^2}\right]^{\frac{1}{2}} \qquad (2.11)$$

where the radius is taken at the $1/e^2$ value, λ is the laser wavelength and w_o is the focal waist radius at position $z = L + d - f$. Now the amplitudes can be rewritten to incorporate the intensity variation due to the focusing geometry (i.e. $A_{P,S} \rightarrow \frac{A_{PS}}{w(z)}$, where $A_{P,S}^2 = \frac{\text{Power}}{\text{Area}}$).

This system of coupled partial differential equations was solved using a non-iterative, numerical algorithm [9,10]. In these reports, solutions were obtained by integrating the phonon amplitude and phase in Equations 2.9 & 2.10. These were then substituted back into the remaining four equations. It is here that terms in units of 'power' occur. The final four equations form a set of coupled partial differential equations which describe transient SBS for the focusing geometry.

The simplest solution to these equations can be found when the signal field is much weaker than the pump field over the entire interaction region, and a steady state time has been reached. This approximation is useful in obtaining an estimate of the threshold energy, gain and reflectivity as well as other properties of the scattering process. In the steady-state regime, the response time of SBS (τ_B) is much less than the pulse duration (τ_P), and therefore, all time derivatives can be set to zero $\left(\frac{\partial}{\partial t} = 0\right)$ with the incident pump intensity taken to be constant $\left(\frac{\partial}{\partial z}, \frac{\partial}{\partial t} A_P = 0\right)$. Using the 'phase-locked' case, the 'phase' terms in Equations 2.9 & 2.10 can be eliminated. From these assumptions, a simplified differential equation can be written in terms of field intensities I_P, I_S:

$$\frac{dI_S}{dz} = -2\tau_B\, g_1 g_2 I_P I_S = -\frac{g_1 g_2}{\Gamma} I_S I_P = -g_B I_S I_P \qquad (2.12)$$

where g_B is the steady-state Brillouin gain usually expressed in cm/MW.

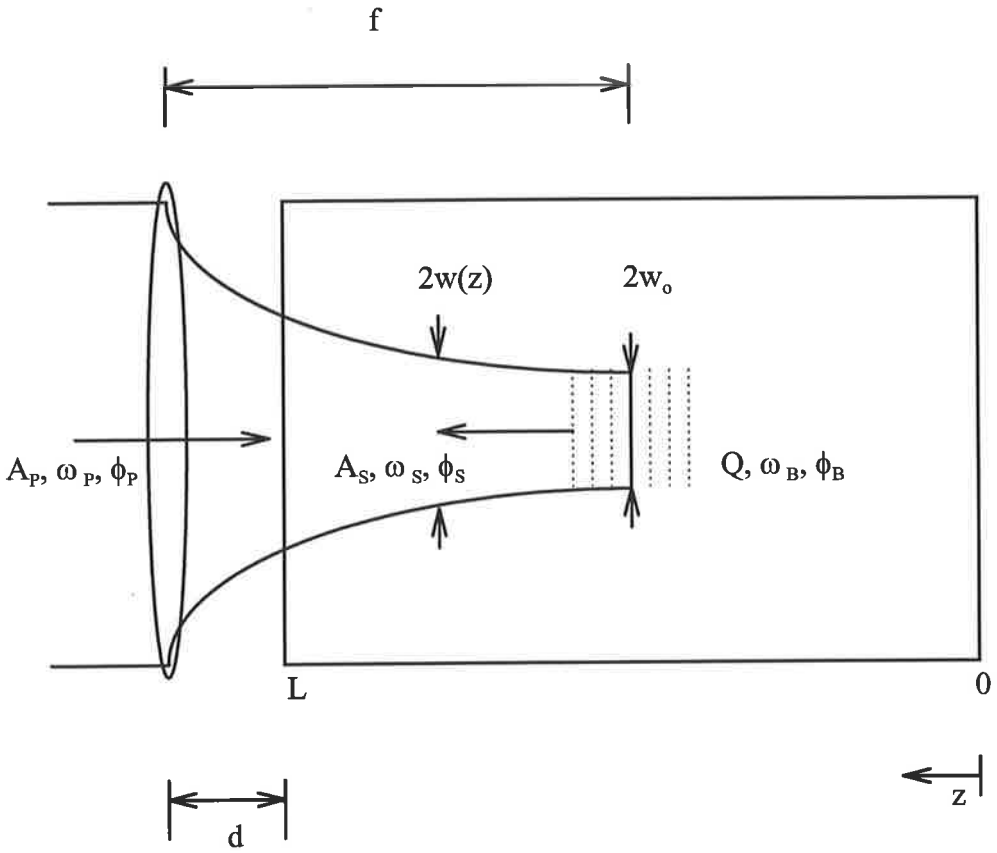

Figure 2.3 Focusing geometry used for transient SBS analysis.

This equation can be solved by integrating I_S over an interaction length (l_i), defining the boundary conditions which allow the amplification of the Stokes wave to be achieved, and by defining the intensity threshold which is a characteristic of SBS. It can easily be shown that the Stokes return intensity increases proportional to $\exp(g_B I_P l_i)$.

The 'threshold' condition can therefore be defined as [11]:

$$g_B I_P l_i = G \cong 25 \tag{2.13}$$

If we consider a typical g_B of 0.02 cm/MW and assume an interaction length of 5cm, we obtain a threshold intensity of 250 MW/cm^2. This intensity level is easily achievable in a simple, focusing geometry with a Q-switched solid-state laser pulse of a few mJ's output energy.

References

[1] W. Kaiser and M. Maier, '*Stimulated Rayleigh, Brillouin and Raman spectroscopy*', in Laser Handbook, vol. 2, F. T Arecchi and E. O. Schulz-Dubois, eds., Amsterdam, North-Holland, ch E2, 1078 (1972).

[2] G. Valley, '*A review of stimulated Brillouin scattering excited with a broad-band pump laser*', IEEE J. Quantum Electron. **QE-22**, 704 (1986).

[3] A. L. Gaeta and R. W. Boyd, '*Stochastic dynamics of stimulated Brillouin scattering in an optical fibre*', Phys. Rev. A **44**, No 5, 3205 (1991).

[4] R. Chu, M. Kanefsky, and J. Falk, '*Transient phase conjugation by stimulated Brillouin scattering: numerical analysis of zero-order solutions*', J. Opt. Soc. Am B **11**, No 2, 331 (1994).

[5] E. M Dianov, A. YA. Karasik, A. V. Lutchnikov, A. N. Pilipetskii, '*Saturation effects of backward-stimulated scattering in the single-mode regime of interaction*', Opt. & Qu. Electronics **21**, 381 (1989).

[6] R. Menzel and H. J. Eichler, '*Temporal and spatial reflectivity of focused beams in stimulated Brillouin scattering for phase conjugation*', Phys. Rev. A **46**, No 11, 7139 (1992).

[7] R. W. Boyd, K. Rzazewski, and P. Narum, '*Noise initiation of Stimulated Brillouin Scattering*', Phys. Rev. A **42**, 5514 (1990).

[8] A. E. Seigman, '*Lasers*', Ch 17, (1986).

[9] S. Afsharvahid, Ph. D thesis, University of Adelaide, 1997 (in preparation).

[10] V. Devrelis, M. O'Connor, J. Munch, S. Afsharvahid, C-J. Wei, and A-M. Grisogono, '*Fidelity of optical phase conjugation using stimulated Brillouin scattering*', IQEC 96, WL (1996).

[11] B. Ya. Zel'dovich, N. F. Pilipetsky, V. V. Shkunov, '*Principles of Phase Conjugation*', T. Tamir (ed.), Berlin: Springer, (1985).

Chapter 3

SBS with Long and Short Coherence Length Pumping

3.1 Introduction

3.1.1 Long Coherence Length Study

One of the most important parameters in defining the performance of the phase conjugate process is phase fidelity. For stimulated Brillouin scattering, phase fidelity describes how well the phase of the SBS reflected beam reproduces the phase of the input beam. Phase fidelity has been the major concern of many experimental studies [1-7]. Some studies have reported that the phase fidelity decreases when the pump energy is well in excess of the SBS threshold energy [1-3], whereas others have reported that the phase fidelity either improves or remains approximately constant at a high value whilst the pump energy increases well above the SBS threshold [4-7].

The small number of recent experimental examinations of time-resolved reflectivity and phase fidelity of the SBS process have been directed towards the measurement of

temporal intensity fluctuations in the SBS return beam [8-13]. It has been proposed that some of the intensity fluctuations observed may be associated with phase fluctuations in the Stokes return beam. The first observations of intensity fluctuations reported to be associated with phase fluctuations in SBS were in 1980 by Basov *et al* [8], Vasil'ev *et al* [9], and Bespalov *et al* [10] but no direct experimental evidence as to their origin was given. Similar intensity fluctuations have been investigated theoretically and observed experimentally by Dianov *et al* [12], where a transient SBS theory incorporating spontaneous noise and phase-pulling effects was used to investigate the occurrence of Stokes intensity fluctuations associated with phase jumps under particular operating regimes. Experimental measurements of the actual phase fluctuations as well as the temporal intensity of the stokes return beam have been made using a heterodyne detection system [13]. Simultaneous temporal variations in SBS reflectivity and phase fidelity have also been reported by Munch *et al* [15] but their origin was unresolved.

The objective of this work was to understand and establish operating regimes for the effective control of phase fidelity in the SBS process. This is required for the subsequent application of SBS to oscillators (see Chapter 4).

In this chapter, SBS reflectivity and phase fidelity (simultaneously time-integrated and time-resolved) will be investigated with long coherence length pumping. Long coherence length SBS is defined as SBS excited by a pump, in which the coherence length is much longer than the interaction length. The interaction length is specified by either the focusing geometry, or the physical length of the SBS cell. Alternatively, long coherence length SBS can be described in terms of a pump bandwidth which is much smaller than the sound decay rate (Brillouin linewidth - Γ). Results demonstrating high time-integrated SBS reflectivity and phase fidelity are presented, as well as the identification of temporal intensity fluctuations associated with phase jumps. The latter was subsequently fully developed by Devrelis [37], while this work concentrated on SBS applied to oscillators.

3.1.2 Short Coherence Length Study

For long coherence length SBS it has been reported that the SBS process occurs independently of the input pump spectrum [16]. As the coherence length of the input pump is reduced, the properties governing the SBS process become more complicated. Short coherence length SBS is defined as SBS excited by a pump in which the bandwidth exceeds the sound decay rate or in which the pulse length is short compared to the sound decay time (τ_B) [14]. Valley [14] reported that there are two factors that tend to disrupt the temporal reproduction and spatial conjugation of the SBS process. The first factor is the group velocity mis-match that reduces the gain when the coherence length of the pump is shorter than the interaction length. Experimental studies performed by Munch *et al* [15] demonstrate that near the steady-state threshold for phase conjugate SBS, the effective interaction length (l_i) should be the shortest of the cell length (L), three times the coherence length ($3xl_c$), or five times the Rayleigh range ($5xl_R$). Mullen *et al* [17] and Davis *et al* [18] have observed a significant drop in reflectivity when the coherence length is shorter than the interaction length (i.e. $l_c < l_i$).

The second factor which may disrupt the SBS process is a pump wave that is composed of many independent temporal modes, each with their own spatial profile [14]. Valley [14] concluded theoretically that in this case, good temporal and spatial reproduction is achieved only if the temporal modes are separated by frequencies greater than the Brillouin linewidth (Γ). Experimental observations have confirmed that SBS is independent of modal structure, if the spacing between individual laser modes is larger than the Brillouin linewidth, and the bandwidth of each line results in a coherence length that is much larger than the interaction length [19-21].

In another study it was proposed that the phase fidelity was destroyed because the medium could not respond to temporal pump intensity variations on time scales less than the phonon lifetime (τ_B) [3]. Betin *et al* [3] concluded that in this case, noise

modes can be created which compete with the Phase Conjugate (PC) mode for energy extraction over the lifetime of the input pulse.

This short coherence length study of SBS forms the major part of the present chapter. The objective of this work is to understand and extend the operational range of SBS-OPC devices under conditions where the extremely high electric field associated with the pump beam, and hence the pump intensity, vary on timescales of the order of the phonon lifetime.

In this chapter, an experiment to measure SBS reflectivity and phase fidelity was designed to investigate SBS using a short coherence length pump. Measurements of optical breakdown caused by these extremely high electric fields were also carried out.

The output pulse from a phase conjugate oscillator using an SBS mirror contains a multitude of longitudinal modes created in part by the successive frequency shift that occurs for each SBS interaction during the build-up phase of the laser pulse. These longitudinal modes interfere inside the cavity, to produce ultra-short pulses each with very high peak power. In designing resonators which incorporate SBS cells, it is essential to characterise their phase conjugate performance under short pulse, high peak power conditions. The design and operation of an oscillator that contains an SBS cell has been developed further in this research, and is the subject of Chapter 4.

3.2 Experiment

Figure 3.1 shows the experimental set-up for the study of the phase conjugate SBS process under different coherence length conditions. The following sections describe the components and diagnostic techniques developed, as well as the approach

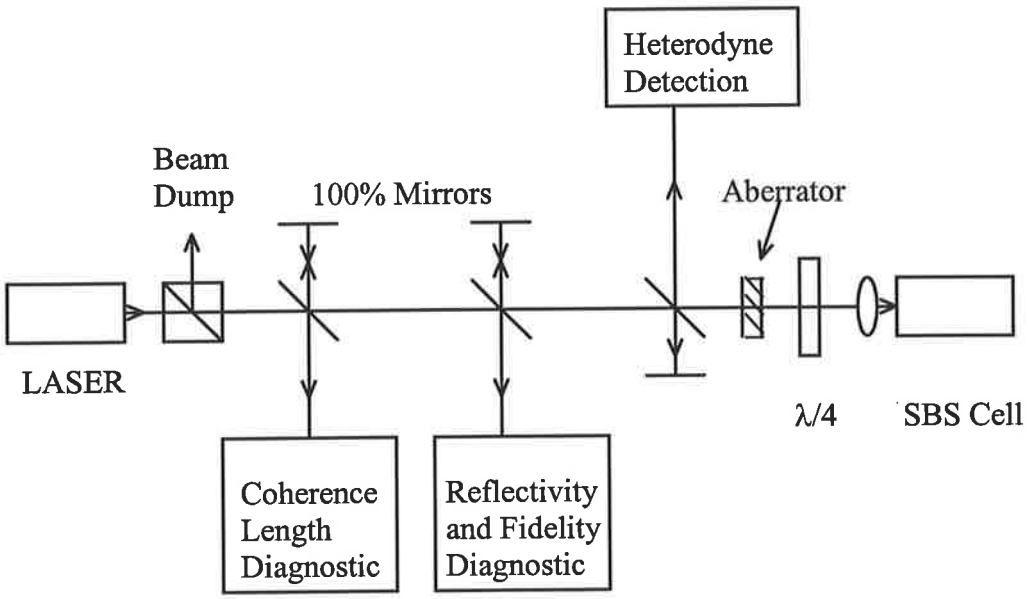

Figure 3.1 Schematic of set-up used to study the phase conjugate SBS process.

used to measure the characteristics of the laser input beam and the SBS backscattered beam.

3.2.1 Laser System

The flashlamp pumped Nd:YAG laser system was operated in two different coherence length regimes. Firstly, a short coherence length of approximately 1cm (linewidth - 30GHz) was obtained from the Nd:YAG laser when free-running. Secondly, injection seeding using a CW diode-pumped Nd:YVO_4 laser, produced a laser beam with a long coherence length of 3m (linewidth - 100MHz). The output beam was linearly polarized and had a maximum energy of 750mJ in a 10ns FWHM pulse (risetime ~ 4ns). Typical examples of the temporal profiles of both the long and short coherence length laser pulses are shown in Figure 3.2.

The laser could be operated at pulse repetition rates between 1 and 15Hz. The measured divergence of the input laser beam (θ_p) was 0.2mrad, and it had a near-field super-Gaussian spatial profile with a beam diameter (D) of 8.5mm. This diameter corresponded to where the intensity dropped to $1/e^2$ of its maximum value.

3.2.2 Detector System

Time-integrated energy measurements were made with a Joulemeter/Ratiometer (Molectron JD2000) using calibrated pyroelectric energy heads (J25). Temporal profile measurements were obtained using silicon photodiodes (Electro-optics Technology ET 2000) which have a quoted rise-time of <200ps and cut-off frequency of >1.75GHz. The pulses were recorded using two transient digitizers (Tektronix SCD1000) with a measured 3dB frequency of 1.86GHz[1]. Two metre lengths of coaxial cable (UR67) were used with N-type connectors in order to maintain the high signal bandwidth.

[1] Refer to Section 3.2.4 for a discussion of the 3dB frequency measurement.

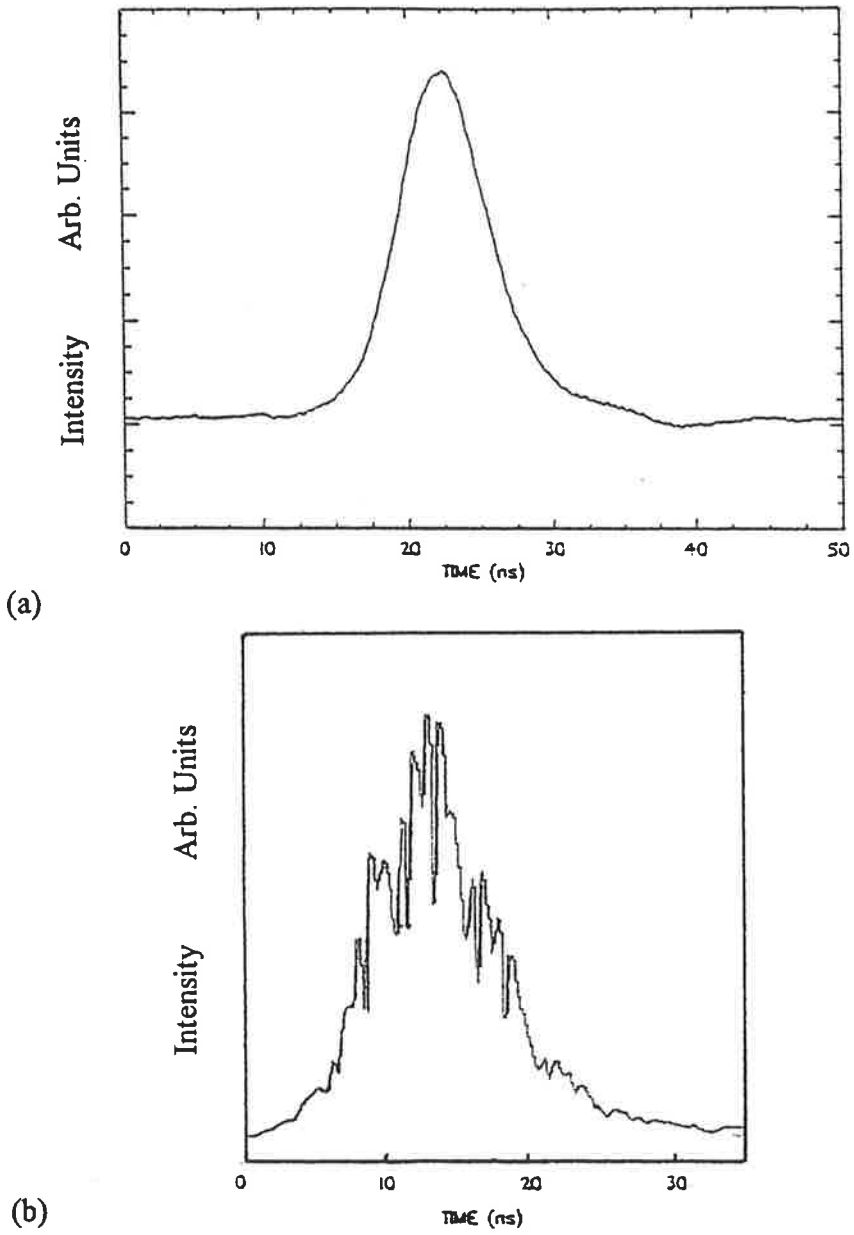

Figure 3.2 Typical temporal profiles for laser pulses,
(a) Long coherence length,
(b) Short coherence length.

Both the time-integrated and the digitized temporal data were stored on a 486 computer via a GPIB interface card. Spatial intensity profiles were obtained by imaging the beam onto a CCD camera (Pulnix TM-620) and stored on computer via a frame grabbing card (PC Vision +).

3.2.3 SBS Reflectivity and Phase Fidelity Diagnostic

Figure 3.3 shows the schematic for the SBS reflectivity and phase fidelity diagnostic. SBS reflectivity is defined as the ratio of the near-field (NF) intensity of the Stokes return beam to the NF intensity of the input beam. These measurements were calibrated by replacing the SBS lens and cell configuration with a flat, 100% reflectivity mirror. By accounting for the losses of the SBS lens and the front surface of the cell, a measurement of the true reflectivity from the non-linear medium was obtained.

For time-integrated measurements, all points on the graphs were obtained by averaging 99 pulse acquisitions. From this, the fluctuation or standard deviation from the mean was determined and displayed on the graphs as error bars.

Phase fidelity is defined as how well the phase of the Stokes return beam matches the phase of the input beam. This can be measured by focusing both beams and comparing the normalized far-field (FF) fluence through a pinhole placed at the beams waist. This is commonly known as the 'Power in the Bucket' technique [4,6]. To calibrate the data, the size of the pinhole was chosen to pass 85% of the input beams intensity. Therefore, the fidelity was measured as the ratio of the energy of the Stokes beam transmitted through the pinhole to the total reflected energy, normalized by the far-field transmission of the pump beam (85%). A concave mirror with a long focal length (f = 1.5m) was used in order to avoid optical breakdown and ablation of the pinhole. The calculated pinhole size to pass 85% of the input beams intensity is $\theta_p \cdot f = 0.3\text{mm}$.

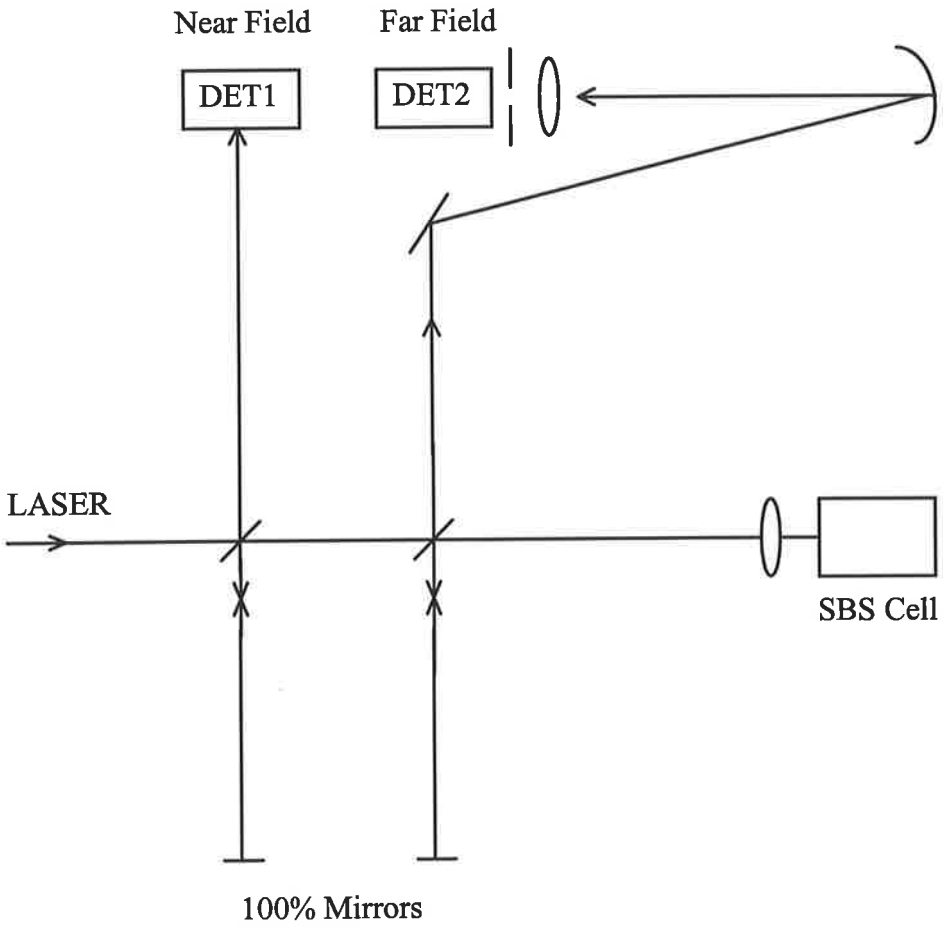

Figure 3.3 Schematic for the SBS reflectivity and phase fidelity diagnostic.

This calculation was confirmed by experimental measurement of a 85% fluence of the input beam intensity through the 0.3mm pinhole.

It should be noted that the diffraction limited pinhole size for a beam with a spatial top-hat profile is $\theta_d \cdot f = 2.44\lambda f/D = 0.46$mm and for a Gaussian is $1.27\lambda f/D = 0.24$mm , where D (=8.5mm) is the spot size ($2\omega_o$) and λ is the wavelength. However, as the measured intensity distribution was neither a top-hat or a perfect Gaussian, an experimental measurement of the laser pump transmission through the pinhole was performed. Alternatively, the Fourier transform of the measured near field intensity can be calculated to determine the spot size in the far field.

3.2.4 Heterodyne Detection Diagnostic

The schematic for the heterodyne detection diagnostic is shown in Figure 3.4. A beat note is formed from the interference of a laser reference beam and the corresponding frequency shifted Stokes return beam. A high-pass filter was applied to subtract the low frequency function (i.e. the laser pulse), leaving only the beat note. By measuring the time between peaks or troughs of this function (i.e. by measuring the zeroes of the beat note) the beat frequency can be determined. This beat frequency is the SBS frequency shift of the Stokes backscattered beam.

By comparing this high frequency sinusoidal signal function to a mathematical sine function of similar but fixed frequency, any changes in the phase of the signal can be identified. However, in this thesis work the heterodyne technique was only used to measure the frequency shift of the Stokes return[2].

The heterodyne diagnostic was calibrated using a 5kHz - 3GHz sine-wave generator (Rohde and Schwarz). A sine-wave with fixed amplitude was added (using load

[2] Devrelis [37] used the heterodyne technique to examine the magnitude of phase changes reported in Section 3.3.1.4 of this thesis.

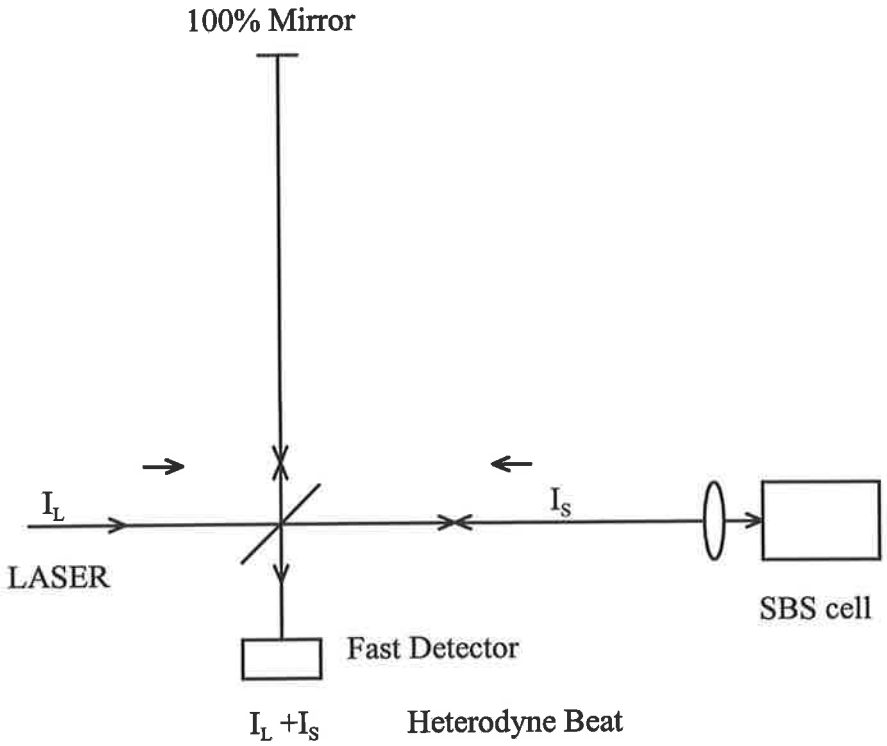

Figure 3.4 Schematic for Heterodyne detection diagnostic.

matching techniques) to a smooth Gaussian laser pulse from a fast Silicon detector and the resultant waveform was propagated through the cables to the transient digitizer.

A ratio of the output sine-wave amplitude to the input sine-wave amplitude for frequencies up to 3GHz was measured. The input frequency to the cables and transient digitizer, at which a 3dB attenuation was measured, was found to be 1.86GHz. The detectors and storage devices used were the same as those used in the SBS reflectivity and phase fidelity diagnostic.

3.2.5 Coherence Length Diagnostic

To study the effect of coherence length on the SBS process, a novel interferometric method for the measurement of coherence length of a single shot was developed. For pulsed lasers, the only method available for a measurement of the complete coherence function was a holographic approach [22]. In that approach, a hologram of an inclined plane was recorded using the laser to be diagnosed. When the hologram is reconstructed, the intensity distribution of the resulting image of the inclined plane can be used to determine the complete coherence properties of the laser on the single laser pulse. Although this method works well, it is limited to parts of the spectrum where holographic emulsions work, and it is neither convenient, nor real-time, nor suitable for modern experiments where lasers operate at high repetition rates with computerized data acquisition systems.

The temporal coherence function of a source is usually determined from an observation of the visibility of the interference fringes formed as a function of path length difference when two parts of the source are made to interfere with each other [23]. When two beams of intensity I_1 & I_2 interfere together, with a path length difference l, the visibility ($V(l)$), and hence the mutual coherence function ($\gamma_{12}(l)$) of the two beams, can be obtained from,

$$I_N(l) = \frac{I_1 + I_2 + 2\gamma_{12}(l)\sqrt{I_1 I_2}\cos kx}{I_1 + I_2}$$

$$= 1 + V(l)\cos kx$$

with,

$$V(l) = \frac{2\gamma_{12}(l)\sqrt{I_1 I_2}}{I_1 + I_2}$$

where all intensities are functions of the transverse coordinates (x,y) and k describes the interference pattern in one dimension (fringes are parallel to the y-axis in this case).

For a pulsed source in an interferometer, an inclined specular reflector of good optical quality was needed in order to produce recognizable interferometric fringes. For this effect, a blazed diffraction grating in a Littrow mount was used. A brief summary of the operation of this diagnostic tool is given below. A more detailed discussion can be found in Reference 24.

The concept is illustrated in Figure 3.5 showing a Michelson interferometer with the inclined grating in one arm. There is a line on the grating marked D, for which the path lengths of the interferometer arms are equal. Excellent fringe visibility will result from light reflected from this part of the grating. Light from other parts (E and F) on the inclined grating will take shorter or longer times to reach the interference plane on the CCD camera. The visibility of the interference fringes from these parts will therefore depend on the coherence length of the laser. The instantaneous, complete coherence function can thus be observed as the visibility of the fringes along the grating as seen on the TV monitor for each pulse.

The grating used was 210mm long with 600 lines per mm, and blazed at 17°. In order to obtain the largest measuring path difference, the inclined grating was reversed and used

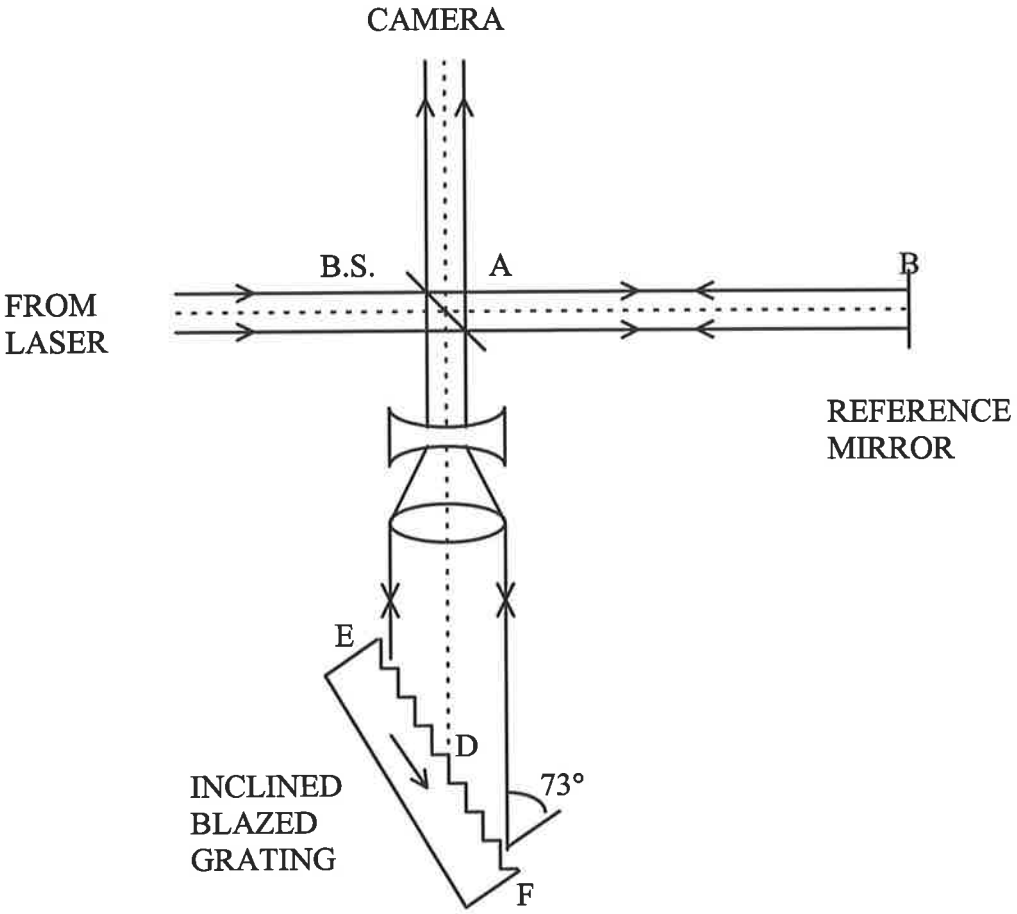

Figure 3.5 Schematic of Coherence length diagnostic.

with an angle of incidence of 73°. This made use of the fact that for the 90° groove shape often used on gratings, the diffraction efficiency is high both at the blaze angle and at its complement. A telescope was used to expand the beam to fill the grating. The closest and furthest points on the grating along the direction of the laser beam were separated by 200mm, allowing coherence lengths of up to 400mm to be measured with the set-up shown.

3.2.6 SBS Material and SBS Cell

Liquid Freon-113 ($C_2F_3Cl_3$) was chosen for the present SBS experiments at 1μm. It has been found that higher SBS reflectivity and phase fidelity is obtained by using media with lower optical absorption [25-27]. This absorption can induce thermal self-stress and refractive index changes at the focus of the laser beam in the medium. Freon-113 has been found to have an absorption coefficient (α) less than $10^{-5}cm^{-1}$ in the 1μm wavelength region [26]. As Freon-113 is chemically inactive it is possible to obtain a high purity liquid with low α. The absorption coefficient for Freon-113 is comparable to, if not lower, than that for other commonly used tetra-chlorides, and high pressure gases. Also, Freon-113 is by far the simplest of the these materials to use [28]. It is not toxic (as are the tetra-chlorides) and being a liquid at room temperature is much safer to handle than gases under extremely high pressures. Freon also has a high 3^{rd}-order nonlinear coefficient, and in particular a high gain coefficient for stimulated Brillouin scattering [29]. As a result of low absorption and high SBS gain, other thermal effects such as optical breakdown and self-focusing, together with stimulated Raman scattering are reduced.

The negative aspect of using Freon-113 is the global ban on the use of all Freons due to their detrimental effects on the earth's atmosphere. It will therefore, have to be replaced with another material of similar chemical characteristics. The SBS parameters for

Freon-113 of greatest interest are the phonon lifetime (τ_B) ~0.84ns, the frequency shift (ν_B) ~1.74GHz and the steady-state gain coefficient (g_B) ~0.0062cm/MW [26].

The purity of the Freon-113 was specified by the manufacturer to be >99.8% [30]. Under closer inspection (observing scatter from a laser - see below) the Freon still contained particles and other impurities which could be detrimental to the SBS process.

To remove the suspended and dissolved impurities, which can increase the absorption of the SBS liquid, a purification procedure involving a distillation and filtration process was adopted. The distillation process was carried out slowly over a period of a day (for two litres of Freon) using a long fractionating column. The filtration process included passing the liquid through a 0.2μm teflon filter twice. The entire purification procedure involved repeating the distillation and filtration processes three times before testing for scatter. After purification, the Freon-113 was kept in glass bottles with teflon seals to avoid contamination.

A qualitative measurement of the particles in our liquid samples was obtained by recording the scattered light from the suspended particles in each sample. A 70mW HeNe laser was focused through the sample and a CCD camera was aligned perpendicular to the cell to record the scattered light. Figure 3.6 shows the images for a purified sample and a sample with suspended impurities. The bright spots indicate the scattered light from dust particles (Mie scattering) measuring fractions of a micron, in the un-purified sample. The faint glow present in the pure sample is most probably due to molecular Rayleigh scattering. Many other researches have reported similar techniques to improve the SBS medium purity and enhance the SBS efficiency [7,26,31].

The SBS cell length and focusing conditions could either be altered independently or together. Cell lengths between 10cm and 60cm, and lenses with focal lengths between

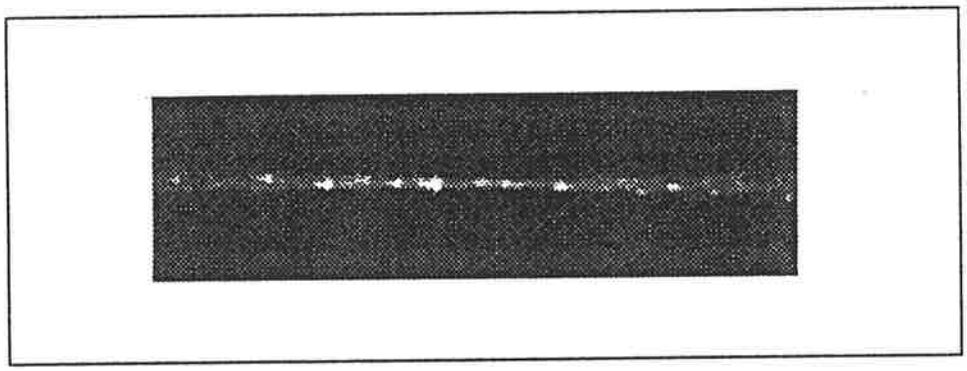

(a)

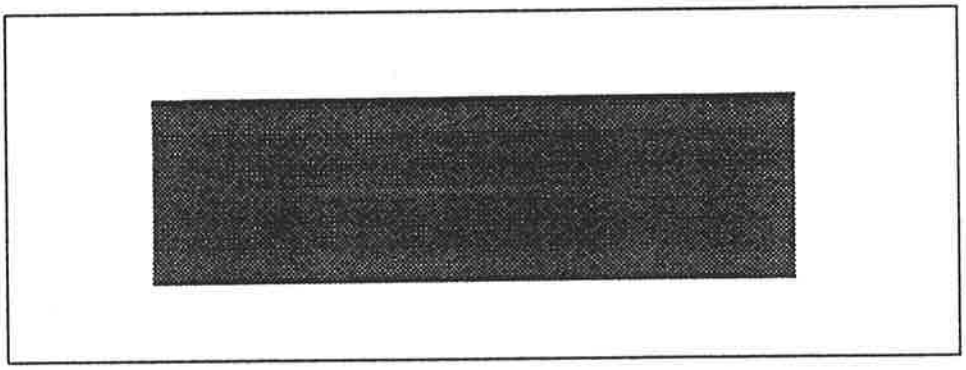

(b)

Figure 3.6 CCD images of a HeNe beam being focused through the SBS cell.

(a) Un-purified Freon-113,

(b) Purified Freon-113.

5cm and 100cm were used. The input energy was controlled by rotating a linear polarizer. The SBS return was isolated from the laser by using a polarizer-quarter wave plate isolator.

3.3 Results and Discussion

3.3.1 Long Coherence Length Pumping

In this section, results from a study of time-integrated and time-resolved SBS reflectivity, and phase fidelity with a long coherence length pump laser (l_c > 3metres) are presented and discussed.

3.3.1.1 Brillouin Frequency Shift for Freon-113

A measurement of the SBS frequency shift for Freon-113 was obtained by optical heterodyne beating of the input laser beam with the frequency shifted SBS return beam (see Figure 3.4). The typical heterodyne signal, measured with a photodiode, is shown in Figure 3.7. Although the beat note can be seen clearly, its amplitude is small. It is known that the measured 3dB frequency of the detection system is approximately the same as the Brillouin frequency shift[3]. Therefore, the signal was significantly attenuated by the detection system. Using the technique described in Section 3.2.4, an SBS frequency shift (ν_B) of 1.8 ± 0.1GHz was measured. From this experimental value, the speed of the acoustic grating (υ_B) was found to be ~704ms^{-1}.

The heterodyne technique has been used in previous experiments for the measurement of the SBS frequency shift [32,33]. The value measured in this experiment agrees with previously reported values of ν_B = 1.74GHz for Freon-113 [26].

[3] Refer to Section 3.2.4 for discussion of heterodyne detection system 3dB frequency measurement.

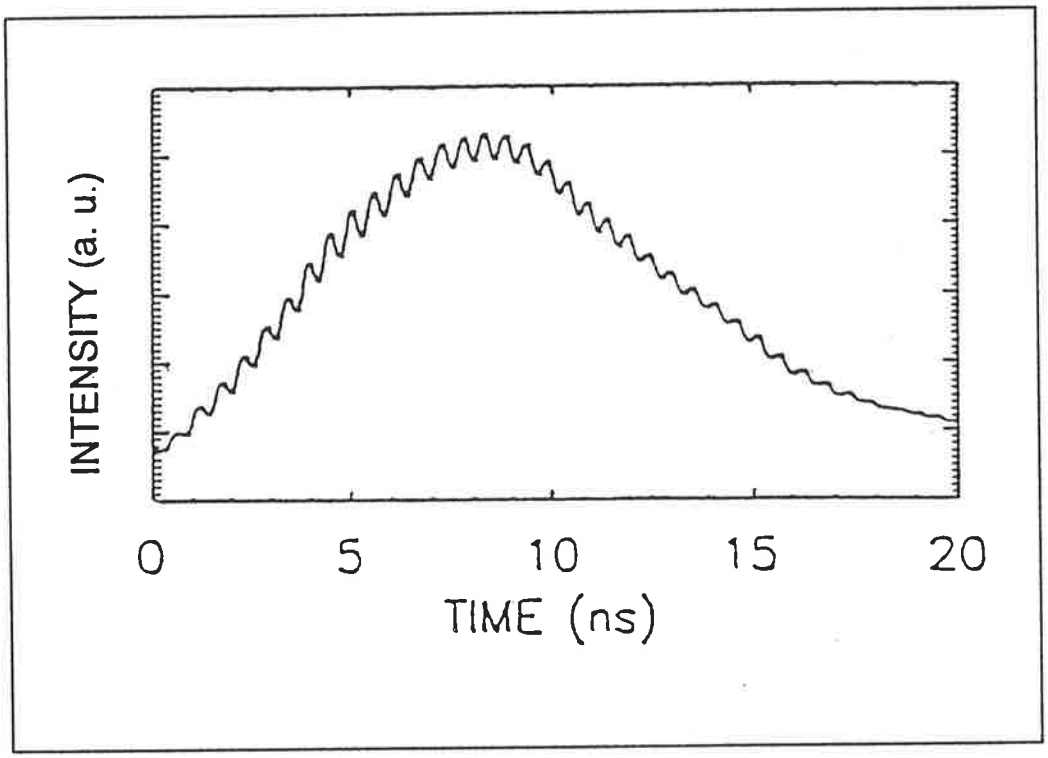

Figure 3.7 Photodiode output from Heterodyne detection diagnostic

3.3.1.2 Time-integrated SBS Reflectivity and Phase Fidelity

The following experiment was carried out to investigate a discrepancy in SBS phase fidelity measurements in the saturation regime, which have been reported in several recent studies [1-7] (described in Section 3.1.1). The experiment also forms part of the characterization of the SBS phase conjugate performance, which is required in Chapter 4 for the incorporation of an SBS mirror within a laser oscillator.

With the experiment set-up as discussed in Section 3.2, the SBS reflectivity of the Freon-113 cell was measured as a function of pump pulse energy. The interaction length (l_i) was <100mm and the Rayleigh range (l_R) was <2mm, both short relative to the coherence length (l_c > 3m). The threshold for the onset of an SBS return was ~2mJ. A reflectivity of up to 94%[4] was obtained when operating greater than ~10 times above threshold (see Figure 3.8). The maximum fluctuation in reflectivity when operating well above threshold was ~4%. The figure also shows the typical characteristics of SBS reflectivity: the threshold, followed by a sharp rise, which levels off to saturation. The corresponding time-integrated phase fidelity versus laser pulse energy is shown in Figure 3.9. For long coherence length pump it can be seen that an excellent fidelity of $90 \pm 7\%$ was achieved.

The results from this experiment are in contrast to some results reported showing large shot-to-shot fluctuations in phase fidelity when the SBS threshold was greatly exceeded [1]. Ottusch et al [1] suggested that the cause of the phase fidelity degradation is connected with a reduced spatial mode discrimination for SBS in the saturation regime. However, in that work, it is important to note that the laser-amplifier system, used to generate the input laser pulses, incorporated an SBS mirror. The threshold turn-on characteristics of such a mirror combined with gain saturation in the amplifier would generate a pulse with a steep leading edge. Therefore, although the pulse width was

[4] Refer to Section 3.2.3 for description of SBS reflectivity diagnostic.

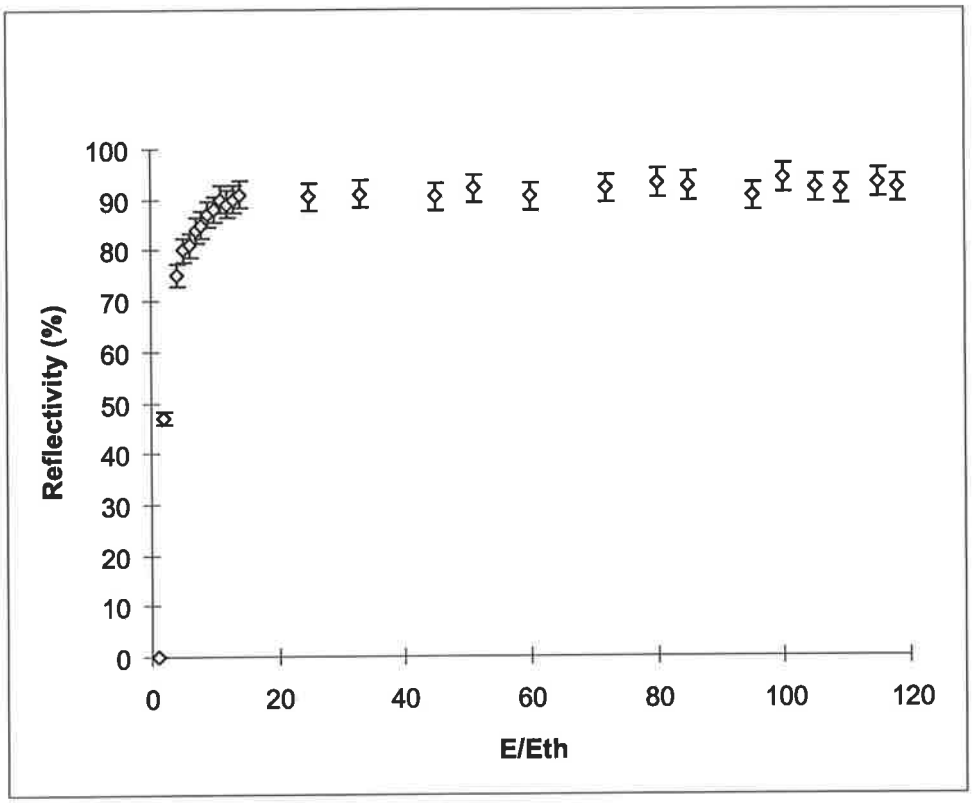

Figure 3.8 Reflectivity vs E/Eth for long coherence length pumping.

Eth ~ 2 mJ

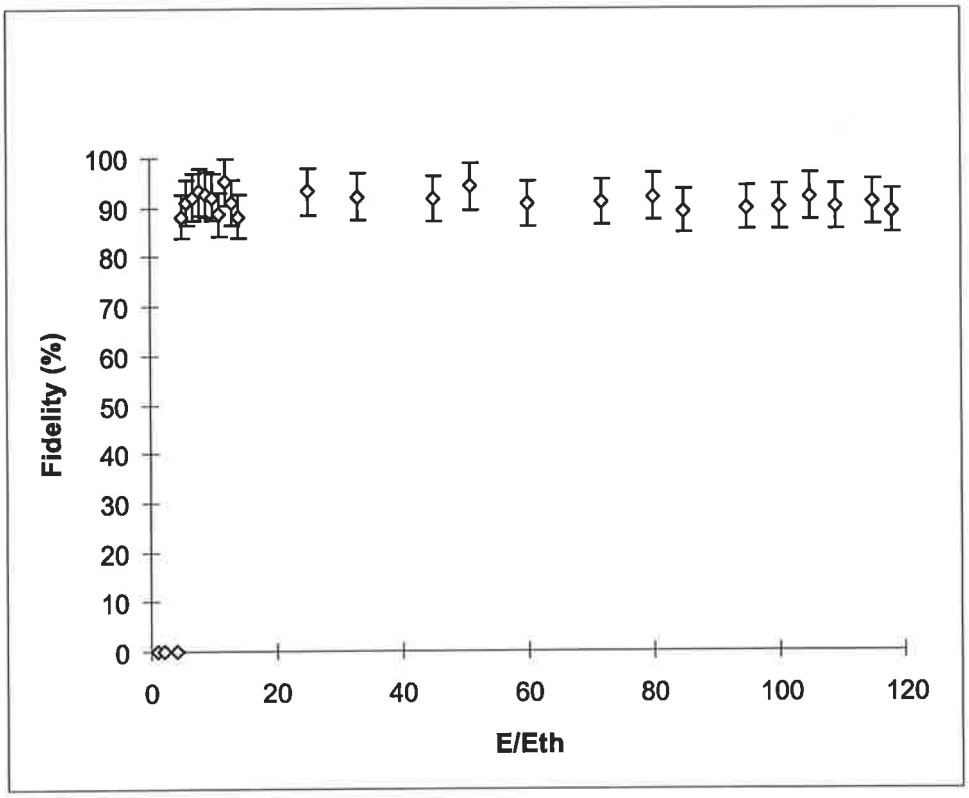

Figure 3.9 Phase fidelity vs E/Eth for long coherence length pumping.

Eth ~ 2 mJ

longer than the acoustic lifetime, the leading edge was shorter. It is well understood that poor phase fidelity can result from input pulse widths that are short relative to the acoustic lifetime [3]. Dane *et al* [6] have obtained experimental results that show strong fluctuations in phase fidelity when using input pulses with steep leading edges, even when the temporal width was longer than the acoustic lifetime. The results from Dane's work indicate that noise modes can be driven by a fast leading edge, even when an input pulse width that is longer than the acoustic lifetime is used. These noise modes can then compete with the Phase Conjugate mode for energy extraction over the duration of the pulse. Similar observations have also been made in measurements that show good phase fidelity up to 50 times above threshold using Freon 113 [4].

The acoustic lifetime (τ_B) for Freon-113 is 0.84ns [26]. The rise-time of the input pulses used in these experiments was ~4ns (refer to Figure 3.2(a)). Therefore, the results shown in Figure 3.9 agree with previous results [4-6] and confirm their observations that pulses with risetimes greater than τ_B do not cause phase fidelity fluctuations like those observed by Ottusch *et al* [1].

3.3.1.3 Effect of Impurities on SBS Reflectivity

Time-integrated SBS reflectivity as a function of input energy was measured for a sample of un-distilled and un-filtered Freon-113 in order to determine the effect of impurities on SBS performance.

The level of impurities in the liquid was found to degrade the SBS reflectivity and the phase fidelity of the Stokes return beam. Figure 3.10 shows the SBS reflectivity curve obtained under the same conditions as above, but using un-purified Freon-113. Whilst the maximum reflectivity reduced from 94% (purified) to ~50% (un-purified), the fluctuations in the reflectivity (well above threshold) increased from 4% (purified) to 20% (un-purified). The threshold energy also increased from ~2mJ to ~4mJ.

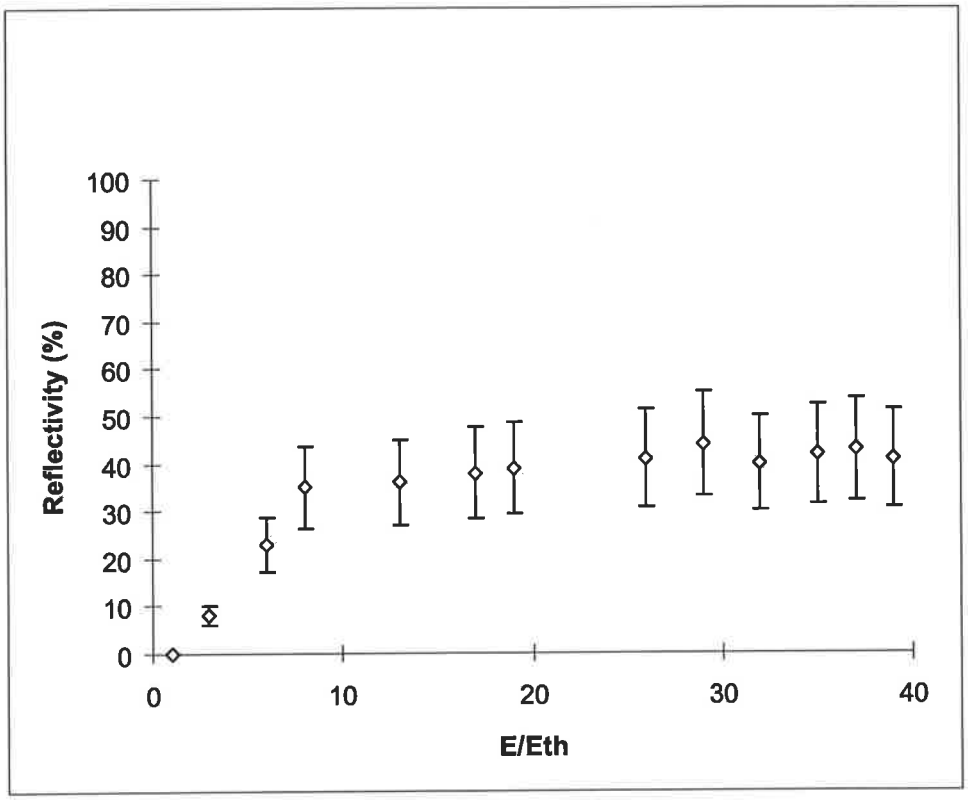

Figure 3.10 Reflectivity vs E/Eth for long coherence length (Freon with impurities).

Eth ~ 4mJ

Optical breakdown (OBD) was observed in the SBS cell for almost every laser pulse.

In this experiment, a considerable reduction in the OBD threshold with increasing dissolved and suspended impurities was observed. A measurement of the approximate OBD threshold for our un-purified and purified samples of Freon-113 was made using the long coherence length pump laser. For purified Freon-113, the OBD threshold was ~600mJ in 10ns FWHM with a 10cm focal length lens ($P_{purified}$(OBD) ~ 67GW/cm^2). For un-purified Freon-113, the OBD threshold was reduced to ~4mJ in 10ns FWHM with a 10cm focal length lens ($P_{un\text{-}purified}$(OBD) ~ 0.4GW/cm^2). A more complete description of optical breakdown will be presented in Section 3.3.2.

It has been found in other experiments that contaminants in the SBS medium tend to lower the optical breakdown threshold, because most contaminants have lower ionization thresholds than the pure molecules of the SBS medium [34]. Therefore, most contaminants are much more readily ionizable, and consequently generate many more free electrons per unit optical flux than would be generated in the pure SBS medium.

3.3.1.4 Time-resolved Measurements of Intensity Fluctuations

The objective of this experiment was to investigate the temporal intensity fluctuations present in the backscattered Stokes beam that were not present in the laser pump. Time-resolved measurements of the laser pump, and Stokes return, as well as the corresponding SBS reflectivity and phase fidelity, were carried out to identify and study the temporal intensity fluctuations.

Figure 3.11 displays time-resolved measurements of the near field (NF) and far field (FF) pulses for the laser pump pulse and corresponding backscattered Stokes pulse, using the set-up shown in Figure 3.3. The parameters used were a long coherence

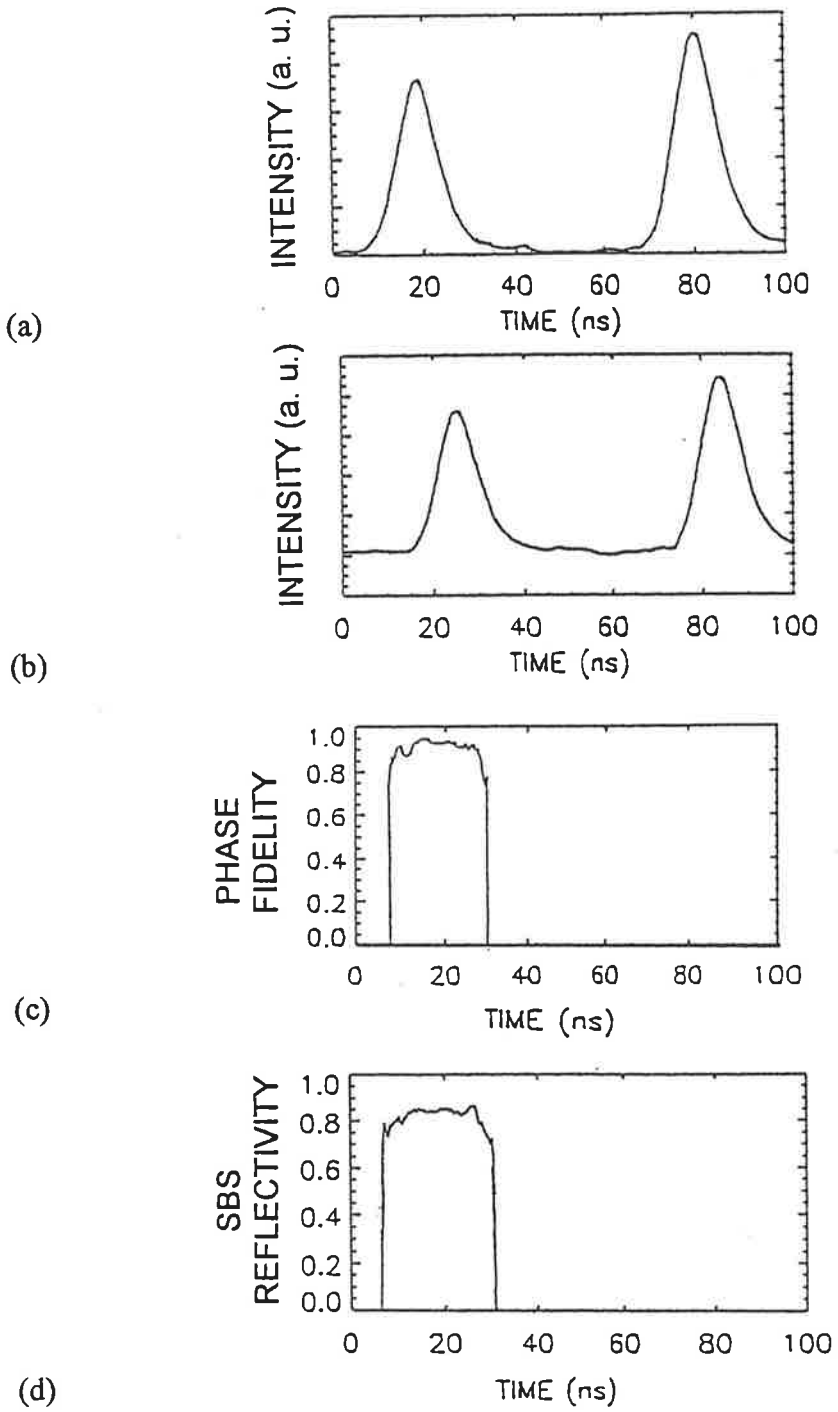

Figure 3.11 Near field and Far field temporal profiles demonstrating high phase fidelity.

(a) NF (right) & FF (left) of laser pulse,

(b) NF (right) & FF (left) of Stokes pulse,

(c) Phase fidelity vs time

(d) SBS Reflectivity vs time

length (l_c > 3m), short interaction length (l_i < 100mm), and short Rayleigh range (l_R < 2mm). These results demonstrate good phase fidelity where the temporal profile of the Stokes beam (both in the NF and FF) reproduces that of the laser pump. Note that the relative intensities of the NF and FF traces in Figure 3.11 are arbitrary.

Two forms of intensity fluctuations were observed in the Stokes return beam. Figure 3.12 shows an example of the first type. These results were obtained with l_c > 3m, l_i > 170mm, and l_R > 5mm. This intensity fluctuation always occurred on the leading edge of the Stokes return temporal profile, and its magnitude (relative to the rest of the pulse) was dependent on the focusing conditions as well as the input energy.

Figure 3.13 displays a comparison of Stokes returns for different focusing depths. The focusing depth is the distance between the SBS lens focal waist, and the front window of the SBS cell. When the focusing depth was less than a few centimetres no apparent fluctuation was measured. However, as the focusing depth increased, the amplitude of the intensity fluctuation increased, and the rise-time of the Stokes temporal profile decreased. It was also observed that the time taken to reach the first peak of the fluctuation increased slightly from ~0.8ns to ~1.2ns as the focusing depth increased.

A reduction in the amplitude of the fluctuation with increasing input energies was measured. The magnitude and position of this intensity fluctuation was very reproducible from shot-to-shot. No degradation in time-resolved phase fidelity was observed during these intensity fluctuations. Intensity fluctuations similar to these have been reported previously [35,36]. The temporal re-shaping of the Stokes return under these operating conditions is a result of strong saturation of the pump wave by the leading edge of the counter-propagating Stokes wave, resulting in considerable amplification [36]. The efficiency or magnitude of this interaction is strongly influenced by the portion of the input pulse that is transmitted through the cell before

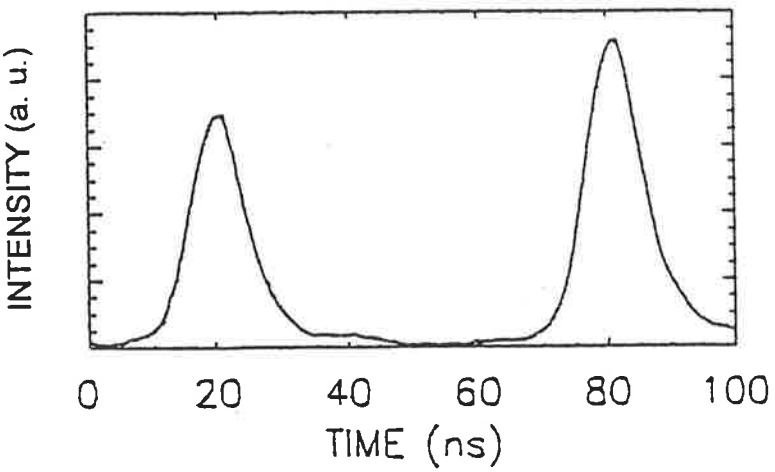

(a)

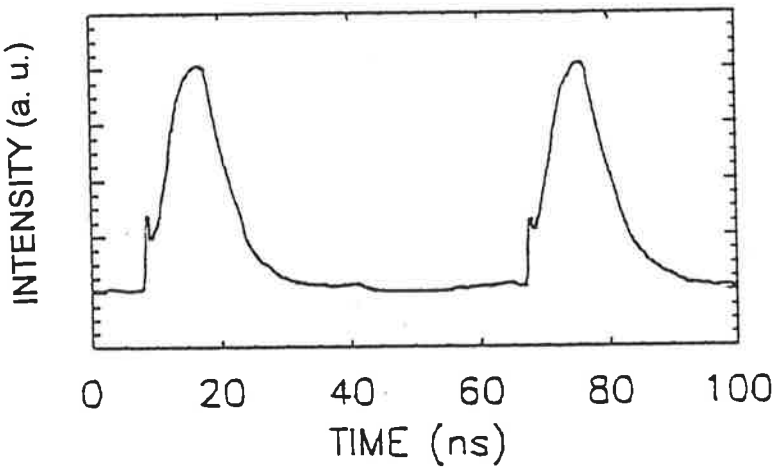

(b)

Figure 3.12 Near field (right) and Far field (left) temporal pulses showing an intensity fluctuation associated with the strong saturation of the input pulse by the Stokes return pulse.

(a) Laser pulse,

(b) Stokes pulse.

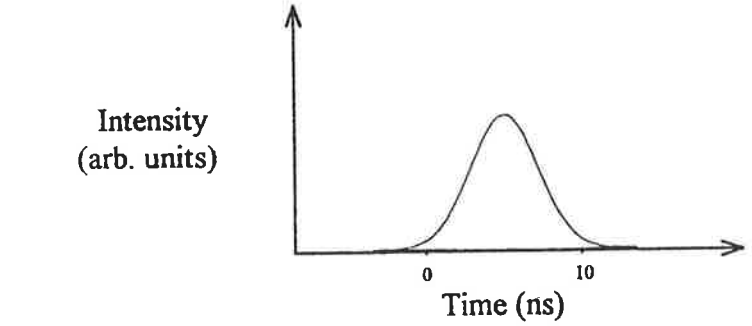

(a)

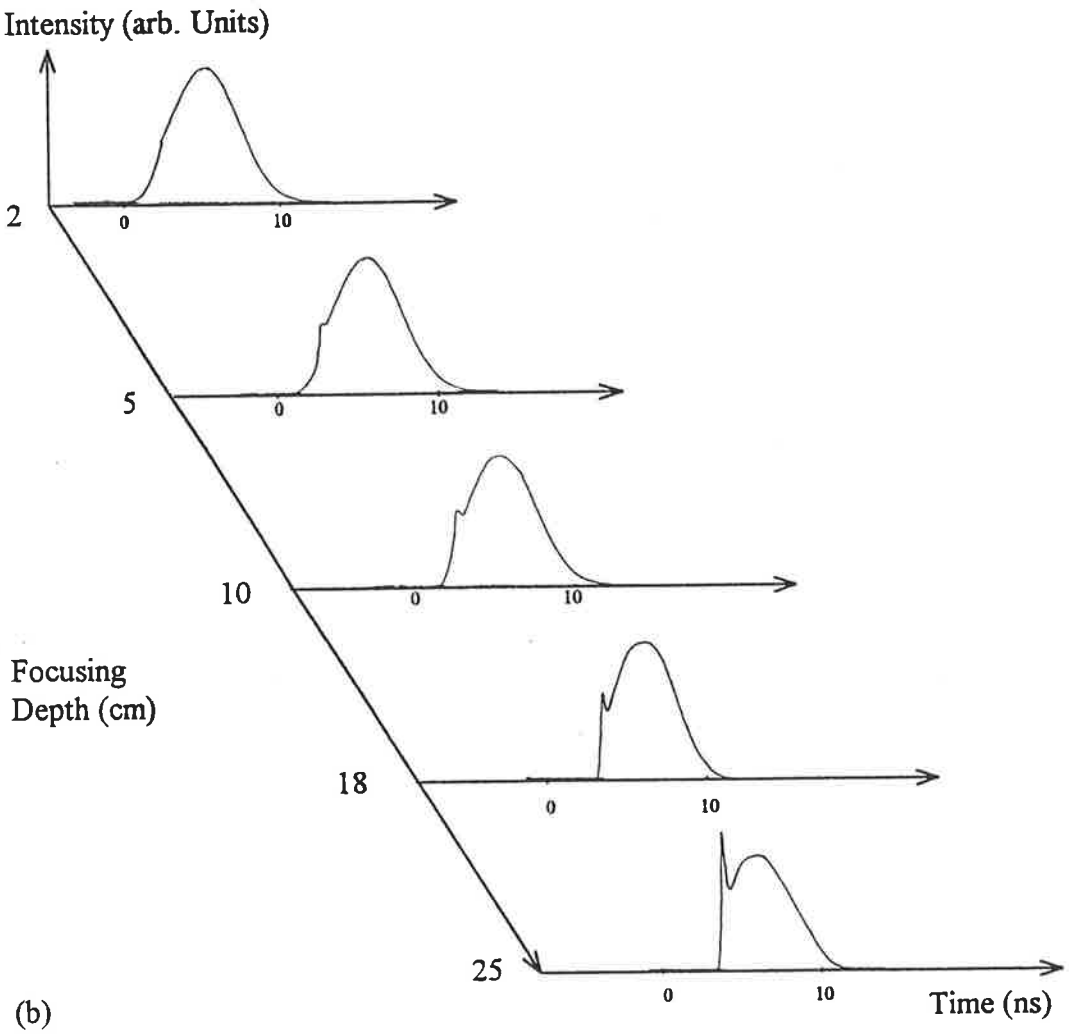

(b)

Figure 3.13 (a) Near field temporal profile of laser input pulse,

(b) Near field temporal profiles of Stokes returns for different focusing depths.

SBS threshold is reached [36]. That is, the fluctuation begins as soon as the SBS threshold is reached. The portion of the input pulse that is involved in this interaction becomes greater with increasing focusing depth (interaction length). Therefore, the saturation of the input pump by the leading edge of the Stokes pulse starts when SBS threshold is reached, and only lasts the time it takes the Stokes return to propagate to the front entrance of the SBS cell. In this experiment, the pulse length was 10ns (~3metres in length) whereas the propagation time varied between 100ps (3cm in length) and 1ns (30cm in length). For higher input energies, SBS threshold is reached closer to the front window thereby reducing the transient interaction time between the leading edge of the Stokes pulse and the input pulse. This results in a decrease in the amplitude of the intensity fluctuation at higher input pump energies. This description is consistent with the position and duration of the fluctuations measured experimentally in this study. Once the compressed portion of the pulse has exited the SBS cell, the intense acoustic wave formed by the pump/Stokes interaction relaxes back within a phonon lifetime (~0.84ns for Freon-113). This results in the relaxation oscillation that appears directly after the peak of the fluctuation. No degradation in time-resolved phase fidelity was observed during these intensity fluctuations, presumably because the entire Stokes return was generated within the interaction length and therefore, coherent phase conjugation would have occurred. The Stokes pulses measured in this work are examples of inefficient pulse compression due to the shortness of the SBS cells and focal lengths used. Many studies optimizing pulse compression of high energy input pulses have been previously reported[5].

Figure 3.14 shows an example of the second type of intensity fluctuation observed in the Stokes pulse. The results in Figure 3.14 were obtained with a long coherence length (l_c > 3m), long interaction length (l_i > 190mm), and long Rayleigh range (2mm<l_R<22mm). This figure shows that although there are no intensity fluctuations in the input laser pulse, intensity fluctuations were observed in the near field and far field

[5] Refer to page 8 of this thesis where several references discussing pulse compression are given.

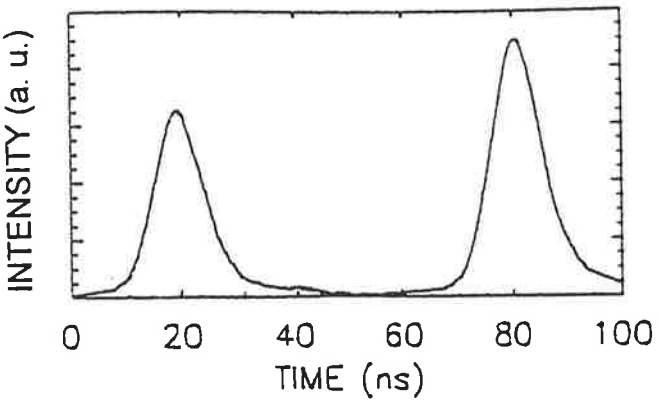

(a)

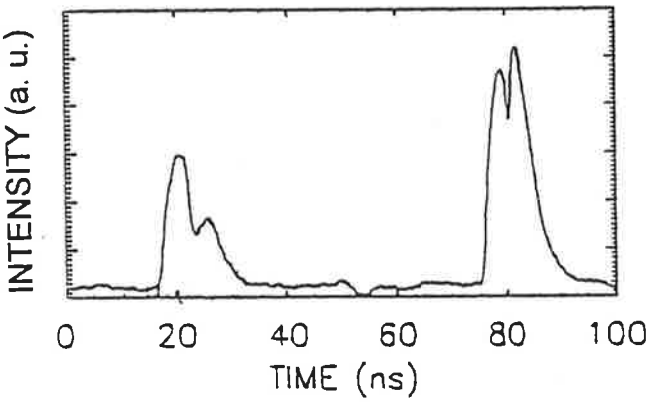

(b)

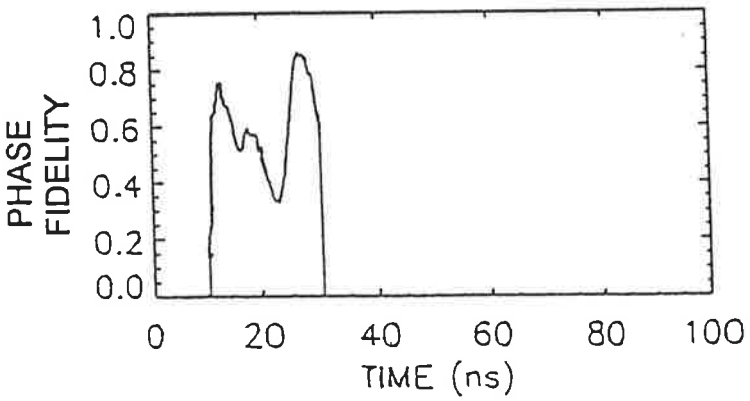

(c)

Figure 3.14 Near field and Far field temporal pulses showing an intensity fluctuation associated with a phase fluctuation.

(a) NF (right) & FF (left) of laser pulse,

(b) NF (right) & FF (left) of Stokes pulse,

(c) Phase fidelity vs time.

of the Stokes return. A reduction in phase fidelity was also observed, corresponding in time with the intensity fluctuation. The percentage of Stokes pulses which contained these temporal intensity fluctuations was typically one pulse in ten. However, this percentage was found experimentally to be dependent on the SBS focusing geometry, as will be discussed later in this section.

Usually only one intensity fluctuation was ever observed on a single pulse, and occurred randomly along the temporal profile of the pulse. The fluctuation starts with a decrease in intensity to a minimum value, then an increase reaching a maximum, followed by another decrease down to the normal intensity without fluctuation. The magnitude of the fluctuations was observed to be almost independent of the input pulse energy (except at very high energies where the number and amplitude of these fluctuations reduced significantly).

The origin of these intensity fluctuations was studied experimentally in another thesis [37], using the heterodyne detection diagnostic as described in Section 3.2.4. From that research it was found that pulses showing intensity fluctuations also had phase jumps associated with them. The same work found the magnitude of the phase jump was directly related to the amplitude of the intensity fluctuation.

Similar phase jumps have previously been predicted [12] and measured [13]. It has been reported that the amplitude of the observed Stokes fluctuation reduces with increasing pump intensity, but becomes greater with increasing interaction length [11,12,37]. In particular, Gaeta et al [38] found that the amplitude of the intensity fluctuations was suppressed for increased energy and short focal length SBS lenses.

A number of research studies have identified the interaction length (distance from the front window of the SBS cell to the focal waist) as being a critical parameter for controlling these intensity fluctuations [11,12,37,39]. A time of propagation parameter

(τ_{prop}) has been reported to define the regime under which these intensity fluctuations may occur. τ_{prop} is the time taken for the input laser pulse to travel from the front window of the SBS cell to the focal plane of the SBS lens,

$$\tau_{prop} = \frac{n l_i}{c} \tag{3.1}$$

where n is the refractive index of the SBS material, and c is the speed of light in air. Devrelis [37] found that when the propagation time (τ_{prop}) was experimentally made smaller than the phonon lifetime (τ_B) of the SBS material, the amplitude of the fluctuations were close to zero, whereas for $\tau_{prop} > \tau_B$ the amplitude of the fluctuations increased. With increasing input energies, the SBS threshold is reached closer to the front window of the SBS cell, thereby reducing the propagation time below the phonon lifetime. This is consistent with observations, made in this experiment, of a reduction in intensity fluctuations at high input energies. Using condition 3.1, for Freon-113 (n=1.36, τ_B=0.84ns), intensity fluctuations associated with phase jumps may be observed when using a SBS lens of focal length >185mm.

Several studies have used optical feedback techniques to reduce the SBS threshold and to eliminate temporal fluctuations due to phase jumps [40-44]. Scott *et al* [40-42] have theoretically and experimentally described a loop scheme where the laser input (duration: 200nsec - 1μsec) is fed back into the SBS medium so that it overlaps with itself near the focal plane where it writes an acoustic grating via 4-wave-mixing. After the initiation of SBS via spontaneous noise, the acoustic grating is rapidly amplified by the loop scheme feedback. This results in a lower SBS threshold. Dane *et al* [43] later used this loop scheme to eliminate temporal fluctuations due to phase jumps. As the acoustic field is continuously seeded over the entire length of the input pulse, phase jumps resulting from fluctuations in the spontaneous noise do not effect the reflectivity and phase fidelity of the SBS process. Recently, the results of Scott *et al* [40], and Dane

et al [43] have been confirmed experimentally by Devrelis [37] using laser pulses with durations of ~10nsec.

3.3.2 Short Coherence Length Pumping

The aim of this section is to study and characterize the effect of a short coherence length pump on Optical Phase Conjugation via SBS.

Results from this work relating to SBS reflectivity and phase fidelity, as well as observations of the competing effects with a short coherence length pump are presented and discussed. Shot-to-shot measurements of the pump coherence length used to characterize the SBS input conditions are also presented.

3.3.2.1 Shot-to-shot Coherence Length Measurement

The coherence length diagnostic as detailed in Section 3.2.5 was used to measure the coherence length of the input pump in real time [24]. Typical examples of long (injection seeded) and short (no axial mode control) coherence length fringe patterns are shown in Figure 3.15. The uneven intensity distribution is due to transverse variations in the intensity of the two interfering beams, $I_1(x,y)$ and $I_2(x,y)$. This unevenness, together with the high contrast of the images seen in Figure 3.15, tends to mask the envelope of the interference fringes used for real time observation of the coherence length. However, on a TV monitor, it was readily observable. Plots of the normalized interference pattern $1+V(l)\cos kx$ (where $V(l)$ is the visibility), for the data shown in Figure 3.15, are shown in Figure 3.16. In this figure, the envelope of the interference pattern is the mutual coherence function. The coherence length is defined as the path length difference required to reduce the visibility by a factor of two as compared to the path matched condition [22,45]. From this experiment, the coherence length of the multi-mode pulse was found to be 17mm (bandwidth - 18GHz), while the

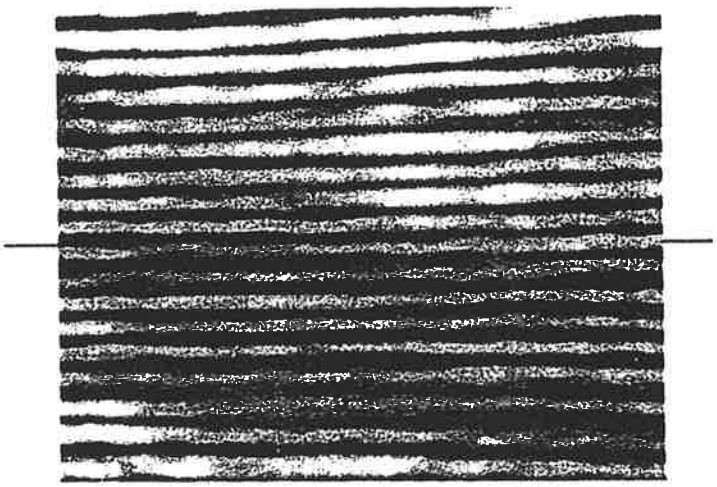

(a)

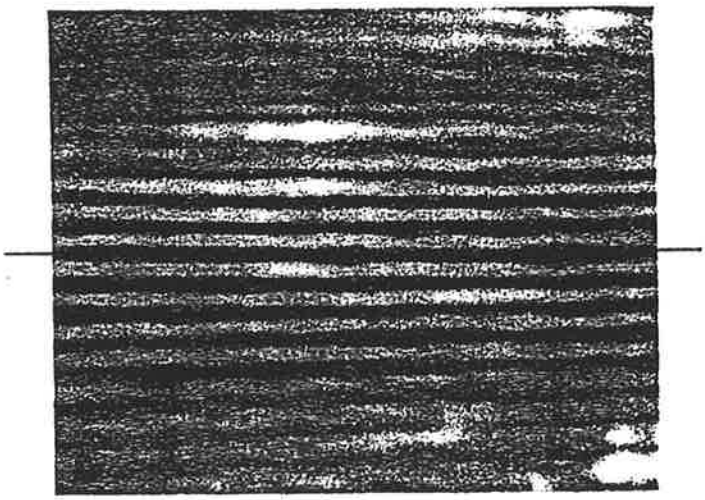

(b)

Figure 3.15 Interference fringes observed on the TV monitor (a) Long Coherence length, (b) Short Coherence length. The horizontal center line on each figure corresponds to path-matched interference. Above the center line corresponds to shorter paths, and below the center line corresponds to longer paths.

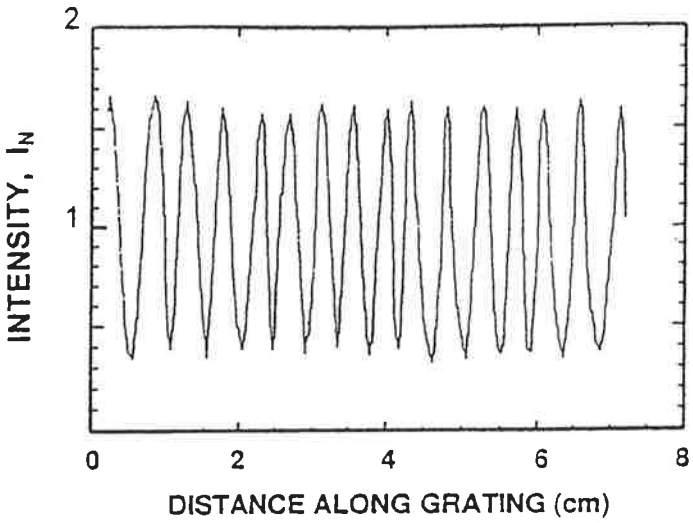

(a)

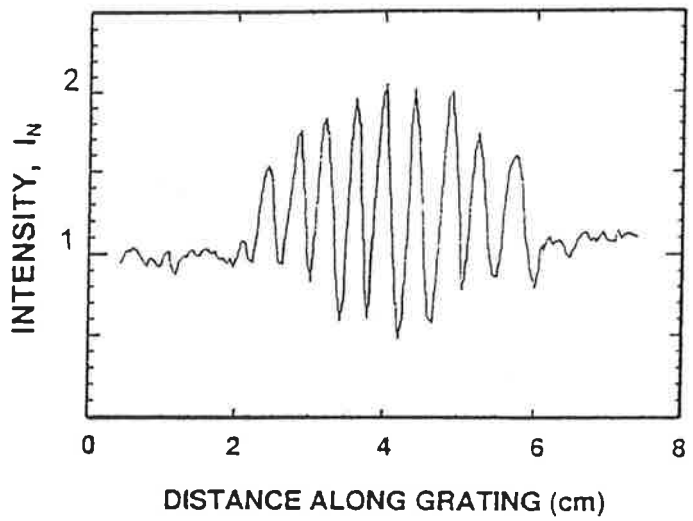

(b)

Figure 3.16 Normalized intensity distributions obtained from a single column of the digitized frame showing the resulting fringe visibility as a function of path-length difference along the grating for the interferograms shown in Figure 3.15. (a) Long coherence length, (b) Short coherence length.

coherence length of the injection seeded pulse exceeded the maximum length measurable (> 0.4m). In a separate experiment the long coherence length was determined to be 3m (linewidth - 100MHz). Therefore, as the pump bandwidth of the multi-mode pulse is significantly higher than the phonon decay rate (Γ~1.8GHz), broadband SBS pumping conditions will occur.

3.3.2.2 Time-integrated SBS Reflectivity and Phase Fidelity

The objective of this section is to characterize OPC via SBS under short coherence length conditions. The approach taken was to measure time-integrated SBS reflectivity and phase fidelity, described in Section 3.2.3, as a function of pump pulse energy and pulse repetition frequency.

With the experiment set-up as discussed in Section 3.2, the SBS reflectivity of the purified Freon-113 was measured as a function of pump pulse energy (see Figure 3.17). The experimental parameters for this data include an input pump bandwidth ~18GHz (l_c~17mm), an interaction length ~140mm and a Rayleigh range <3mm. The results shown in Figure 3.17 were taken for pulse repetition frequencies (PRF) of 2Hz and 15Hz. In this case, the SBS threshold energy was ~4mJ (compared with ~2mJ for long coherence length pumping). The maximum reflectivity obtained was 50% at 2Hz and only 10% at 15Hz (compared with 94% - long coherence length). Note also the large fluctuations in reflectivity at all energies.

This experiment was performed with other pulse repetition frequencies. The results for PRF's between single shot and 2Hz operation gave the same magnitude and fluctuation in SBS reflectivity as the 2Hz PRF results shown in Figure 3.17. At PRF's greater than ~4Hz, the time-integrated SBS reflectivity degraded with increasing PRF. At 15Hz PRF the first pulse gave an SBS reflectivity similar to that obtained for single shot operation, whereas the pulses that followed resulted in considerably lower reflectivity.

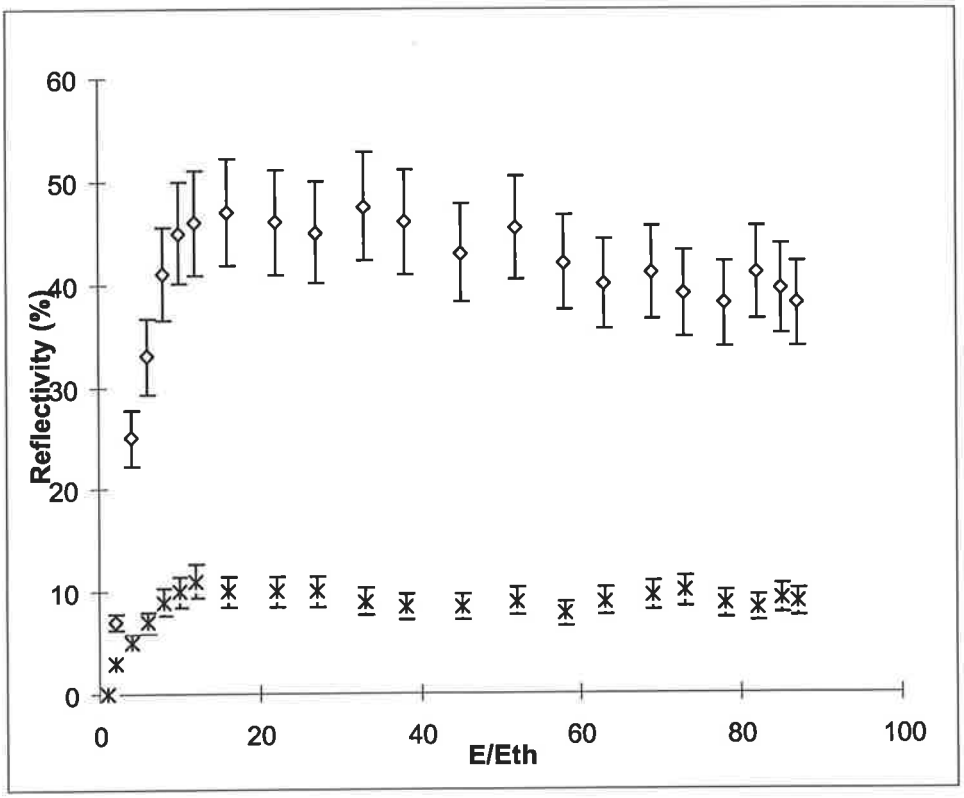

Figure 3.17 Reflectivity vs E/Eth for short coherence length pumping. Eth ~ 4mJ.
◊ - 2Hz PRF,
x - 15Hz PRF.

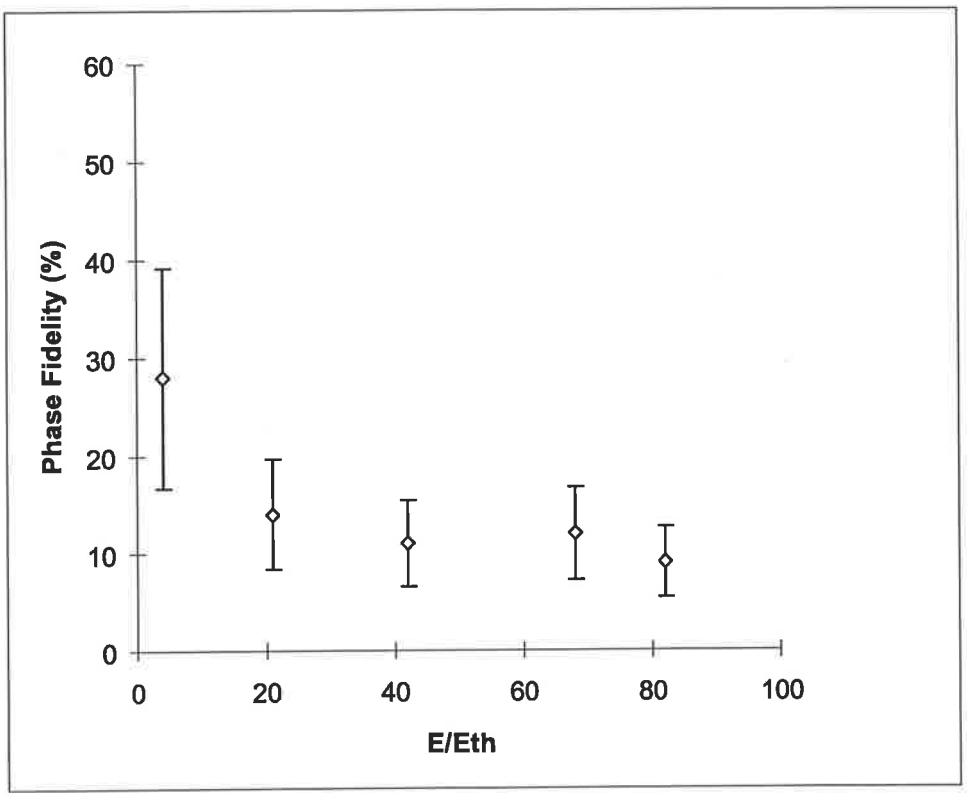

Figure 3.18 Phase fidelity vs E/Eth for short coherence length pumping. Eth ~ 4mJ

Figure 3.18 shows the corresponding phase fidelity as a function of input energy above threshold, for SBS with short coherence length pumping at 2Hz PRF. It can be seen that the phase fidelity just above threshold is higher, but more variable, than when well above threshold.

Between single shot and ~4Hz PRF operation, erratic visible signs of optical breakdown (OBD) were observed at, and in front of the focal waist at lower input energies (i.e. E/Eth ≤4). At higher energies, visible signs of OBD were observed on every pulse. The intensity of the spark/s, the number of sparks per input pulse, and their physical extent along the beam path became greater with increasing input energy. At 15Hz PRF operation, visible signs of OBD were seen on every pulse with input energies above threshold and in greater magnitude and extent than for the 2Hz PRF operation. Filaments of plasma extending along the beam path in the focal volume were also observed. Although the occurrence of these filaments was erratic, their number and magnitude increased with increasing input pulse energy.

In Figure 3.2(b) it was shown that the input pump pulse used in these experiments contained high amplitude modulations forming many very short pulses, each with very high peak power. It is known that the occurrence of competing effects to SBS, such as stimulated Raman scattering, self-focusing and optical heating become greater with increasing input peak power [46]. Also, some competing effects respond to input intensity modulations on time scales considerably shorter than that for SBS [47]. On account of their quicker response times, these competing effects can achieve higher gain compared with that for SBS when intensity modulations are present in the input pump [19,46]. The major competing effect observed in these experiments was optical breakdown (OBD) in the form of visible plasma sparks, and extended filaments in the focal volume. OBD has been observed during many other SBS experiments [31,49,50,52,54]. Breakdown results in the massive ionization of gas being created in the focal volume within a few nanoseconds [61] and therefore, the effectiveness of the

focal region for PC-SBS becomes significantly degraded. The OBD effect can extend itself in the form of a shock wave that can move faster than the speed of sound [14, 58].

There are three important frequency scales which need to be considered for broadband SBS experiments: the SBS decay rate or Brillouin linewidth (Γ), the pump bandwidth ($\Delta\nu_P$), and the speed of light divided by the interaction length (c/l_i) [14,17]. Narrow bandwidth SBS occurs when the pump bandwidth is smaller than the Brillouin linewidth, as described in previous sections of this chapter. When $\Delta\nu_P > \Gamma$, which is the case in this present experiment, the magnitude of the broadband SBS gain depends on the magnitudes of the laser coherence length and the SBS interaction length [14,17].

Mullen *et al* [17] used a dual spectral-line pump whose line separation was variable between 0GHz to 4.4GHz to investigate broadband SBS. A significant drop in reflectivity was measured when the interaction length (l_i) for SBS was longer than the pump coherence length (l_c). This drop was attributed to the fact that when $l_i > l_c$, the effective interaction length, and therefore SBS gain was reduced. In Mullen's study [17], with a focused geometry, the effective interaction length was the shorter of the coherence length or the Rayleigh range. Narum *et al* [19] also found that the SBS reflectivity was independent of the number of input pump modes when $l_i < l_c$, and the laser mode separation was larger than the spontaneous Brillouin linewidth. Munch *et al* [15] found that at the steady-state SBS threshold, the effective interaction length was the shorter of the following parameters: the cell length, 3 times the coherence length, or 5 times the Rayleigh range. In addition, results by Fillippo et al [46] showed that there was no difference in broadband pumping compared with narrowband pumping as far as the gain coefficient is concerned for interaction lengths up to 16 x l_c. In our experiments, the Rayleigh ranges studied were all less than the pump coherence length (17mm), and the SBS cell length was ~7 times the coherence length. Therefore, following the conditions derived from Valley [14], Mullen [17], Munch [15] and Narum [19], the parameters used in this present experiment should result in achieving a

broadband SBS gain that is nearly equal to the narrowband gain (ie. SBS reflectivity for our broadband pumping comparable to our narrowband pumping results). However, this was not found to be the case.

Another study examined broadband SBS phase fidelity with input pumps at 28 and 45GHz linewidth [48]. High phase fidelity was measured for the 28GHz input pump with f/36 and f/90. Good conjugation fidelity occurred, despite the fact that the coherence length used was smaller than the interaction length. However, for the 45GHz linewidth pump, poor phase fidelity was measured. A significant difference in the two input pumps was their temporal modulations. The 28GHz pump had a temporally smooth profile whereas the 45GHz pump had a highly amplitude modulated temporal profile compared with the phonon lifetime. Lefebvre *et al* [48] concluded that the temporal modulations on the input pulse led to a transient response in developing the conjugate return resulting in low SBS reflectivity. It has been reported that poor wavefront reversal can result from input pulse widths that are short relative to the decay time (τ_B) in the SBS medium [3,14]. Under these conditions, the acoustic grating can not respond to temporal modulations that occur on time scales shorter than τ_B [14]. The temporal modulations in the input pulses used in this experiment (see Figure 3.2(b)) varied on time scales <1ns which is comparable with the SBS phonon lifetime (τ_B=0.84ns) for Freon-113. Other studies have demonstrated high SBS reflectivity and phase fidelity for broadband SBS using input pulses with temporal modulations that vary slowly compared with the phonon decay time [15,46].

The degradation in reflectivity and phase fidelity shown in Figures 3.17 and 3.18 may also be due to the very high intensities in the focal volume causing competing effects such as optical breakdown (OBD) that were observed in the SBS cell. OBD, as well as other competing effects, have been observed during the SBS process in many other studies [49,50,52], and are the topic of the following section.

3.3.2.3 Competing Effects

In the previous section, poor SBS reflectivity and phase fidelity were obtained even though focusing conditions ($l_c > l_i$) were set-up in order to achieve high SBS gain. A significant contribution in obtaining this result was the optical breakdown (OBD) observed in, and in front of the focal region inside the SBS cell.

The aim of this section is to study in greater detail the competing effects observed in our present experiments, and examine their effect on the SBS gain and Optical Phase Conjugation.

Optical Breakdown:

Optical breakdown usually initiates when one or more electrons are freed from an atom or molecule when the laser radiation is sufficiently intense (multi-photon absorption). The ionization of the medium can lead to the formation of a high temperature opaque plasma. This absorbing plasma can form in less than 1ns [52], expand and produce a visible spark, sound, and bubble formation [51,53]. Avalanche ionization can follow from multi-photon absorption and takes as little as a few tens of picoseconds to produce breakdown effects [54].

Figure 3.19 shows several typical optical breakdown events observed during this present experiment. Using a CCD camera, the spatial extent of the plasma sparks was measured and found to vary between ~100μm and a few millimetres. Multiple OBD sparks sometimes linked by a thin plasma filament were often observed (see Figure 4.19(b)). When multiple OBD occurred, it was found that OBD generation initiated at the focus, and progressively occurred in the backward direction towards the front window of the SBS cell.

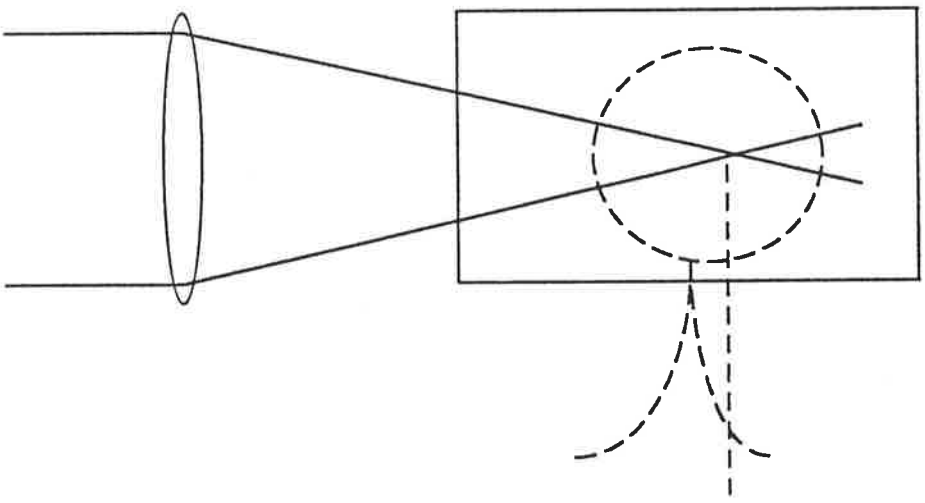

(a)

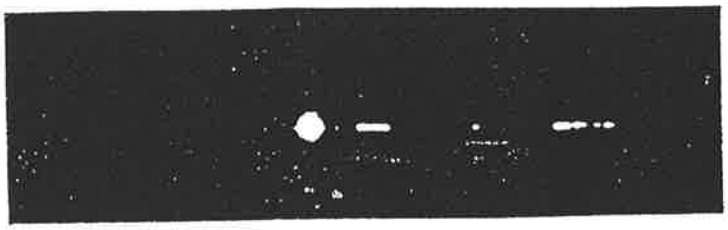

(b)

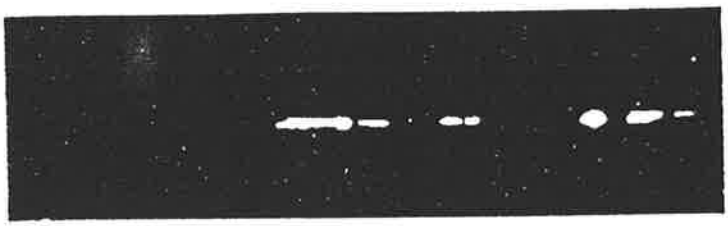

Figure 3.19 CCD images of the confocal region inside the SBS cell showing typical examples of optical breakdown.

Using a fast silicon-avalanche photodiode[6], the temporal extent of the visible sparking event was measured to exceed the laser pulse duration and sometimes lasted up to 10ms.

As described in Section 3.3.1, other studies have found that opaque sparks formed near the focal region can prevent the laser radiation from propagating through the interaction length, resulting in poor reflectivity and phase fidelity [7,31,48]. Teslenko [55] found that for the multiple OBD case, the sparks were progressively formed in the same direction as in this present experiment (ie. starting at the focus and moving closer to the front SBS cell window). In Section 3.3.1, relatively large particulate impurities (size >2μm) were observed to lower the breakdown threshold. In this case, using purified Freon-113, it is proposed that the rapidly varying, extremely high electric fields associated with the multi-mode pumping laser beam result in peak powers that reach the breakdown threshold [18]. OBD can cause the creation of new chemical species through a dissociation process. This can increase optical absorption and lower the breakdown threshold. During this present experiment, a degradation in the SBS reflectivity and an increased amount of OBD was observed over several months of operation (with short coherence length pumping). The purity of the SBS medium was found to be essential for OPC via SBS. Every attempt was made in our experiments to continually purify our Freon-113 SBS samples (see Section 3.2.6).

From Figure 3.17, it can be seen that the SBS reflectivity reduces with increasing pulse repetition rate. It was observed that for a train of pulses (PRF >8Hz) allowed to enter the SBS cell, usually only the first pulse had relatively good reflectivity and fidelity. It has been reported that OBD and sparks can result in a shock wave forming, which propagates through the medium faster than the speed of sound [14,58]. As a result of OBD, the vibration and disturbance effects on time scales of 100's of milliseconds, was believed to be responsible for the decrease in reflectivity at higher pulse repetition

[6] Newport 877

frequencies. This reduction in reflectivity with increasing PRF when using short coherence length pumping has been reported in previous studies [34].

Bubble Formation:

The presence of sub-micron particles or dissolved impurities with higher absorption than the pure SBS liquid can initiate the creation of bubbles [60]. Under high peak power conditions, these impurities can absorb radiation and begin to ionize and conduct energy to the surrounding liquid. As the surface temperature exceeds the boiling temperature of the liquid (~47° for Freon-113), a bubble of hot gas forms around the plasma / ionized particle.

In this experiment, using a CCD camera, a cavitation bubble was always detected whenever optical breakdown was observed. Figure 3.20 shows an example of the cavitation bubbles formed. The bubbles can be more easily identified in the CCD image due to the scattering of the visible light generated by the plasma. These bubbles were observed to rise to the top of the SBS cell and form a small pocket of gas. Using a sequence of CCD images, the lifetime of the bubbles was measured to vary between one and a few hundred milliseconds. The bubble generation followed that of the plasma. They were created initially near the focus and then progressively towards the front window of the SBS cell all within a pulse duration time period. These observations can be explained by the self-focusing of the input beam in the SBS medium. For the experimental parameters used in this study, the self-focusing threshold was ~3 times the SBS threshold [55-58]. The intensity at the waist of the SBS lens rises quickly as the input laser beam propagates through the region. As laser beams are typically more intense at the centre than at the edge, the beam slows at the centre and consequently converges. Due to this intensity induced index change, the laser beam collapses towards the front of the cell forming a damage track consisting of breakdown

sparks extending along a single filament[7]. Similar self-focusing observations have been reported in SBS with high pressure gases [57]. In that study, by comparing the electrostrictive self-focalisation threshold with the SBS threshold, the transient self-focusing was found to be due to the electrostrictive effect. Other studies have also observed rapidly expanding cavitation bubbles reaching ~400μm after ~200ns [59].

[7] Other mechanisms that result in intensity dependent changes to the refractive index include the Kerr effect, and electronic polarizability [58].

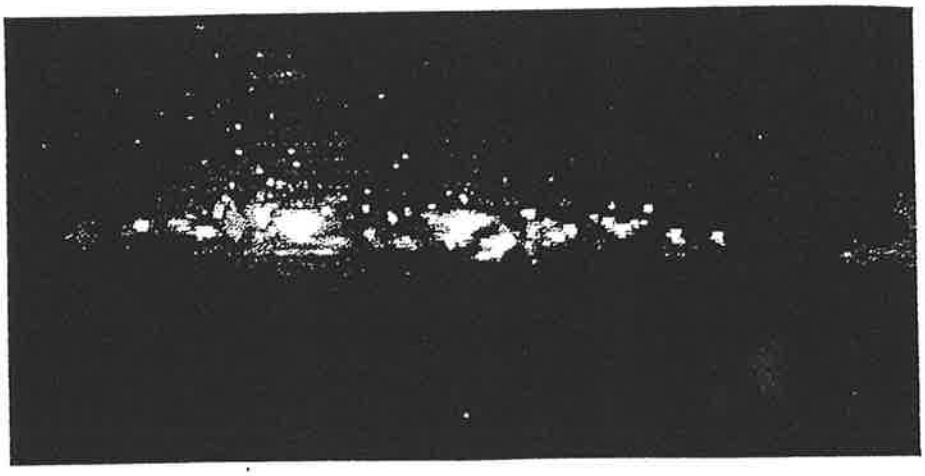

Figure 3.20 CCD image of the confocal region inside the SBS cell showing the typical formation of cavitation bubbles.

3.4 Summary

A heterodyne detection scheme was used to measure the frequency shift of Freon-113. The measured value of 1.8±0.1GHz indicates a good agreement with previously reported values.

Time-integrated measurements of SBS reflectivity and phase fidelity were performed using a long coherence length pump at various input energies. In the saturated regime (energy well above threshold), an SBS reflectivity of ~94% and phase fidelity of 90% were measured, with liquid Freon-113 as the SBS medium. No significant shot-to-shot variations in the phase fidelity were observed at high energies.

Impurities were found to lower the breakdown threshold. With an un-purified sample of liquid Freon-113, an optical breakdown (OBD) threshold of ~0.4GW/cm^2 was recorded. This can be compared with the increased value of ~67GW/cm^2 obtained when the sample had been purified. With further purification it may be possible to increase the threshold for OBD closer to the limit for the Freon-113 molecules.

Time-resolved measurements of the long coherence length input pump and Stokes return, as well as the SBS reflectivity and phase fidelity were carried out. Although good temporal phase fidelity was observed in most cases, intensity fluctuations in the Stokes return pulse were measured and categorized into two types. The first type of intensity fluctuation always occurred on the leading edge of the Stokes return pulse. Its amplitude was found to become greater with increasing focusing depth, but reduce with increasing input energy. This intensity fluctuation was not observed when short focal length lenses and high input energies were used. However, no degradation in phase fidelity was observed when this fluctuation occurred, indicating coherent SBS. The temporal re-shaping of the Stokes return was a result of the strong saturation of the

pump beam by the leading edge of the counter-propagating Stokes wave. This resulted in considerable amplification of the acoustic grating.

The second type of intensity fluctuation recorded, occurred at random times during the pulse and resulted in temporal degradation of the SBS reflectivity and phase fidelity throughout the lifetime of the fluctuation. The amplitude of the fluctuation was dependent on the propagation time[8] and was reduced at high input energies. The suppression of these fluctuations was found to depend strongly on the ratio of the propagation time to that of the phonon lifetime in the medium. Optimum suppression was observed when this ratio was reduced. This work has demonstrated the operating regimes (i.e. the focusing geometries) where the presence of phase jumps and intensity fluctuations created by spontaneous noise can be eliminated.

During this work a novel interferometer was designed that enabled shot-to-shot measurements of the complete coherence function of the input laser pulses. From these observations of the whole visibility pattern, accurate, real-time measurements of the coherence length were made.

In short coherence length pumping, the single pulse SBS reflectivity and phase fidelity were significantly degraded compared with the long coherence length pump case. A further degradation in reflectivity and phase fidelity was observed at input pump pulse repetition frequencies (PRF) greater than ~4Hz. In our experiment, the Rayleigh range was ~6 times shorter than the input coherence length. In this case, the interaction length is confined by the Rayleigh range of the SBS lens and not by the coherence length of the input. This condition, by itself, should have resulted in broadband gain close to that of the narrowband case. However, the extremely high electric fields associated with the multi-mode input pulse were sufficient to cause OBD and gas bubble formation. Also, the magnitude of these competing effects may have dominated the SBS process as they

[8] The propagation time is defined in Section 3.3.1.4 as the time taken for the input laser pulse to travel from the front window of the SBS cell to the focal plane of the SBS lens.

have quicker response times than SBS to fast temporal modulations occurring on the input pulse.

In order to avoid the interaction length being restricted by the coherence length, it is advantageous to focus the input laser beam sharply so that the Rayleigh range defines the interaction length. However, to avoid OBD, it is beneficial to use lenses with long focal lengths in order to reduce the peak intensities in the focal region. Still, in this regime, the interaction length becomes restricted by the coherence length resulting in reduced OPC-SBS gain.

The further reduction in reflectivity with increasing pulse repetition frequency (PRF) was found to be due to the long-term effects of the OBD. Although the opaque plasma spark lasts only ~10ms, the vibration and disturbance effects caused by the shock wave can last ~100ms. The observed increase in competing effects with increased PRF is a serious limitation of broadband SBS for practical applications. Preparing ultra-pure SBS samples, and operating below the OBD power threshold has been found continually during this thesis work to be essential for reliable SBS performance.

If the spatial and temporal variations in the input pump are on time scales longer than the phonon lifetime of the medium, the interaction length is shorter than the input coherence length, and the competing effects are reduced with suitable SBS geometries, then coherent, phase conjugate SBS will be obtained.

References

[1] J, J, Ottusch, and D. A. Rockwell, '*Stimulated Brillouin scattering phase-conjugation-fidelity fluctuations*', Opt. Lett. **16**, No 6, 369 (1991).

[2] A. F. Vasil'ev, and V. E. Yashin, '', Sov. J. Quant. Electron. **17**, 644 (1987).

[3] A. A. Betin, A. F. Vasil'ev, O. V. Kulagin, V. G. Manishin, and V. E. Yashin, '*Phase conjugation in nonstationary stimulated Brillouin scattering of focusing beams*', JETP Lett. **62**, 468 (1985).

[4] R. St. Pierre, H. Injeyan, and J. Berg, "Investigation of SBS phase conjugation fidelity fluctuations in Freon-113', in Conf. Lasers Electro-Optics, OSA Tech. Dig. Ser. (Opt. Soc. Amer., Washington, DC) **12**, 180 (1986).

[5] L. P. Schelonka, and C. M. Clayton, '*Effect of focal intensity on stimulated-Brillouin-scattering reflectivity and fidelity*', Opt. Lett. **13**, 42 (1988).

[6] C. B. Dane, W. A. Neuman, and L. Hackel, '*Pulse-shape dependence of stimulated-Brillouin-scattering phase-conjugation fidelity for high input energies*', Opt. Lett. **17**, No 18, 1271 (1992).

[7] C. B. Dane, L. E. Zapata, W. A. Neuman, M. A. Norton, and L. A. Hackel, 'Design and operation of a 150W near diffraction-limited laser amplifier with SBS wavefront correction', IEEE J. Quantum. Electron. **31**, No 1, 148 (1995).

[8] N. G. Basov, I. G. Zubarev, A. B. Miranov, S. I. Mikhailov, and A. Yu. Okulov, '*Phase fluctuations of the Stokes wave produced as a result of stimulated scattering of light*', JETP Lett. **31**, 645 (1980).

[9] M. V. Vasil'ev, A. L. Gyulameryan, A. V. Mamaev, V. V. Ragul'skii, P. M. Semenov, and V. G. Siderovich, '*Recording of phase fluctuations of stimulated scattered light*', JETP Lett. **31**, 634 (1980).

[10] V. I. Bespalov, A. A. Betin, G. A. Pasmanik, and A. A. Shilov, '*Observation of transient field oscillations in the radiation of stimulated Mandel'shtram-Brillouin scattering*', JETP Lett. **31**, 630 (1980).

[11] A. L. Gaeta, and R. W. Boyd, '*Stochastic dynamics of stimulated Brillouin scattering in an optical fibre*', Phys. Rev. A **44**, 3205 (1991).

[12] E. M. Dianov, A. Ya. Karasik, A. V. Lutchnikov, and A. N. Pilipetskii, '*Saturation effects at backward-stimulated scattering in the single-mode regime of interaction*', Optical and Quantum Electron. **21**, 381 (1989).

[13] M. S. Mangir, J. J. Ottusch, D. C. Jones, and D. A. Rockwell, '*Time-resolved measurements of stimulated Brillouin scattering phase jumps*', Phys. Rev. Lett. **68**, No 11, 1702 (1992).

[14] G. C. Valley, '*A review of Stimulated Brillouin Scattering Excited with a Broad-Band Pump Laser*', IEEE J. Quantum. Electron. **22**, No 5, 704 (1986).

[15] J. Munch, R. F. Wuerker, and M. J. Lefebvre, '*Interaction length for optical phase conjugation by stimulated Brillouin scattering: an experimental investigation*', Appl. Opt. **28**, No 15, 3099 (1989).

[16] V. I. Popovichev, V. V. Ragul'skii and F. S. Faizullov, '*Stimulated Mandel'shtam-Brillouin scattering excited by radiation with a broad spectrum*', JETP Lett. **19**, No 6, 196 (1974).

[17] R. A. Mullen, R. C. Lind, G. C. Valley, '*Observation of stimulated Brillouin scattering gain with a dual spectral-line pump*', Opt. Comm. **63**, 123 (1987).

[18] G. M. Davis and M. C. Gower, '*Stimulated Brillouin scattering of a KrF laser*', IEEE J. Quantum. Electron. **27**, No 3, 496 (1991).

[19] P. Narum, M. D. Skeldon and R. W. Boyd, '*Effect of laser mode structure on stimulated Brillouin scattering*', IEEE J. Quantum. Electron. **22**, No 11, 2161 (1986).

[20] A. A. Filippo, M. R. Perrone, '*Experimental study of Broad-band XeCl double-pass amplifier with SBS mirror*', Appl. Phys. B **55**, No 1, 71 (1992).

[21] A. A. Filippo, M. R. Perrone, '*Reflectivity of broad-band stimulated Brillouin scattering mirrors*', Opt. Comm. **91**, No 5,6, 395 (1992).

[22] R. F. Wuerker, J. Munch, and L. O. Heflinger, '*Coherence length measured directly by holography*', Appl. Opt. **28**, 1015 (1989).

[23] For an excellent review, see A. S. Marathery, *Elements of Optical Coherence Theory* (Wiley, New York, 1987), Chap. 5, or W. Koechner, *Solid-State Laser Engineering*, 3rd ed. (Springer, New York, 1992), section 5.2.

[24] V. Devrelis, M. O'Connor, and J. Munch, '*Coherence length of single laser pulses as measured by CCD interferometry*', Appl. Opt. **34**, No 24, 5386 (1995).

[25] E. L. Bubis, V. V. Vargin, L. R. Konchalina, and A. A. Shilov, '*Study of low-absorption media for SBS in the near-IR spectral region*', Opt. Spectrosc. **65**, No 6, 757 (1989).

[26] N. F. Andreev, E. Khazanov, and G. A. Pasmanik, '*Applications of Brillouin Cells to High Repetition Rate Solid-State Lasers*', IEEE J. Quantum. Electron. **28**, No 1, 330 (1992).

[27] S. F. Grigor'ev, O. P. Zaskal'ko, and V. V. Kuz'min, '*Some features of stimulated Brillouin scattering in light absorbing media*', JETP Lett. **65**, No 4, 697 (1987).

[28] 'Thermodynamic properties of Freon-113, Trichlorotrifluoroethane, ClCF2-CCl2F, with addition of other physical properties', Du Pont, Wilmington, DE 19898, Barley Mill Plaza, 1979.

[29] W. Kaiser and M. Maier, *'Stimulated Rayleigh, Brillouin and Raman spectroscopy*', in Laser Handbook, vol 2, F. T. Arecchi and E. O. Schulz-Dubois, eds., Amsterdam, North-Holland, ch E2, 1078 (1972).

[30] Freon product information, *'Freon Fluorocarbons: Properties and Applications*', Du Pont, Wilmington, DE 19898, Barley Mill Plaza, 1985.

[31] H.J. Eichler, R. Menzel, R. Sander, and B. Smandek, '*Reflectivity enhancement of stimulated Brillouin scattering liquids by purification*', Opt. Comm. **89**, 260 (1992).

[32] M. J. Damzen and M. H. R. Hutchinson, '*Technique for measuring phase-conjugation fidelity by heterodyning signals*', Opt. Lett. **10**, No 1, 40 (1985).

[33] J. Czarske, and H. Miller, '*Heterodyne detection technique using stimulated Brillouin scattering and a multi-mode laser*', Opt. Lett. **19**, No 19, 1589 (1994).

[34] R. A. Mullen, and J. N. Matossian, '*Quenching optical breakdown with an applied electric field*', Opt. Lett. **15**, 601 (1990).

[35] M. J. Damzen and M. H. R. Hutchinson, '*High-efficiency laser pulse compression by stimulated Brillouin scattering*', Opt. Lett. **8**, No 6, 313 (1983).

[36] C. B. Dane, W. A. Neuman and L. A. Hackel, '*High-energy SBS pulse compression*', IEEE J. Quantum Electron. **QE-30**, No 8, 1907 (1994).

[37] V. Devrelis, '*Fidelity of Optical Phase Conjugation using stimulated Brillouin scattering*', PhD Thesis, University of Adelaide , 1997, (unpublished).

[38] A. L. Gaeta, R. W. Boyd and T. R. Moore, '*Stochastic dynamics in stimulated light scattering*', IEEE proceedings, IQEC'94, (1994).

[39] R. W. Boyd, K. Rzazewski and P. Narum, '*Noise initiation of stimulated Brillouin scattering*', Phys. Rev. A **42**, No 9, 5514 (1990).

[40] A. M. Scott, W. T. Whitney, and M. T. Duigan, '*Low threshold phase conjugation for 2μm lasers*', CLEO'93, CThJ3, 426 (1993).

[41] A. M. Scott, W. T. Whitney, and M. T. Duigan, *'Stimulated Brillouin scattering and loop threshold reduction with a 2.1μm Cr, Tm, Ho:YAG laser'*, J. Opt. Soc. Am. B **11**, No 10, 2079 (1994).

[42] A. M. Scott, W. T. Whitney, '*Characteristics of a Brillouin ring resonator used for phase conjugation at 2.1μm*', J. Opt. Soc. Am. B **12**, No 9, 1634 (1995).

[43] C. B. Dane, L. A. Hackel, and M. J. Lefebvre, *'Long coherence length, low threshold 1μm SBS phase conjugation'*, CLEO'95, CMA1,1 (1995).

[44] G. K. N. Wong, and M. J. Damzen, '*Investigations of optical feedback used to enhance stimulated scattering*', IEEE J. Quantum Electron. **QE-26**, No 1, 139 (1990).

[45] A. A. Michelson, *Studies in Optics* (U. Chicago Press, Chicago, 1927), pp. 34-45.

[46] A. A. Filippo, and M. R. Perrone, '*Stimulated Brillouin scattering in SF_6 with a free-running XeCl laser as pump*', Appl. Phys. B **57**, 103 (1993).

[47] I. V. Tomov, R. Fedosejevs and D. C. D. McKen, *'High-efficiency stimulated Brillouin scattering of KrF laser radiation in SF_6'*, Opt. Lett. **9**, No 9, 405 (1984).

[48] M. Lefebvre, S. Pfeifer and R. Johnson, '*Dependence of stimulated Brillouin scattering phase conjugate correction on the far-field intensity distribution of the pump light*', J. Opt. Soc. Am. B **9**, No 1, 121 (1992).

[49] M. R. Osborne and M. A. O'Key, '*Temporal response of stimulated Brillouin scattering phase conjugation*', Opt. Comms. **94**, 346 (1992).

[50] H. J. Eichler, C. Jun, A. Kummrow, R. Menzel and D. Schumann, '*Nd:YAG laser with SBS Q-switching mirror and repetition rate up to 50Hz*', Int. J. Nonlinear Opt. Phys. **2**, No 2, 247 (1993).

[51] D. L. Bullock, N-M. Nguyen-Vo and S. J. Pfeifer, '*Numerical model of stimulated Brillouin scattering excited by a multiline pump*', IEEE J. Quantum Electron. **30**, No 3, 805 (1994).

[52] A. Kummrow, '*Effect of optical breakdown on stimulated Brillouin scattering*', J. Opt. Soc. Am. B **12**, No 6, 1006 (1995).

[53] B. Zysset, J. G. Fugimoto and T. F. Deutsch, '*Time-resolved measurements of picosecond optical breakdown*', Appl. Phys. B **48**, 139 (1989).

[54] Y. S. Huo, A. J. Alcock and O. L. Bourne, '*A time-resolved study of sub-nanosecond pulse generation by the combined effect of stimulated Brillouin scattering and laser induced breakdown*', Appl. Phys. B **38**, 125 (1985).

[55] V. S. Teslenko, '*Initial stage of extended laser breakdown in liquids*', IEEE Trans. On Elec. Insulation **26**, No 6, 1195 (1991).

[56] E. L. Kerr, '*Filamentary track formed in transparent optical glass by laser beam self-focusing. 2. Theoretical Analysis*', Phys, Rev. A **4**, No 3, 1195 (1971).

[57] W. Koechner, '*Solid-State Laser Engineering*', Springer-Verlag:New York, 3rd ed. (1992).

[58] Y. R. Shen, '*The Principles of Non-Linear Optics*', Wiley, New York, (1984).

[59] M. A. O'Key, M. R. Osborne, '*Broadband stimulated Brillouin scattering*', Opt. Comm. **89**, 269 (1992).

[60] J. A. Sell, '*Photothermal investigations of solids and fluids*', Academic Press Inc., **10**, (1989).

[61] F. Dizier, J-L. Ayral, J. Montel and J-P. Huignard, 'A phase conjugate Nd:YAG laser with beam steering', Int. J. Nonlinear Opt. Phy. **2**, No 2, 229 (1993).

Chapter 4

SBS Oscillator Design and Performance

4.1 Introduction

Phase conjugated systems are usually configured as master oscillator power amplifier (MOPA) systems [1-6] (Figure 4.1). However, such systems can be complex, because a high quality, low power seed laser must be followed by many (or large) amplification stages, each one of which must be adequately isolated to avoid amplified spontaneous emission (ASE). An attractive approach is the design of a simple, high power oscillator which incorporates the gain of the active host, and the aberration correction properties of a phase conjugate mirror (PCM).

There has been many experimental and theoretical investigations on phase conjugate oscillators [7-33,38,40,44]. From this body of work it has been demonstrated that PCM's can be used to improve the beam quality and reduce the sensitivity to phase and amplitude perturbations in laser oscillators.

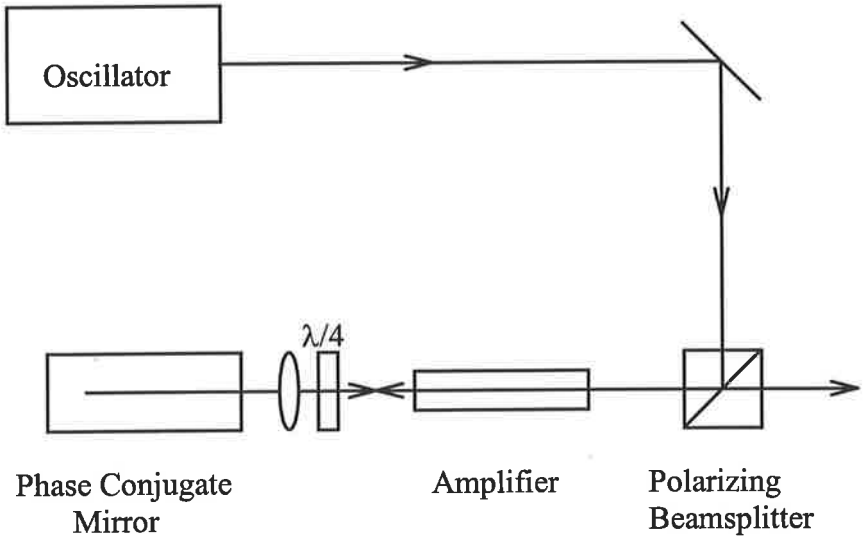

Figure 4.1 Schematic of MOPA (double-pass) system.

Stimulated Brillouin scattering (SBS) has become the preferred nonlinear process used in phase conjugate, solid-state laser oscillators due in part to the simple resonator geometries employed to generate the phase conjugate wave. Throughout the past 15 years, researchers have devised many resonator configurations which overcome the threshold power required for SBS. However, most recently, there have been three resonator designs which have become the subject of more extensive research studies (see Figure 4.2). All designs include two conventional mirrors which form a 'start-up cavity' to overcome the SBS threshold power requirement, and a third SBS mirror to perform the phase conjugation[1].

Figure 4.2(a) shows the 'intracavity SBS cell' arrangement [8,12,15,21-26,28-30,32,44]. The start-up cavity surrounding the cell generates powerful relaxation spikes. The energy in these spikes is used to reach the threshold condition for SBS. Once threshold has been reached, the SBS reflectivity of the nonlinear medium increases rapidly with the incident wave intensity. The energy is then coupled into the SBS cavity. Self Q-switching can occur if the losses in the start-up cavity are significantly higher than in the SBS cavity. Eichler *et al* [26] recently reported successful operation using gaseous (SF_6) intracavity SBS cells. However, both Eichler *et al* and Agnesi *et al* [23] have reported that competing effects such as optical breakdown and filamentation occurring within the focal region of the SBS lenses have been the main limitation of the intracavity SBS cell arrangement when liquids are used as the SBS media.

Figure 4.2(b) shows the 'side-arm SBS cell' configuration. Chandra *et al* [16], Agnesi *et al* [23], and Perrone *et al* [31] have reported the use of a side-arm geometry employing a polarizing element to control the coupling fraction to the SBS cell. Chandra *et al* found this arrangement to be easier to align than an intracavity SBS cell, and also the intensity coupled to the SBS cell could be controlled by the rotation of a

[1] Recently, one research group has successfully demonstrated a phase conjugate excimer oscillator without the need for a start-up cavity [40].

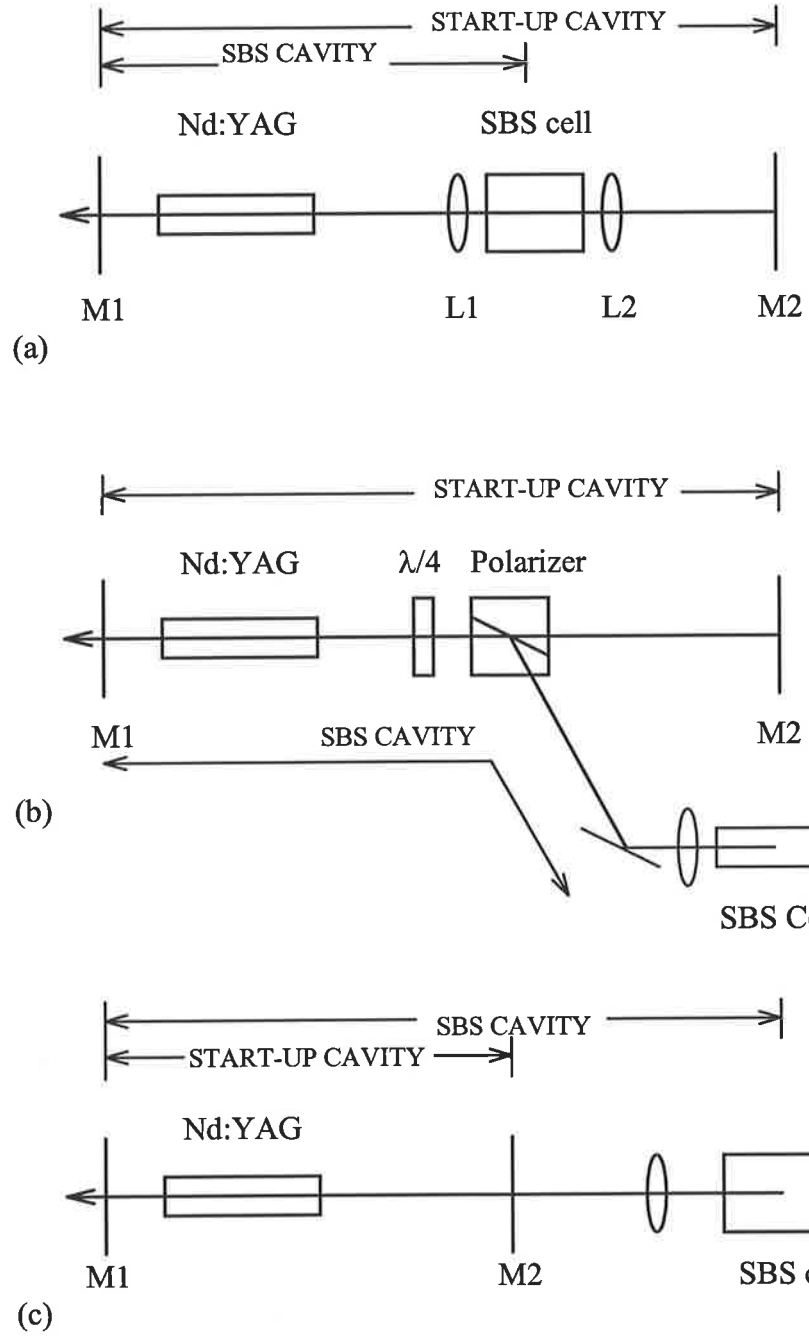

Figure 4.2 Schematic of three SBS oscillator configurations.
(a) Intracavity SBS cell,
(b) Sidearm SBS cell,
(c) External SBS cell.

polarizing element. However, Agnesi *et al* did not observe self-Q-switching using this arrangement, but found that an additional passive Q-switch was required in order for the SBS threshold to be reached and a short high peak power laser pulse to be generated.

Figure 4.2(c) shows the 'external SBS cell' configuration. Pashinin *et al* [18,20] and Lamb *et al* [27,38] have studied this design with the aim to overcome the high intracavity intensities experienced with intracavity SBS cell designs.

Although the SBS threshold in all three designs is reached by a relaxation oscillation, the first design differs from the other two because of the oscillating intracavity modes, and the extremely high intracavity electric fields that exist inside the SBS cell. From these three major configurations, the intracavity SBS cell has been the subject of the greatest number of recent studies. A great deal of progress has been made in realizing a PC oscillator using this design. However, many problems that limit the usefulness of this device have also been identified. These mainly arise from competing effects occurring in the focal volume of the SBS cell as a result of the high intracavity oscillating fields. For these reasons, the research presented in this chapter centres on the intracavity SBS cell configuration.

For intracavity cells, the phonon field responsible for SBS has been reported to initiate from density waves formed by oscillating modes in the start-up cavity, and not from random (spontaneous) noise [22,30,34]. The most efficient excitation of the acoustic sound wave is achieved when the frequency difference between resonator longitudinal modes (ν_i, ν_{i-m}) is equal to the Brillouin shift (ν_B) for the medium [22]. ie.

$$\nu_i - \nu_{i-m} = m\left(\frac{c}{2L_{startup}}\right) = \nu_B \quad \text{with } m = 1,2,3,... \tag{4.1}$$

In this case, a beat frequency of the longitudinal modes of the start-up resonator coincides exactly with the frequency (ν_B) of the sound wave which is, therefore, resonantly excited by electrostriction. This results in a start-up cavity length given by:

$$L_{startup} = \frac{mc}{2\nu_B} \quad \text{with } m = 1,2,3,... \tag{4.2}$$

When the acoustic sound wave reflectivity is high enough, the laser radiation is confined to the SBS cavity with length L_{sbs}. The field reflected by the phonon is down-shifted in frequency by ν_B. The following condition describes the length of the SBS resonator such that each lasing mode will shift into another longitudinal mode supported by the SBS resonator:

$$L_{sbs} = \frac{nc}{2\nu_B} \quad \text{with } n = 1,2,3,... \tag{4.3}$$

Therefore, for maximum effective gain, the start-up and SBS cavities must be a multiple of the resonance length $L_R = c/2\nu_B$. If the start-up cavity length is detuned from resonance, the effective gain is reduced. Assuming two longitudinal modes (with a beat frequency, $\Omega = 2\pi\nu = \pi c/L$) exciting a sound wave in the SBS medium (with a Brillouin shift, $\Omega_R = 2\pi\nu_B$) by electrostriction, the effective SBS gain coefficient (g_{eff}) can be described by [34]:

$$g_{eff} = \frac{g_{max}\,\Omega_R\Gamma}{\sqrt{(\Omega^2 - \Omega_R^2) + \Omega^2\Gamma^2}} \tag{4.4}$$

where,

g_{max} is the maximum steady-state SBS gain coefficient.

Γ is the inverse phonon lifetime ($=1/\tau_B$).

This resonance condition has been observed in other experiments when high pressure SF_6 gas is used as the SBS medium, but not when acetone is used as the SBS medium

[26,30]. In these reports, it was concluded that the resonance condition is not observed in acetone and most other liquids due to a combination of their resonance length (L_R) being considerably smaller than that of most gases (i.e. most liquids have much higher ν_B than most gases), and also due to their considerably larger SBS bandwidths (i.e. most liquids have much shorter phonon lifetimes than most gases). Therefore, when using liquids as SBS media, the resonances as specified by Equation 4.4 for different integer multiples overlap, whereas discrete resonances exist when gases are used.

At threshold, the reflectivity of the SBS mirror is exponentially dependent on the intensity in the cavity. The SBS cell reflectivity rises rapidly to ~50-70% within a few nanoseconds. The geometrical losses in the start-up cavity can be controlled so that its Q-factor is low. As the Q-switching time is in the order of a few nanoseconds, the SBS cell itself can provide passive Q-switching to generate giant pulses with high peak powers. Using SBS for passive Q-switching was first reported by Pohl [35].

As well as the longitudinal modes, an understanding of the intracavity transverse modes is important to control the coupling of radiation from the start-up cavity to the SBS cavity. The start-up cavity must support transverse modes which will couple directly into the SBS cavity.

Coupling the energy between the two cavities is critical as it is a major factor in determining the efficiency of the self-Q-switching process. If the start-up resonator's Q-value is too high (i.e. the losses are too low) the SBS starts so early that only a relatively small population inversion has been stored in the active medium. This depletes quickly and the intensity builds up once more in the form of a relaxation oscillation, and Q-switches again before a large population inversion can be established. This process can occur many times during the flashlamp pulse lifetime. Several smaller Q-switched pulses result from this operation [22]. If the Q-value is too low, then the intensity built up in the start-up resonator will be insufficient to reach the

SBS threshold. The magnitude of the loss in the start-up resonator must be such that SBS turn-on occurs toward the end of the flashlamp pulse, when population inversion is maximized.

The objective of the work in this chapter is to study an SBS oscillator using an intracavity SBS cell arrangement with Freon-113 as the SBS medium. This includes optimizing the passive Q-switching performed by the SBS mirror, reducing the effects of competing phenomena and improving the beam quality of the resonator close to diffraction limited using the phase conjugate properties of the intracavity SBS mirror.

In this chapter, a simple model is presented which describes the growth of the Q-switched pulse with the cavity losses determined by the intensity dependent intracavity SBS cell reflectivity. A detailed experimental investigation follows, describing the operation and performance of a Q-switched phase conjugated oscillator using an intracavity liquid-SBS cell.

4.2 Modelling of SBS Oscillator Operation

4.2.1 Relaxation Oscillations

Figure 4.3 shows the schematic of a 4-level atomic system. When strong pumping begins (W_{pump}), a population inversion (N) is created in the gain medium. Under steady-state conditions, where the gain per pass equals the cavity losses ($\frac{dN}{dt} = 0$), the population of level 2 (N_2) can never exceed the inversion threshold population (N_{2t}) [2]. However, in the transient regime, N_2 can be raised above the threshold value as no laser oscillation has yet been built up, and no radiation exists to deplete the population inversion via the stimulated emission process. Then the oscillation level is amplified due to stimulated emission, reducing the population inversion below the threshold value. If the pumping duration is much longer than the time taken to saturate the gain, re-pumping of the gain medium can occur, resulting in the laser output consisting of a series of relaxation oscillations.

By setting the cavity losses to a high level (low Q-factor), the lasing oscillations can be inhibited and both the energy stored, and the gain of the active material can be increased. In this case, the population inversion can reach a value far above the threshold for normal lasing action. If the Q factor is then rapidly increased by reducing the cavity losses, the cavity flux will quickly rise to a high value since the optical system is subjected to low loss and high gain. The result is a powerful pulse with a duration typically of a few tens of nanoseconds for Nd:YAG.

[2] The inversion threshold population occurs when energy levels 1 and 2 have equal populations.

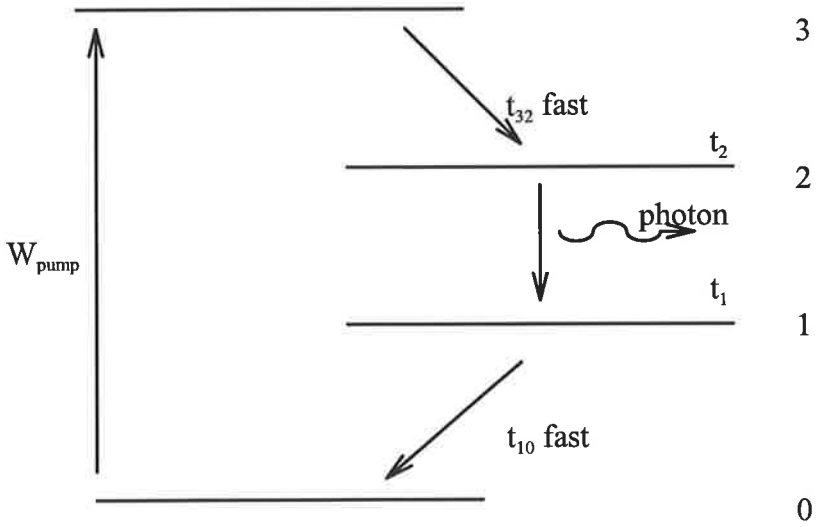

Figure 4.3 Schematic of an Ideal 4-level atomic system.

4.2.2 Rate Equations for Q-switching

The theory of Q-switching is well known [41], and will be briefly reproduced in part here to help with the analysis of intracavity SBS Q-switching. In this analysis, spontaneous emission and optical pumping processes have been ommitted intentionally in forming the rate equations due to the very short Q-switch pulse duration.

An ideal 4-level system with t_{10} fast implies $N_1 \sim 0$. This is assumed to simplify the rate equations. The stimulated emission process between levels 2-1 is characterised by the cross section (σ_{21}).

$$\sigma_{21}(\nu) = \frac{A_{21}\lambda_o^2}{8\pi n_r^2} g_{lineshape}(\nu) \tag{4.5}$$

where A_{21} is Einstein's coefficient for spontaneous emission and is equal to $\frac{1}{t_{21}}$, and n_r is the refractive index of Nd:YAG. $g_{lineshape}(\nu)$ is the line-shape factor, which is Lorentzian for homogeneously broadened (Nd:YAG) gain media.

$$g_{lineshape}(\nu) = \frac{\Delta\nu}{2\pi\left[(\nu - \nu_0)^2 + (\Delta\nu/2)^2\right]} \tag{4.6}$$

At line centre ($\nu = \nu_0$) it has a maximum value given by,

$$g_{lineshape} = \frac{2}{\pi\Delta\nu_o} \tag{4.7}$$

$$\Rightarrow \sigma = \frac{\lambda_o^2}{4\pi^2 n_r^2 \Delta\nu\, t_{21}} \tag{4.8}$$

Therefore, the rate of change of the population inversion (N) can be written as,

$$\frac{d\,\mathrm{N}}{dt} = -\gamma\sigma c\Phi \mathrm{N} \tag{4.9}$$

where Φ is the photon density, c is the speed of light, and γ is the inversion reduction factor. It has been assumed that for a 4-level Nd:YAG system, the 'inversion reduction factor' after the emission of a single photon is 1. The term on the right hand side of Equation 4.9 expresses the net stimulated emission between levels 2-1.

The build up of the cavity flux (Φ) is primarily determined by two factors: firstly, the amplification of the flux due to stimulated emission and the corresponding saturation of the gain; secondly, the simultaneous loss of flux due to transmission through the cavity mirrors and scattering losses. Therefore, the rate of change of the photon density (Φ) can be written as,

$$\frac{d\Phi}{dt} = \Phi \mathrm{N}\sigma c\left(\frac{\mathrm{L_{rod}}}{\mathrm{L_{cavity}}}\right) - \frac{\Phi}{\mathrm{t_c}} \tag{4.10}$$

where, $\mathrm{L_{rod}}$ is the length of the active material, $\mathrm{L_{cavity}}$ is the length of the resonator, and $\mathrm{t_c}$ is the photon decay time which is dependent on the optical system parameters.

In order to determine how Q varies in time, the time dependent photon lifetime ($\mathrm{t_c}$) in the cavity must be determined. Therefore, expressions for the optical gain (g) and transient losses are needed.

At equilibrium, the total round-trip losses equal the round-trip optical gain experienced by the flux. If the cavity mirrors have reflectivities of $\mathrm{R_1}$ and $\mathrm{R_2}$ and we let the dissipative losses (absorption) be α per unit length, then the threshold condition can be written as,

$$R_1 R_2 \, exp\left(g_t - \alpha\right) 2L_{rod} = 1 \tag{4.11}$$

where g_t is the gain at threshold, and the round trip is accounted by the $2L_{rod}$ factor. Note that propagation of the flux throughout the cavity is not explicit in this simple result.

When deriving gain coefficients for stimulated emission, an interaction between an atomic system having a finite transition linewidth ($\Delta\nu$) and a signal with bandwidth $d\nu$ must be considered. In the case of Nd:YAG, thermal lattice vibrations are the dominant homogeneous broadening factor which can be written in a Lorentzian form (see Equations 4.6 & 4.7). The general gain coefficient can then be written in terms of the material dependent parameters of Nd:YAG,

$$g(\nu) = \frac{N c^2 g_{lineshape}(\nu)}{8\pi^2 n_r^2 \nu^2 t_{21}} \tag{4.12}$$

where N is the population inversion, n_r is the refractive index of Nd:YAG, and t_{21} is the spontaneous upper-state lifetime.

The photon cavity lifetime (t_c) can be described in terms of the fractional power loss (ε) per round trip:

$$\varepsilon = \frac{t_R}{t_c} \tag{4.13}$$

where $t_R = 2L_{cavity}/c$ is the round-trip time of a photon in a resonator having an optical length L_{cavity}. Rearranging Equation 4.11 yields,

$$2g_t L_{rod} = -ln\, R_1 R_2 + 2\alpha L_{rod} \tag{4.14}$$

The right hand side of Equation 4.14 is the total fractional power loss per round trip. Therefore, combining Equations 4.13 & 4.14 we obtain t_c in terms of the cavity loss parameters,

$$t_c = \frac{2L_{cavity}}{c\left[-ln\,R_1R_2 + 2\alpha L_{rod}\right]} \tag{4.15}$$

In this case, the loss mechanism is controlled by the SBS process.

4.2.3 Loss Mechanism for an Intracavity SBS Resonator Configuration

Figure 4.4 shows the schematic of a start-up cavity with an intracavity SBS mirror. The reflectivity R_2, used in previous equations must include the SBS mirror reflectivity which is intensity dependent. We can replace R_2 with an effective reflectivity (R_{eff}) which is intensity dependent and, for an intracavity SBS cell, is given by,

$$R_{eff} = R_{SBS}\left[1 - R_2\right] + R_2 \tag{4.16}$$

Seidel *et al* [29] used a transient SBS analysis to model R_{SBS}. This group were particularly interested in modelling the timing of the reflectivity of the power reflected from the SBS cell for pulse-lengthening experiments using an SBS oscillator. Other groups [23,24,26,30,38] have used the steady-state analysis to model R_{SBS} and the characteristics of the Q-switched output laser pulse. The analysis in this chapter uses the SBS equations incorporating the steady-state approximation (see Equation 2.12). This approximation is justified for phonon lifetimes that are short relative to the round-trip time of the cavity, and the laser pulsewidth.

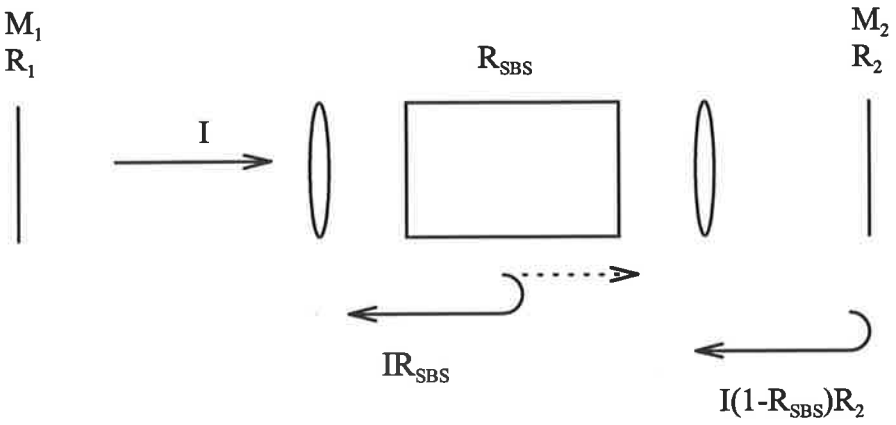

Figure 4.4 Schematic displaying the three mirrors present in an intracavity SBS oscillator.

For an interaction length 'l_i', there are three boundary conditions which are required to solve the steady-state SBS equations:

$$R_{SBS} = \frac{I_S(l_i)}{I_P(l_i)}$$

$$I_P(z) - I_S(z) = \text{constant} \tag{4.17}$$

$$\frac{I_S(l)}{I_S(0)} = e^G$$

where I_P & I_S are the field intensities of the input pump, and Stokes backscattered beams, respectively. G (=25) is the typical exponential factor required before the SBS threshold is reached [37].

Using these conditions an equation in R_{SBS} can be derived [23,30,37]:

$$\frac{\exp(-G)}{R_{SBS}} = \frac{1 - R_{SBS}}{\exp\left[\left(1 - R_{SBS}\right) g_B \, l_i \, I_P\right] - R_{SBS}} \tag{4.18}$$

Therefore, we can now obtain a relation for the photon cavity decay time (t_c) with an intracavity SBS resonator configuration:

$$t_c = \frac{2L_{cavity}}{c\left[-ln\, R_1 R_{eff} + 2\alpha L_{rod}\right]} \tag{4.19}$$

where $R_{eff} = R_{SBS}\left[1 - R_2\right] + R_2$

and R_{SBS} is given by Equation 4.18.

A computer model was written which numerically solves the rate equations 4.9 and 4.10 using a finite difference approach as follows:

$$\Phi^{i+1} = \Phi^{i}\left[1 + \Delta t c\sigma\, N^{i}\frac{L_{rod}}{L_{cavity}} - \frac{\Delta t}{t_c^{i}}\right]$$

$$N^{i+1} = N^{i}\left[1 - \Delta t c\gamma\sigma\Phi^{i}\right] \tag{4.20}$$

with initial conditions:

$$N(t=0) = N_{initial} = N_{threshold} = \frac{4\pi^2 n_r^2 \nu^2 t_{21} g_t \Delta\nu}{\lambda^2}$$

$\Phi(t=0)$ takes the spontaneous emission value.

where,

Δt is the time stepsize between the i^{th} and $i^{th}+1$ terms.

$\Phi^{i,i+1}, N^{i,i+1}$ are the i^{th} and $i^{th}+1$ terms of the Photon Flux and Population Inversion, respectively.

t_c^i is the i^{th} term of the photon cavity decay time.

However, since the gain is typically pumped slightly above threshold, a $(1+\delta)$ multiplication factor for $N(t = 0)$ is used ($\delta \sim 5\%$). This factor is included because the cavity flux does not build up immediately when the gain has reached its threshold value, due to the spontaneous nature of the initial emission. Taking into account the mode cross section inside the laser rod (A), the power (P) can be found from the cavity flux (Φ) by,

$$P = h\nu c A \Phi \tag{4.21}$$

Figure 4.5 shows a typical set of results from this computer simulation. Figure 4.5(a) displays the time-resolved effective reflectivity of the SBS mirror and M_2 combination in time. For this set of initial conditions, the time-resolved effective reflectivity takes

approximately 10ns (2-3 round trips) to switch from a low R_{eff} (~10%) to a high R_{eff} (~90%). This risetime corresponds to the switching time for the cavity Q.

The evolution of the cavity flux (Φ) and the population inversion (N) as a function of time are shown in Figures 4.5(b) and (c). The constant mirror M_2 reflectivity allows the cavity flux (Φ) to build slowly until the SBS threshold is reached[3]. The rapidly increasing R_{eff} results in an increased photon cavity lifetime (t_c), which in turn increases the cavity flux (Φ), with the corresponding depletion in the population inversion (N). Also, from Figure 4.5(b), it can be seen that the trailing edge of the Q-switched pulse is slower than the leading edge. The rise-time is controlled by the extreme amplification in the laser gain medium whereas the fall-time is mainly a function of the photon cavity lifetime (t_c).

Several parameters were varied to investigate the sensitivity and magnitude of any changes to the resultant Q-switched pulse. These included the steady-state SBS gain (g_B), the back mirror reflectivity (R_2), and the initial population inversion (N(t=0)).

For an intracavity SBS cell, the effective SBS gain (g_{Beff}) will depend not only on the properties of the non-linear medium itself, but may be reduced by the presence of suspended and dissolved impurities, and enhanced by the beat frequency between two longitudinal modes inside the cavity[4] [30,34]. However, only the effect on the output pulse of a reduction or increase in the effective SBS gain is modelled here, and not the mechanism which led to the change.

---

[3] The entire pumping process has not been modelled here. Therefore, the relatively long time required for the gain to exceed the losses (in the form of a relaxation oscillation) is not simulated. This simulation starts with the population inversion already slightly above threshold.

[4] This condition arises from the ability to reduce the SBS threshold by constructing counter-propagating cavity modes whose interference pattern excites the required Brillouin sound wave in the non-linear medium (refer to page 100 of this thesis).

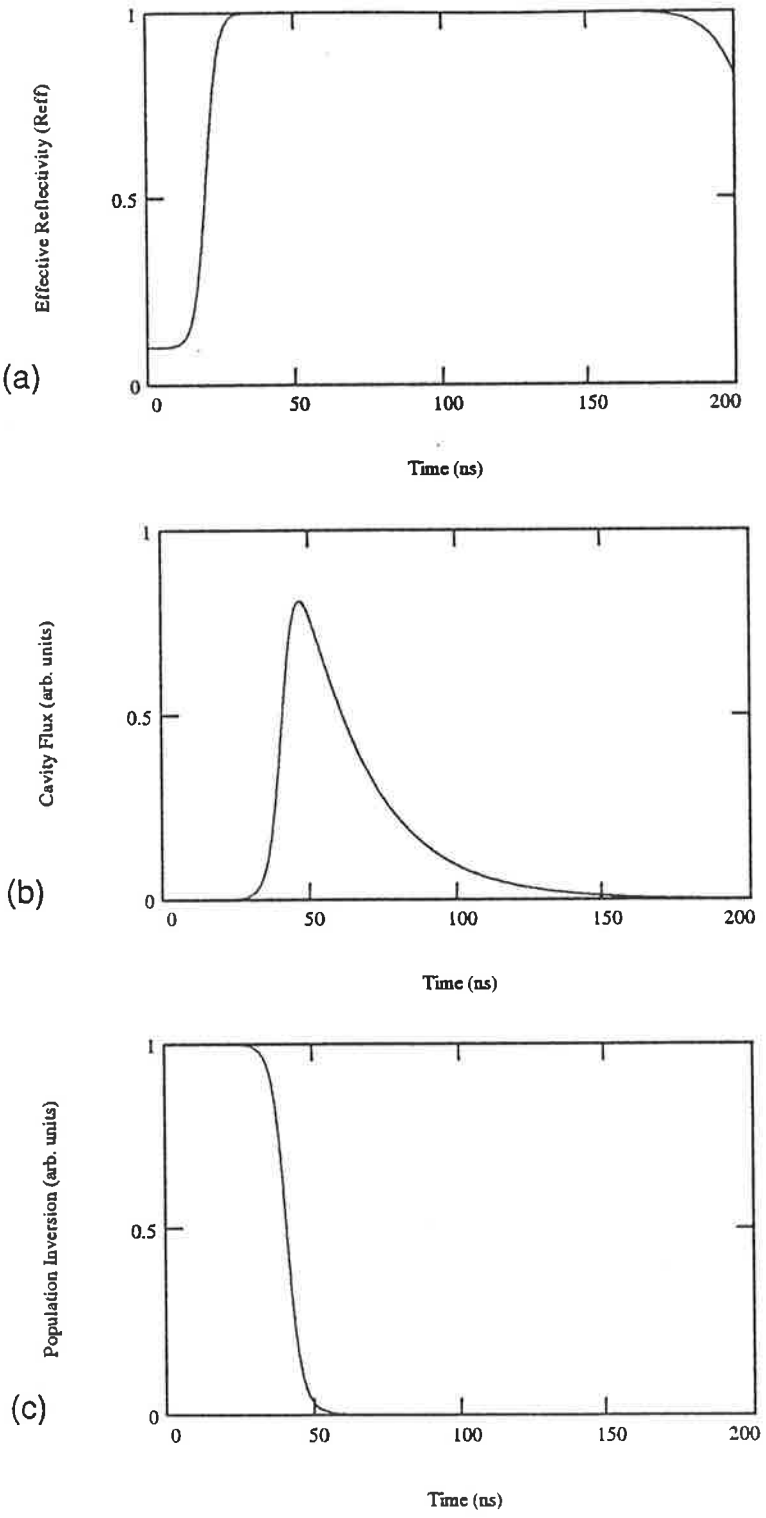

Figure 4.5 Numerical Simulation (R_2=10%),
(a) Time-resolved Effective Reflectivity (R_{eff}) as a function of time,
(b) Cavity Flux (Φ) as a function of time,
(c) Population Inversion (N) as a function of time.

Reducing g_{Beff} in this model reduced the maximum value achieved by the effective reflectivity (R_{eff}). The change in cavity losses was also reduced, resulting in a pulse with lower peak power and larger pulsewidth (i.e. an inefficient Q-switched process). As the change in cavity losses is further reduced, the following qualitative results were observed from this model. The cavity flux pulse length approached that of a relaxation oscillation which indicated in effect that the oscillator failed to Q-switch. With increased values of g_{Beff}, the time required to saturate the time-dependent effective reflectivity was reduced, resulting in a shorter Q-switch pulse length with higher peak power.

When the initial population inversion was lowered, a Q-switch pulse with a longer pulse width and lower peak power resulted. Experimentally, this condition can occur if the flux in the start-up cavity reaches the SBS threshold before the population inversion stored in the active medium reaches its threshold value. Also, as shown in Figure 4.6, the model predicts that an increase in the back mirror reflectivity (R_2), will result in a Q-switch pulse with a longer pulse length and a lower peak power.

The fundamental cavity conditions for high Q-switch extraction efficiency have been well documented [41]. When the transition from low Q to high Q is made instantaneously, a high gain-to-loss ratio is the major requirement to maximize the Q-switching extraction efficiency. In this case, the optimum output coupling fraction is the key parameter in obtaining a high gain-loss ratio. In a slow Q-switch, the development of a Q-switch pulse depends on the ratio of the pulse build-up time to the switching time. If the Q-switch pulse is emitted when the cavity losses are minimum (i.e. the pulse build-up time and switching time are equal), then the Q-switch operation is optimized.

In this section, however, the particular characteristics of the intracavity SBS process that are required for passive Q-switching have been presented, namely: maximizing the

effective SBS gain which results in the time-dependent effective reflectivity saturating at a higher level and at a faster rate. This, in turn, will lead to a shorter switching time and Q-switch pulse width; and choosing an initial start-up cavity loss within the following contraints: firstly, as high as possible to maximize the change in cavity Q; secondly, high enough to avoid the early build-up of the SBS reflectivity which results in a slower switching time (compared with the pulse build-up time), and a longer pulse width[5]; and thirdly, low enough for relaxation oscillations with the SBS threshold power, to be produced.

[5] A switching time which is slow compared with the build-up time can lead to an early, inefficient Q-switch pulse, and the occurrence of multiple pulsing.

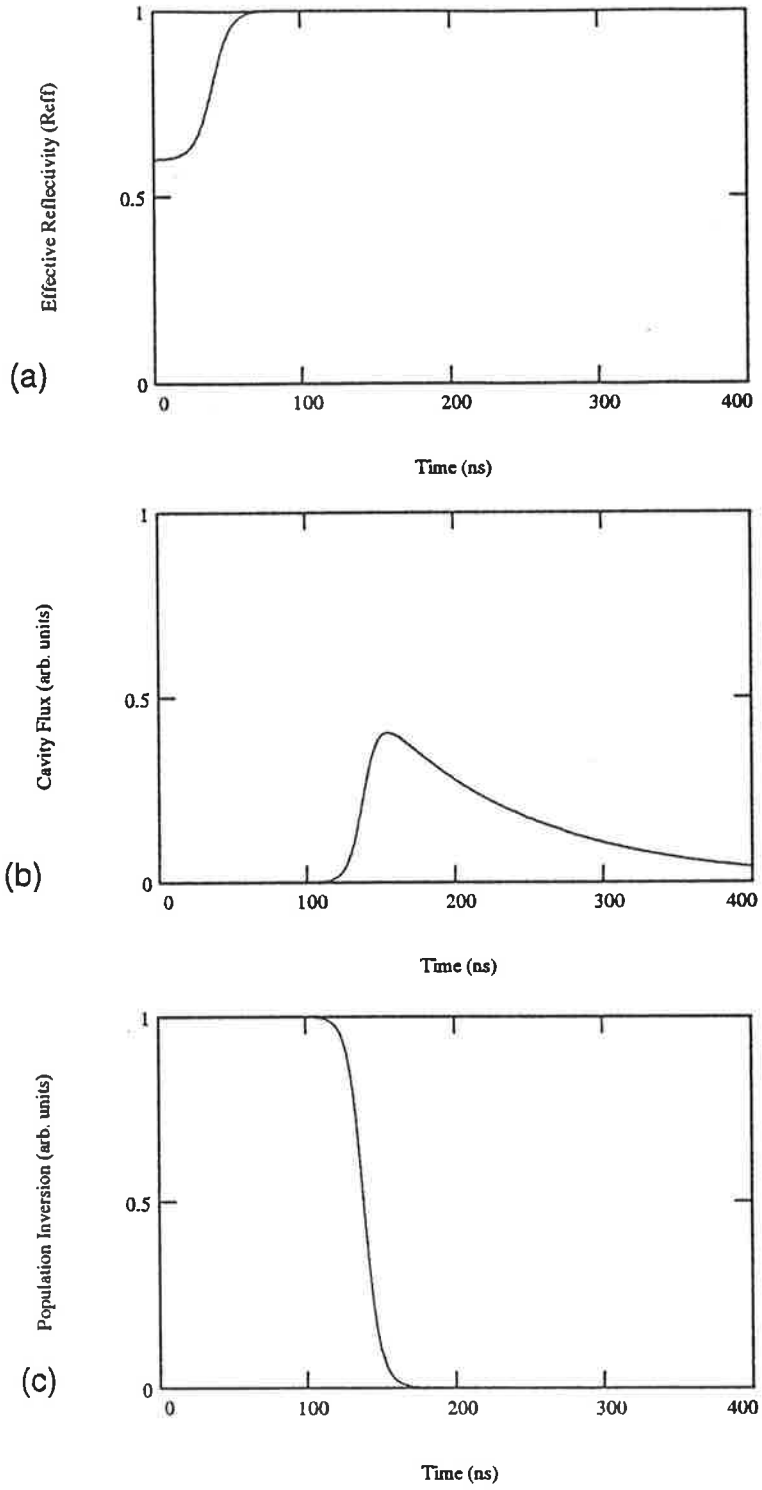

Figure 4.6 Numerical Simulation (R_2=60%),
(a) Time-resolved Effective Reflectivity (R_{eff}) as a function of time,
(b) Cavity Flux (Φ) as a function of time,
(c) Population Inversion (N) as a function of time.

4.3 Experiment

This section describes the components and diagnostic techniques developed to measure the performance of the intracavity SBS phase conjugate mirror, and the output characteristics of the SBS oscillator. References to Section 3.2 are given as many of the techniques and approaches used in this chapter are similar to those used in Chapter 3.

The initial oscillator design used in these experiments is shown in Figure 4.10. Two plane mirrors were used to form the start-up cavity. The initial reflectivity of the two mirrors were, R1 chosen between 20% and 50%, and R2 = 100%. Neutral density filters were used to lower the effective reflectivity of R2. The Nd:YAG rod had anti-reflection (AR) coatings, and physical dimensions of 8mm diameter x 80mm length. The rod was pumped by a single Xenon flashlamp in an elliptical cavity. The SBS cell contained purified Freon-113 and was positioned as close to the Nd:YAG rod as possible (~8cm). R1 and the SBS cell formed the SBS cavity. Two anti-reflection coated lenses, with focal lengths of 100mm were used to form a telescope to focus the intracavity radiation into the SBS cell. Lenses with other focal lengths between 38mm and 100mm were also used. An aperture was placed in front of the output coupler to provide near-field control of the transverse modes in the cavity. The SBS cells were all glass except for teflon stoppers, and had optical flat glass windows.

The schematic of the diagnostics used is shown in Figure 4.11. Three separate lasers were used to align the SBS resonator. Reflections from non-refracting elements (i.e. mirrors and other flat surfaces) were aligned using a 10mW HeNe laser, whilst the SBS cell and lens conbination were aligned using either a pulsed Nd:YAG laser or a continuous (CW) Nd:YVO_4 laser. Time-integrated and time-resolved SBS reflectivity measurements were obtained in the same way as described in Section 3.2. In some cases, an oscilloscope with 500MHz bandwidth was used instead of the 1GHz Transient Digitizer.

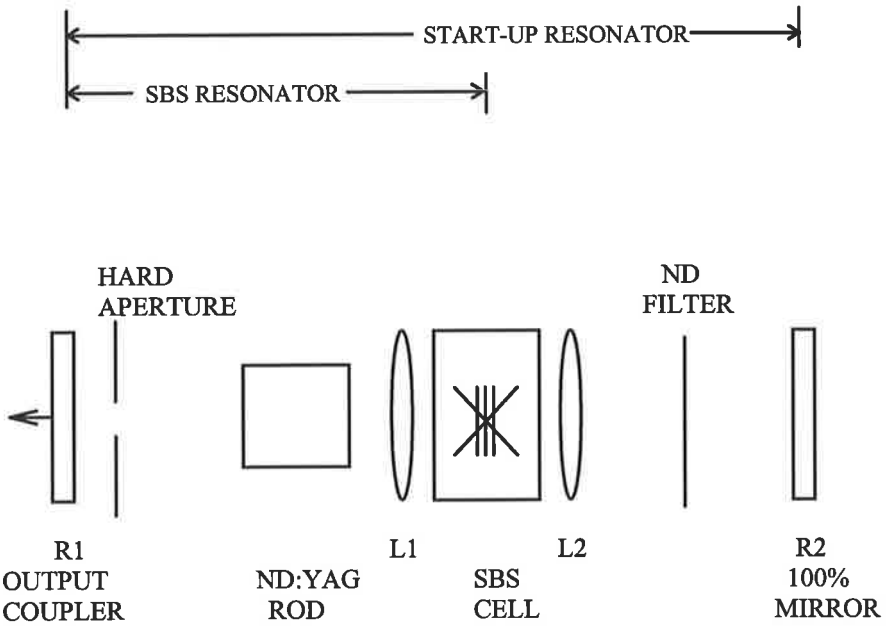

Figure 4.10 Initial resonator design.

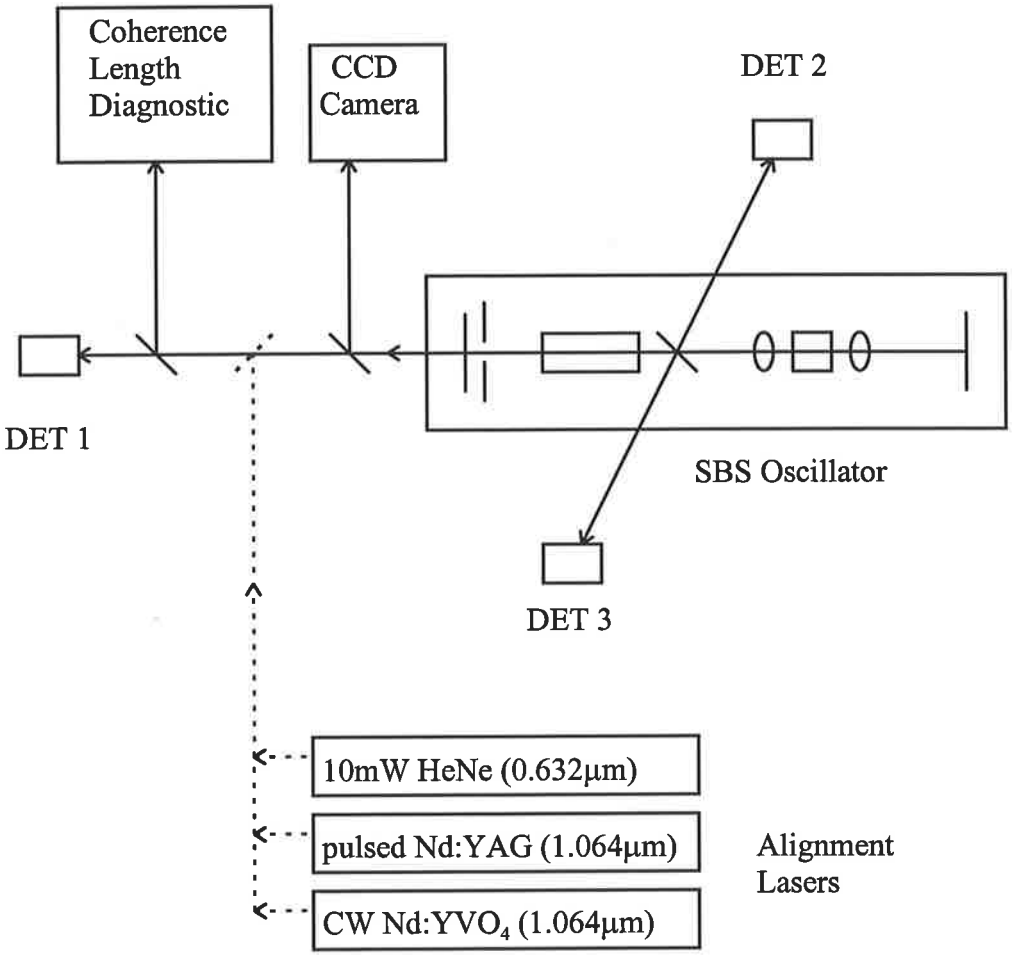

Figure 4.11 Schematic of the resonator diagnostics.

4.4 Results and Discussion

A suitable start-up resonator must be designed in order to produce successful operation of the SBS resonator. The lasing action, in the form of relaxation oscillations, creates the initial conditions for the SBS process. This includes achieving the required threshold power, as well as building suitable density waves in the SBS medium from the oscillating modes. An analysis of the operation of the start-up resonator is presented first as a basis for the design of the SBS resonator.

4.4.1 Start-up Resonator

A schematic of the start-up resonator is shown in Figure 4.12. The empty SBS cell and telescope combination were included in order to simulate the operating conditions before the SBS threshold was reached. In this experiment, lens L2 was translated in order to change experimentally the stability of the resonator during the alignment procedures.

The slope efficiency of this laser is shown in Figures 4.13(a) and (b) for different output coupling fractions. The line overlay represents a best fit of 0.5% slope efficiency. This low efficiency is partly attributed to the low performance of the flashlamp and cavity design. The maximum output energy achieved with the optimum output coupling for the free-running laser, without the SBS medium, was 270mJ. The stability of the output energy was <2%. The divergence of the output beam with a 4mm spot size ($2\omega_o$) at the output coupler was measured to be ~1.9mrad.

The relaxation oscillations achieved when the resonator was tuned for maximum output are shown in Figure 4.14. In this figure the flashlamp intensity is overlayed in order to show the relative timing of the relaxation oscillations.

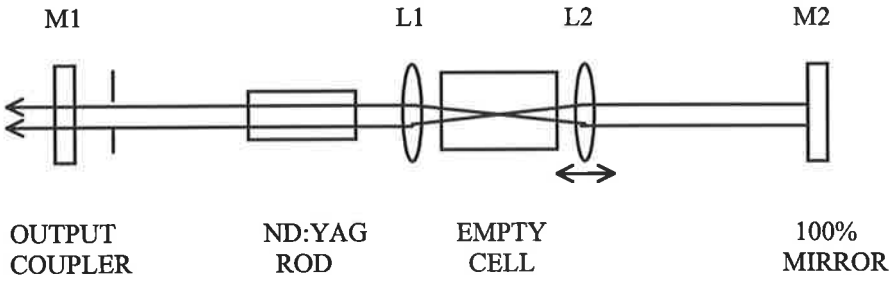

Figure 4.12 Start-up resonator design

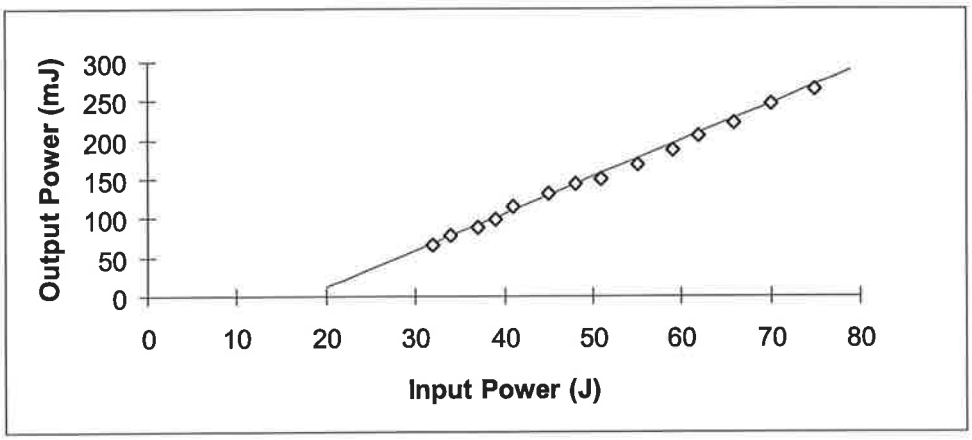

(a)

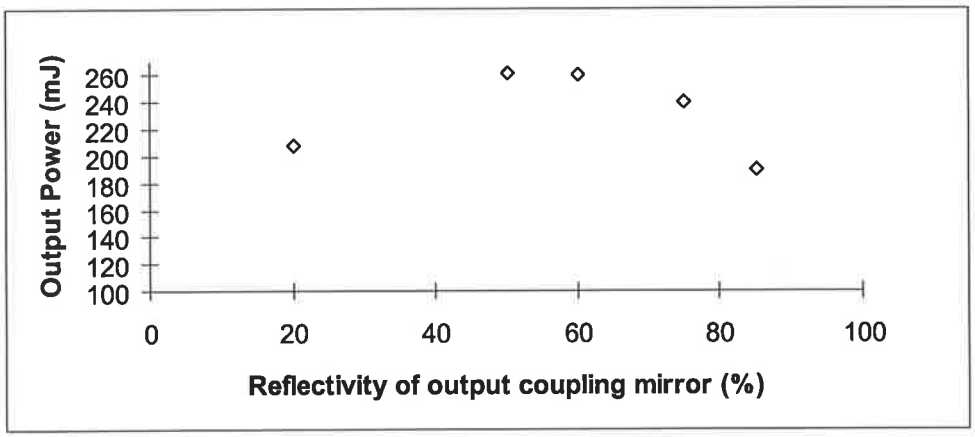

(b)

Figure 4.13 (a) Slope Efficiency of the start-up resonator with an output coupling mirror reflectivity of 60%, (b) Output Power versus Output coupling mirror reflectivity for Input power = 70J.

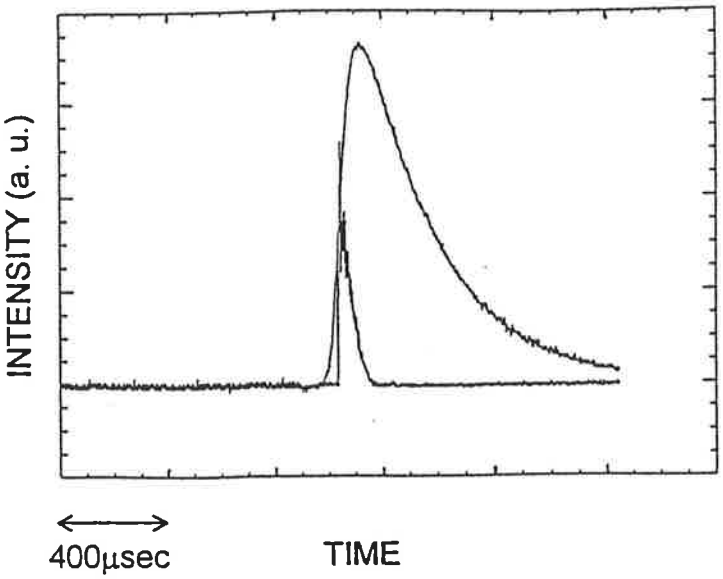

(a)

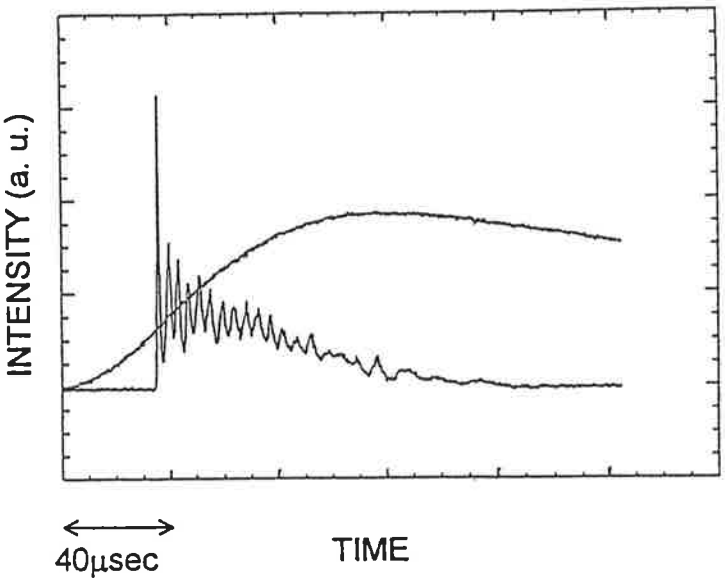

(b)

Figure 4.14 Start-up resonator relaxation oscillations,
(a) Plot showing the entire flashlamp pulse and the timing of the laser relaxation oscillation, (b) Plot showing a close-up of the relaxation oscillation.

There were approximately 20-30 relaxation oscillations each with a temporal width of 0.5-1μs FWHM, separated by ~3μs. The duration of the entire oscillation was ~120μs, (compared with the duration of the flashlamp pump pulse ~400μs FWHM).

The initial SBS threshold is reached by a relaxation oscillation that is generated in the start-up oscillator. The peak power, energy and number of oscillations can be controlled by varying the losses in the start-up cavity. Figure 4.15 shows typical temporal profiles of relaxation oscillations under different start-up cavity loss conditions. If the losses are chosen suitably, a single relaxation spike with high peak power, and with energy of ~3mJ's can be obtained from the laser. This relaxation spike was reproducible in time to ±10μs and in peak power to ±10%.

It is advantageous to alter the start-up cavity losses in that part of the cavity that is outside the SBS cavity. This can be done by choosing a back mirror with a suitable reflectivity, or adding a neutral density filter in front of the back mirror. Fine adjustment can be made by angle tuning the back mirror. The net effect of this is to inhibit lasing action. This, in turn, increases the initial inversion, and leads to a more powerful relaxation spike. This factor also increases the storage capacity of the rod and leads to greater output energies. It is essential for this optimization that the single relaxation spike occurs late in the lifetime of the flashlamp pump pulse.

Seigman [36] states that it is not necessary to supply pumping power to a Q-switched laser for longer than about one or two population decay times (~200μsec for Nd:YAG) before the Q-switching takes place, since the inverted population no longer continues to grow after this length of time [36]. This technique is widely used in active Q-switching methods such as electro-optic Pockell cells. As can be seen in Figure 4.15(b), a single stable relaxation spike can be generated which starts the passive Q-switch ~130μsec

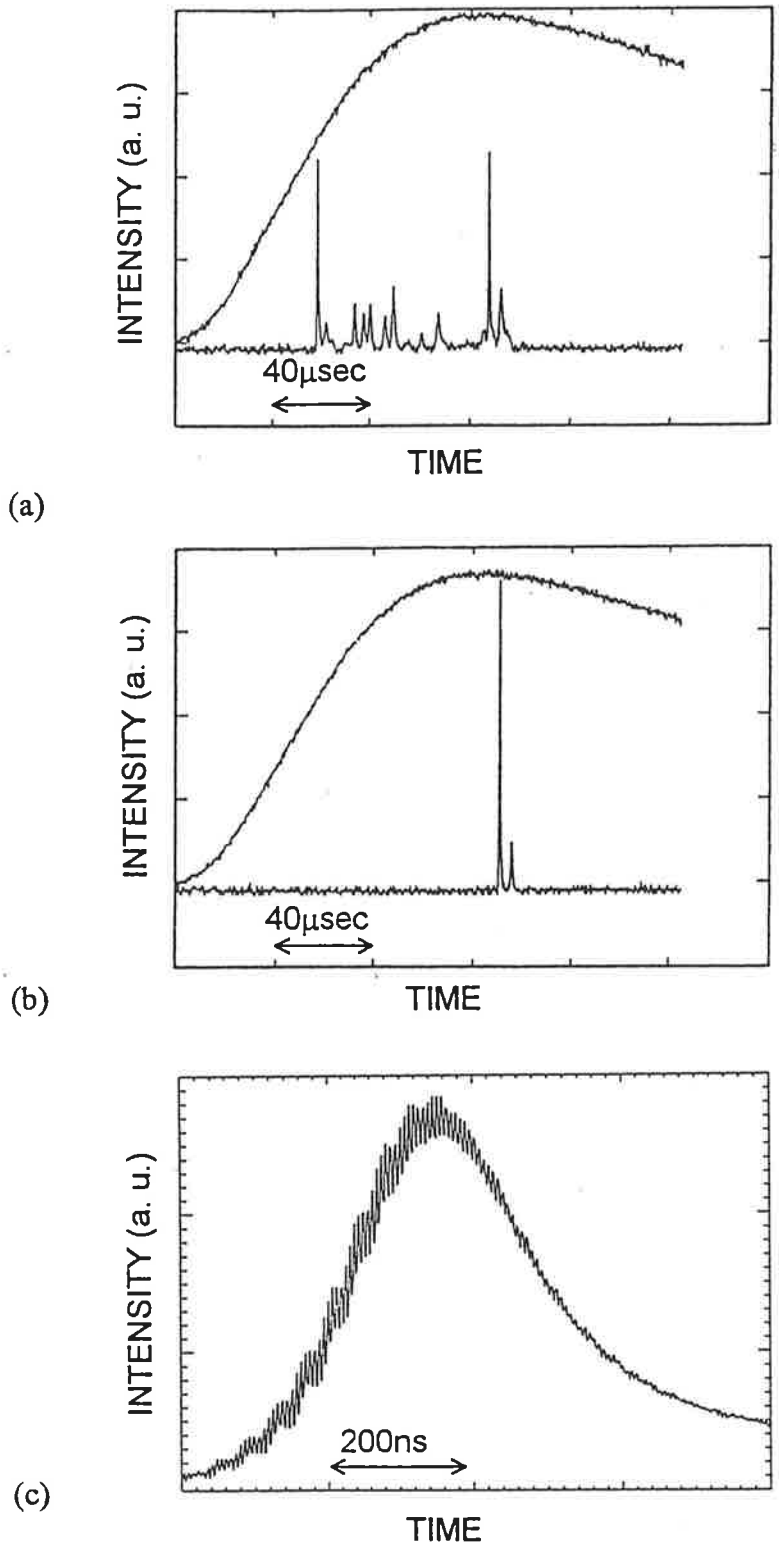

Figure 4.15 Relaxation oscillations under different loss conditions.
(a) Increased loss resulting in fewer relaxation oscillations, (b) Optimum loss resulting in one stable, reproducible oscillation, (c) A typical stable relaxation oscillation.

after pumping begins. Whilst maintaining a stable oscillation, the maximum delay achieved was 150μsec. Ideally, this hold-off should be for longer (i.e. 230-260μsec) in order to extract the highest possible gain, however, this could not be achieved in our experiment by controlling the losses of the back section of the resonator. The end result is a Q-switched pulse with lower energy than expected. One solution is to use a separate Pockels cell, instead of the non-linear SBS, to perform the Q-switching later in time. However, an important part of the research in this chapter was the study of SBS Q-switching, therefore an additional Q-switch was not used in this work.

Figure 4.15(c) shows a typical oscillation that reaches the SBS threshold. Its FWHM is 400ns and has an intracavity energy ~10mJ. The peak power is therefore up to approximately 25kW. The strength of the temporal modulations seen in this figure varied from pulse to pulse. With closer inspection, the period of this oscillation was about 5.4ns, which corresponds approximately to the resonator cavity round trip time ($L_{start\text{-}up}$ ~ 81cm).

4.4.2 SBS Resonator

Purified Freon-113[6] was added to the SBS cell within the start-up cavity described in the previous section. The addition of the Freon-113 introduced absorption, and refractive index changes into the resonator. As the refractive index of Freon-113 (n_{freon} = 1.37) is closer to that of glass (n_{glass} = 1.5) than air (n_{air} = 1.0), the reflected loss from the inside surfaces of the SBS cell is reduced. The linear absorption of the YAG rod, SBS cell and lens combination was measured with and without Freon-113. Without Freon-113, the single pass loss through the Nd:YAG rod, empty SBS cell and two AR coated lenses was ~18%±0.5%. This corresponds to ~1.2% reflection from each AR coated surface, and ~4% reflection from each non-AR coated surface. With Freon-113, the single pass loss reduced to ~15.5%±0.5%. The losses due to the reflections from surfaces were considerably higher than the losses due to linear absorption of Freon-113. Also the increase in refractive index required a corresponding change to the length of the telescope. This was achieved by translating lens L2.

In order to obtain the highest effective gain in the interaction region, and to optimize the output power from an oscillator with an intracavity SBS cell, the lengths of the two resonators were matched to the Brillouin shift. As described in Section 4.1, the resonance length (L_R) is:

$$L_R = \frac{c}{2\nu_B} \tag{4.22}$$

where ν_B is the Brillouin frequency shift.

For the start-up cavity, matching to the Brillouin shift maximizes the contribution of the two-wave mixing on the amplitude of the acoustic wave [34]. When using only a focusing geometry, SBS initiates from thermal noise. In this case, due to the

[6] Refer to Section 3.2 for purification process.

surrounding resonator configuration, resonant cavity modes will be co-propagating and contra-propagating in the SBS medium. As described in Section 4.1, if these modes are spaced by the frequency shift of the acoustic wave, two-wave mixing may provide an additional gain mechanism for the acoustic wave. The strength of this two wave mixing effect on the acoustic field is dependent on the cavity detuning from resonance.

Length matching of the SBS cavity is necessary due to the frequency shift that occurs once SBS threshold has been reached. If the cavity is slightly detuned from resonance, then the frequency shifted radiation will progressively walk-off the longitudinal cavity mode structure. Although this condition was set-up in our experiments, it has previously been reported that, for SBS media (typically liquids) with Brillouin shifts (ν_B) >1GHz and phonon lifetimes (τ_B) ~1ns, there are practically always resonator modes whose frequency difference coincides with ν_B to an accuracy of the scattering bandwidth (Γ) [26,30,37]. However, no detailed experiments were performed to confirm this theory.

The temporal profile, beam quality, output energy, intracavity SBS reflectivity and coherence length of the SBS oscillator are discussed separately in the following five sections.

4.4.2.1 Temporal Profile

When the cavity losses were properly adjusted, one giant Q-switched pulse with a duration of approximately 20-30ns resulted (see Figure 4.16(a)). Figure 4.16(b) shows in more detail the relaxation oscillation initiating the SBS process, resulting in the cavity losses being reduced within a few nanoseconds. An indication of the threshold power for SBS Q-switching was obtained by measuring the peak power of the relaxation spikes emitted from the start-up cavity that were just below the SBS threshold. A threshold value of a few kilowatts was obtained. This can be compared

with the calculated threshold for the simple, Generator-SBS focusing geometry without feedback,

$$P_{th} \cong \frac{G}{l_i\, g_B}\pi\left(\frac{\lambda f}{2D}\right)^2 \approx 10-30\,\mathrm{kW}$$

for G=25, g_B(freon)=6.2x10^{-3}cm/MW, λ=1μm, f=10cm, D=4mm and l_i = 1-2cm.

Large fluctuations in the temporal profile were observed. Pulses with FWHM's ranging between 10ns and 80ns were observed. This can be compared with the original relaxation oscillation FWHM of ~400ns.

It was found that when the cavity losses in the start-up resonator were reduced, laser output consisting of many discrete pulses, each having a duration between 50-100ns was observed. The total output energy in the many smaller Q-switched pulses was approximately the same as the energy when only a single Q-switched pulse was generated. This type of output has been reported in other studies [16,21,22,38].

The model developed in Section 4.2 was used to investigate the effect of a reduction in cavity losses in the start-up cavity on intracavity SBS Q-switching performance. From these computer simulations and our experimental observations it can be concluded that a reduction in the cavity losses in the start-up cavity results in relaxation spikes that occur earlier during the flashlamp pump pulse and with sufficient energy to initiate the SBS process. The relatively poor Q-switching performance is due to a smaller population inversion stored in the active medium. This process can continue many times during the flashlamp pumping lifetime.

Energy values of up to 80mJ were measured. This is compared with the maximum conventional resonator output, measured to be 270mJ. This value was limited in part by the flashlamp input energy and the design of the elliptical flashlamp reflector. Since Q-

switching occurs only 150μsec (instead of ~240μsec) after the flashlamp pulse begins, at least one third of the input pump energy is wasted. This early Q-switching contributes to the difference between the measured output energy of the start-up and SBS resonators. The efficiency of SBS to perform the Q-switching process may also be a contributing factor and is discussed later in the chapter.

The temporal modulation of the pulse had a period of ~3.4ns. This corresponds closely to the round-trip time of the SBS cavity (SBS cavity length ~52cm). The depth of modulation varied from pulse to pulse.

The observed fluctuations in pulse length always occurred with optical breakdown (OBD) events. OBD has been previously observed in SBS oscillators using liquid cells [21,26,29]. In fact, it has been found to be the main limitation using an intracavity cell. Figure 4.16(c) shows a temporal profile of the output laser pulse when an OBD event occurred. It is proposed that the opaque plasma, which forms within nanoseconds, as a result of OBD, prevents the laser radiation from propagating into the SBS interaction length. SBS reflectivity and phase fidelity reduce, and lasing ceases prematurely. Figure 4.16(c) shows that for the first ~8ns the cavity flux appears to be increasing as normal, with the characteristic cavity round-trip modulation, until the intensity flattens out, all cavity modulations stop and the flux decreases rapidly to zero. As in Section 3.3.2, OBD was usually observed in this intracavity SBS cell in the form of sparks or a train of sparks at or in front of the focal region. These sparks varied randomly in intensity and number from pulse to pulse. In some cases several sparks along the laser propagation axis were linked by plasma filaments. Bubbles were formed as well as the plasma.

Other observed changes to the output beam characteristics when OBD occurred included a reduction in output energy and a degradation of the near-field transversal mode pattern.

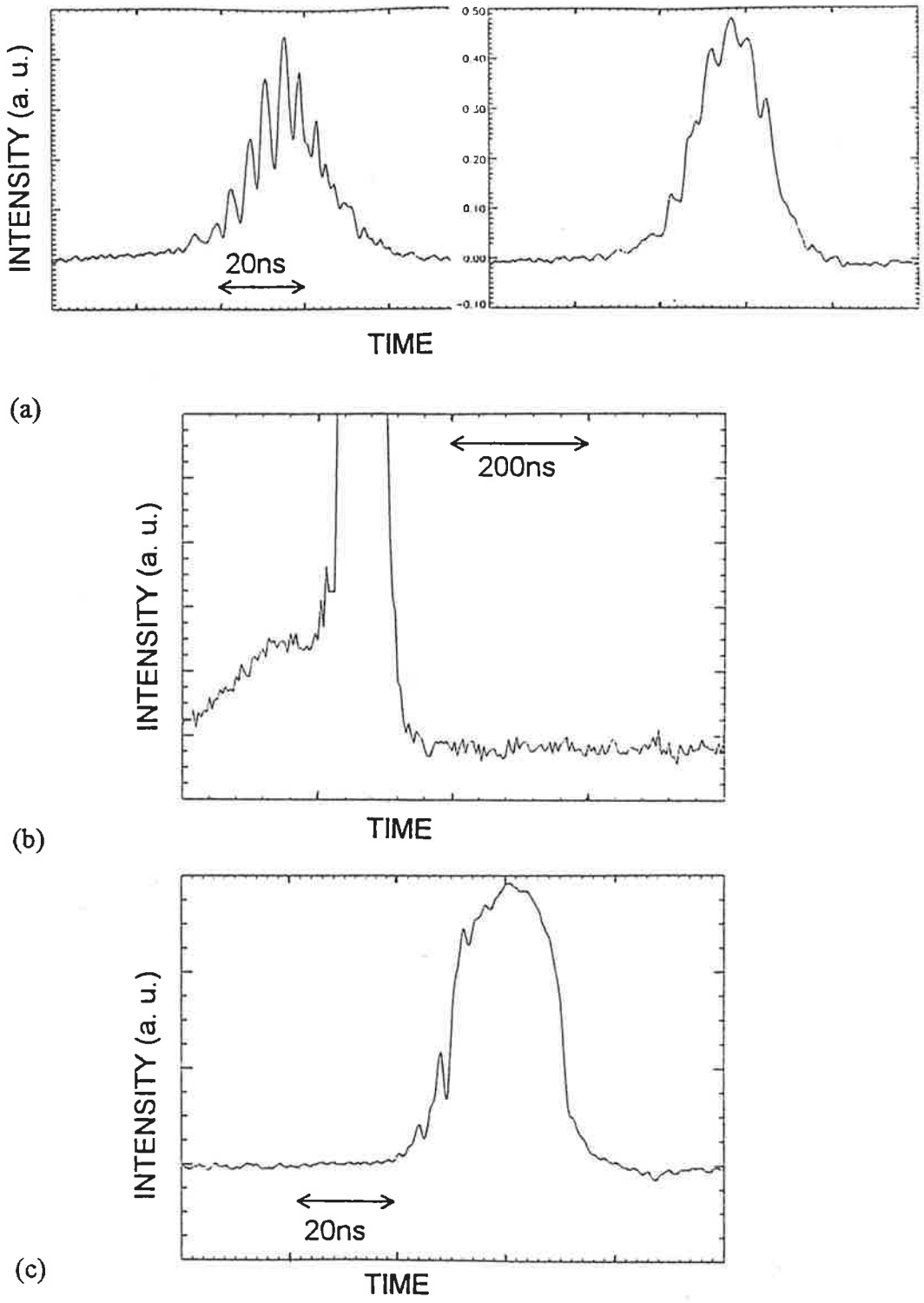

Figure 4.16 Temporal profile.
(a) Typical Q-switched pulses, (b) Q-switched pulse magnified to show the relaxation oscillation which initiated SBS process, (c) Example of a laser pulse when visible signs of OBD where observed at, and in front of the focus.

4.4.2.2 Output Laser Beam Quality

Figure 4.17(a) shows the near-field transversal mode pattern from the SBS oscillator.

When an aberrator (thin microscope slide etched with acid) was placed inside the SBS cavity between the Nd:YAG rod and the SBS lens (L1), the total output energy was reduced, but the spatial profile and divergence remained unchanged, whereas, when the same aberrator was placed in the resonator with conventional mirrors only, lasing ceased altogether. From this, we can conclude that the aberrations created by the etched microscope slide were partially corrected by the SBS process.

The far-field divergence of the SBS Q-switched output, when no plasma or bubbles formed, was measured to be 0.41mrad compared with the start-up cavity output which had a divergence of 1.9mrad. In order to evaluate quantitatively the measured divergence of the laser output, the diffraction limited divergence expected from theory, must be determined. In the following calculation, a beam at the exit of the output coupler with a TEM_{00}, Gaussian near-field profile, and with a spot size of 4mm was used. In this case the diffraction limited full angle divergence is given by:

$$\theta_d = 1.27\left(\frac{\lambda}{D}\right) \tag{4.23}$$

where, λ is the wavelength, and D is the spot size of the waist. This results in a calculated value for the full-angle diffraction limited divergence of θ_d = 0.34mrad. Therefore, the beam quality of the phase-conjugated Q-switched laser beam was found to be 1.5x diffraction limited (compared with ~6x diffraction limited for the start-up resonator).

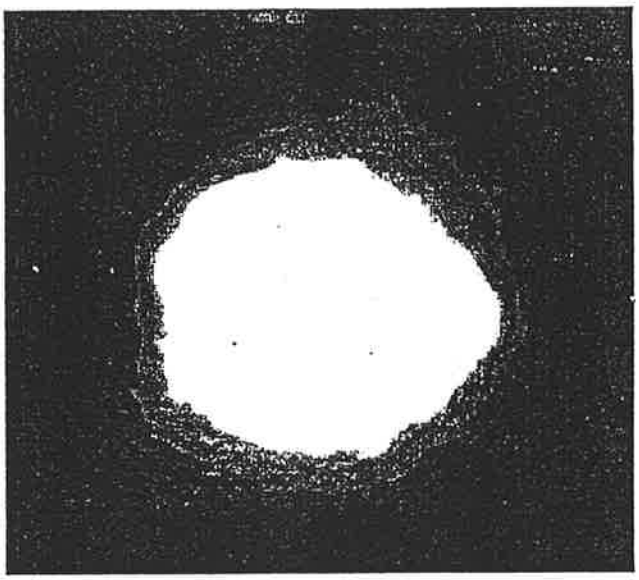

(a)

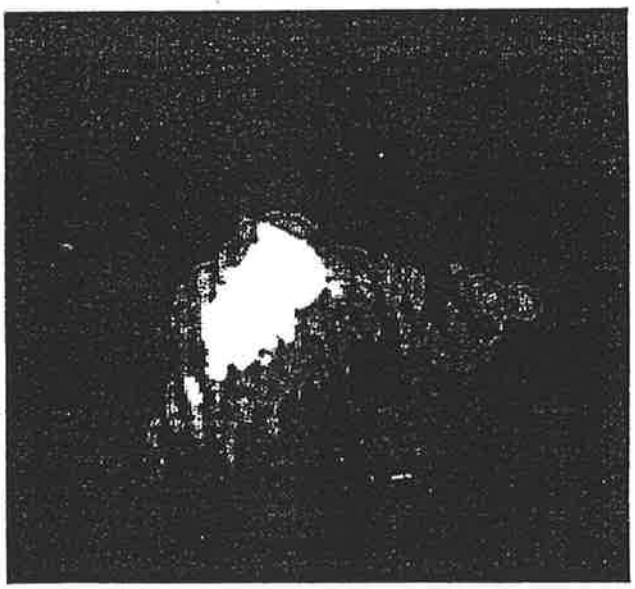

(b)

Figure 4.17 Near-field transversal mode pattern of the laser beam from the SBS oscillator.
(a) without visible signs of OBD in the SBS cell,
(b) with visible signs of OBD in the SBS cell.

The near-field transversal mode pattern of the output laser beam became severely degraded in the presence of OBD (see Figure 4.17(b)). Several hot spots were formed in the beam, and together with the high peak power, led to some optical damage of the SBS cell windows. Although the divergence of the laser output with OBD was observed to increase greatly, a quantitative value was difficult to measure due to the separate hot spots in the spatial profile.

4.4.2.3 Output Energy Fluctuations

Large shot-to-shot output energy fluctuations were observed. Figure 4.18(a) shows a histogram of the number of laser pulses at each output energy when the laser was operated at 1Hz pulse repetition frequency (PRF). At the higher energy range, there is a peak at 33mJ, where no visible sparks or bubbles associated with OBD were seen. A broad, lower energy peak can be seen at ~18mJ. Pulses from this peak were associated with sparks and filamentation in the SBS cell due to OBD. The number and magnitude of the sparks varied greatly from shot to shot giving rise to its broad shape (i.e. laser pulses associated with larger than average OBD had lower output energy).

When operated at higher PRF's, the output energy fluctuations increased (see Figure 4.18(b)). In this case, visible signs of OBD occurred on almost every pulse. Optical breakdown causes shock waves to form which propagate through the SBS cell. The vibration and disturbance effects exist in the SBS cell for hundred's of milliseconds and are believed to be responsible for the increased degradation of reflectivity at higher PRF's. At 1Hz operation, where each pulse was unaffected by the preceeding pulses, shot-to-shot fluctuations were a direct result of plasma formation on nanosecond timescales. At 15Hz operation, the disturbance effects due to shock waves affect the pulses that follow and contribute to the other major competing effect, plasma formation. This was also reported in Section 3.3.2, where at high PRF's the longer-term effects of OBD affected the SBS performance. As will be described later in this chapter,

the fluctuations in output energy were found to be associated with similar fluctuations in the reflectivity of the intracavity SBS cell.

Even longer term effects over time scales of days were observed. It is suspected that continued ionization of the Freon-113 may cause new molecules to be formed, which in turn may increase the absorption and occurrence of competing effects and decrease the SBS gain coefficient. This has detrimental effects to the Q-switching performance, as described in Section 4.2.3.

4.4.2.4 Averaged and Time-resolved Intracavity SBS Reflectivity

The objective of this experiment was to measure the reflectivity of the intracavity SBS cell under various start-up cavity configurations. As shown in Figure 4.11, the approach was to insert an uncoated wedge inside the cavity between the gain medium and the SBS cell, and obtain time-integrated and time-resolved reflectivity measurements from the reflections off the wedge.

Without the visible signs of OBD in the SBS cell, an effective energy reflectivity (R_{eff}), averaged over the pulse, of 65±2% was observed. Using Equation 4.16, the SBS reflectivity (R_{sbs}) yields 61±2% (with R_2~10%). Under the same conditions, but when visible sparks associated with OBD were observed in the cell, the effective energy reflectivity was measured to be 48±10% and the SBS reflectivity, 42±10%. This data displays a similar trend to the histogram of 'Number of Laser Shots versus Energy' shown in Figure 4.18(a). This trend is a relatively narrow peak measured for the higher SBS reflectivity/output energy, and a broad peak for the lower SBS reflectivity/output energy.

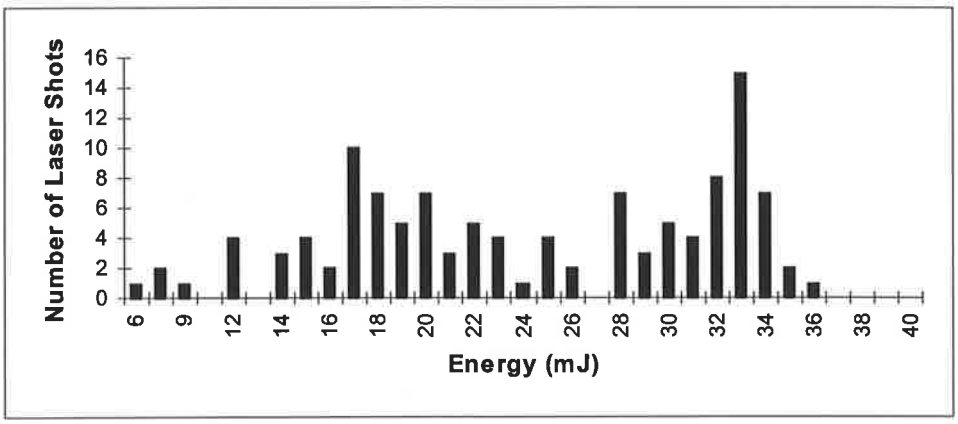

(a)

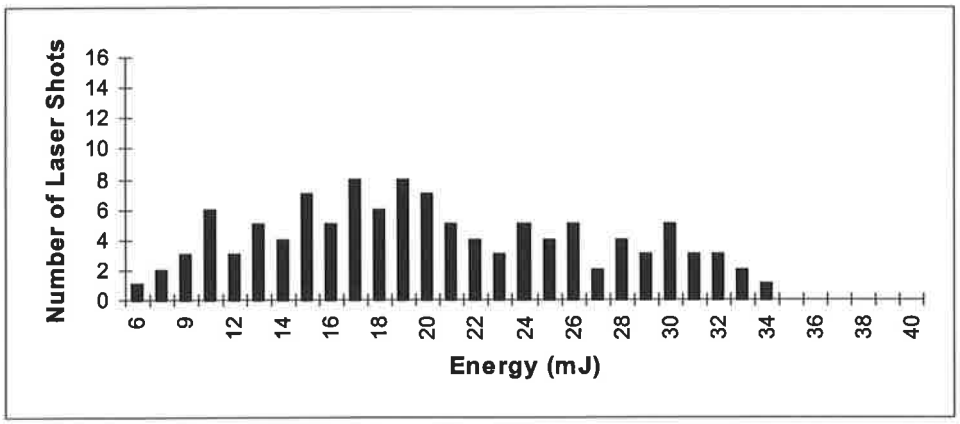

(b)

Figure 4.18 Histogram plot of the Number of laser shots vs Energy at two different pulse repetition frequencies.
(a) 1Hz PRF, (b) 15Hz PRF.

Figure 4.19 shows the time-resolved SBS reflectivity for a typical pulse where no OBD was seen in the SBS cell. There is an initial rise from 0% up to 65% within 10-15ns. This lasts for approximately 15-20ns, at which time the reflectivity begins to reduce and oscillate with a period approximately equal to the cavity round-trip time. The modulation seen in Figure 4.19 corresponds temporally with the latter section of the falling edge of the laser pulse, and was very reproducible from shot-to-shot.

4.4.2.5 Coherence Length

The coherence length diagnostic as described in Section 3.2 was used to measure the coherence length of the output laser beam. Figure 4.20 shows the measured fringe visibility for a laser pulse where no sparks due to OBD were observed in the SBS cell. From this, the coherence length was measured to be ~2.5cm (12GHz). From results described in Section 3.3.2, it seems likely that the OBD events seen in the SBS resonator occur for the same reasons as they do in simple focusing SBS with a broadband pump. That is, the high electric fields associated with the short coherence length Q-switched pulse cause plasma formation which restricts propagation of laser radiation into the interaction length.

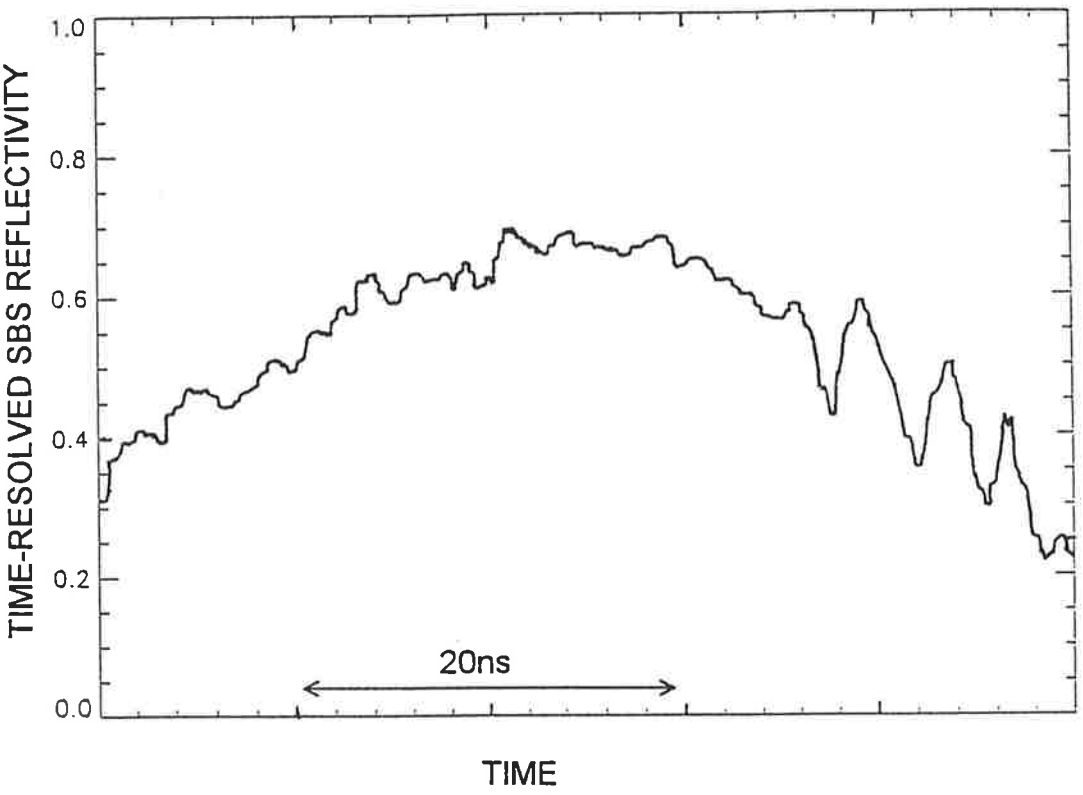

Figure 4.19 Time-resolved SBS Reflectivity (R_{SBS}) vs Time,
for pulses where no sparks associated with OBD were observed in the SBS cell.

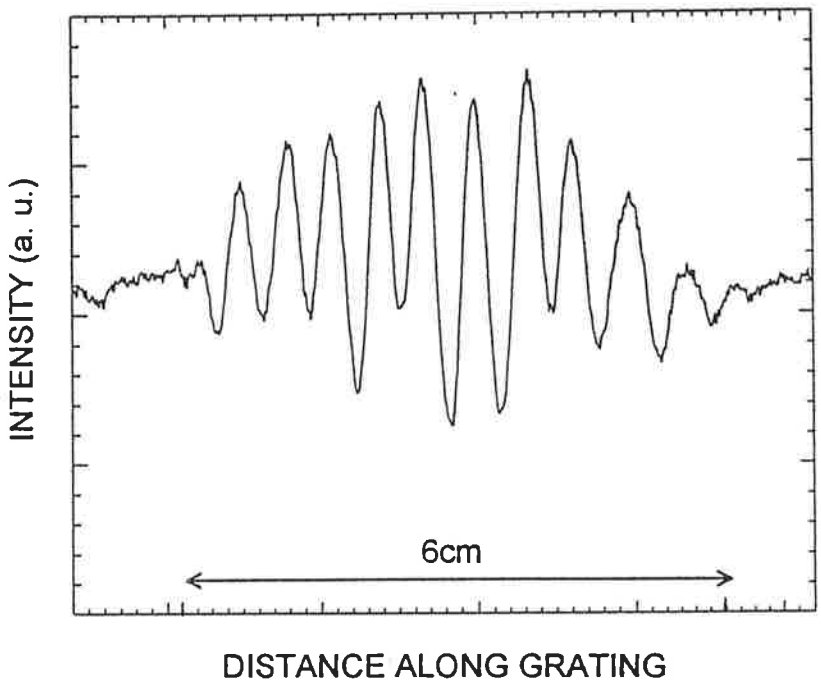

Figure 4.20 Intensity Distribution obtained from a single column of the digitized frame showing the resulting Fringe Visibility as a function of path-length difference along the grating.

4.4.2.6 Conclusion

The initial resonator design described previously resulted in SBS passively Q-switched pulses with high peak power. However, large fluctuations were observed in the temporal profile, output energy and near-field transversal mode pattern of the laser beam. These fluctuations increased with increasing pulse repetition frequency (PRF).

It was found in Section 3.3.1, that for long coherence length laser pumping, SBS performance was enhanced by eliminating OBD competing effects through a purification process. In Section 3.3.2, with short coherence length laser pumping, OBD effects due to high pump peak powers were observed, even in purified Freon-113. Therefore, although the purification process increased the OBD threshold power, it seems likely that the extremely high electric fields present in the intracavity SBS cell were sufficient to cause OBD effects in the purified Freon-113. The effect of the OBD plasma, as described previously, is to restrict the laser radiation from propagating to the SBS interaction region, resulting in poor SBS reflectivity and phase fidelity.

4.4.2.7 Proposed Solution

There are a number of ways to ensure that the intensity at the focus of the SBS lenses is kept below the OBD threshold intensity.

It was found in Section 3.2 that the onset of optical breakdown (which competes with SBS) in the focal region depends on the pump beam intensity. This has also been reported by other authors [42,43]. Therefore, longer focal length lenses could be used to form the telescope in order to increase the waist size and lower the focal intensity. However, this technique is limited by the requirement that the Rayleigh length of the SBS lens must be shorter than the coherence length of the laser (see Section 3.3.2).

Alternatively, controlling the bandwidth of the laser radiation may reduce the high intensities in the focal region. Soan *et al* [44] successfully used a Littrow grating and an etalon to narrow the bandwidth of the circulating radiation in order to achieve coherent SBS excitation in a flashlamp pumped, dye laser.

In the following work, the longitudinal mode structure of the start-up cavity is controlled to lower the bandwidth of the circulating laser radiation.

4.4.2.8 Longitudinal Mode Control

The longitudinal mode structure of a 1 metre long start-up cavity with a Finesse ~15 can be calculated using a simple Fabry-Perot analysis and is shown in Figure 4.21. To control the mode content of the start-up cavity, an intracavity etalon was introduced into the existing setup as shown in Figure 4.22. The etalon used was ~1/8inch thick, and had uncoated surfaces, each with a reflectivity of ~4%. The transmission curve for this etalon (Finesse ~0.17) is shown in Figure 4.21(a). The aim was not to force the cavity to run single longitudinal mode, but to contribute transmission losses to a number of modes and thereby suppress them. An etalon of 1/8inch in length does not give the suitable modulation in frequency required for this purpose. Therefore, the etalon was aligned with the back mirror, separated by ~10cm. The resonance characteristics of a 10cm cavity (Finesse ~0.17) are shown in Figure 4.21(b).

With longitudinal mode control (LMC), no sparks associated with optical breakdown were observed at pumping energies up to 75J and pulse repetition frequencies up to 15Hz. Figure 4.23 displays the temporal profile and output energy of the laser beam when longitudinal mode control was employed within the SBS laser cavity. No significant fluctuations in the temporal profile were observed. The amplitude of the modulations in the temporal profile were, on average, larger than when no LMC was used. This indicates the existence of fewer axial modes which gave rise to a beat note

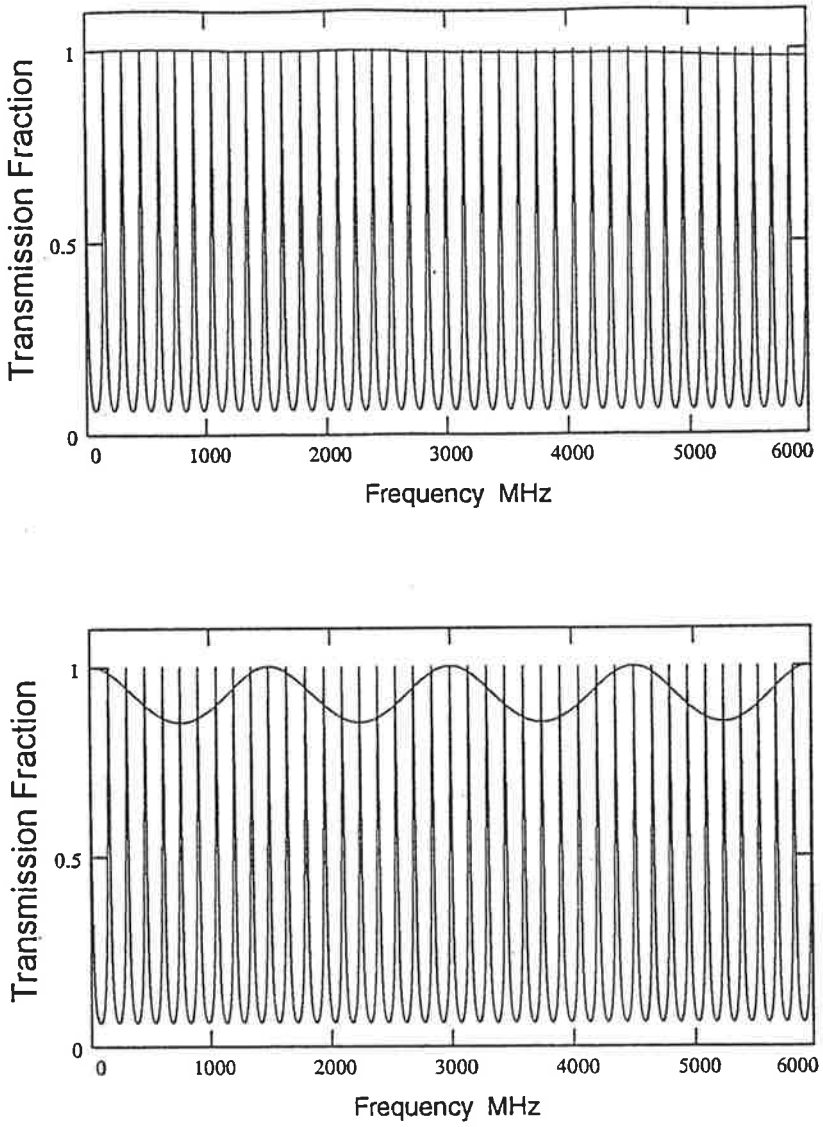

Figure 4.21 Transmission versus Frequency for a 1 metre long start-up cavity. Overlay: (a) 1/8inch cavity spacing, (b) 10cm cavity spacing.

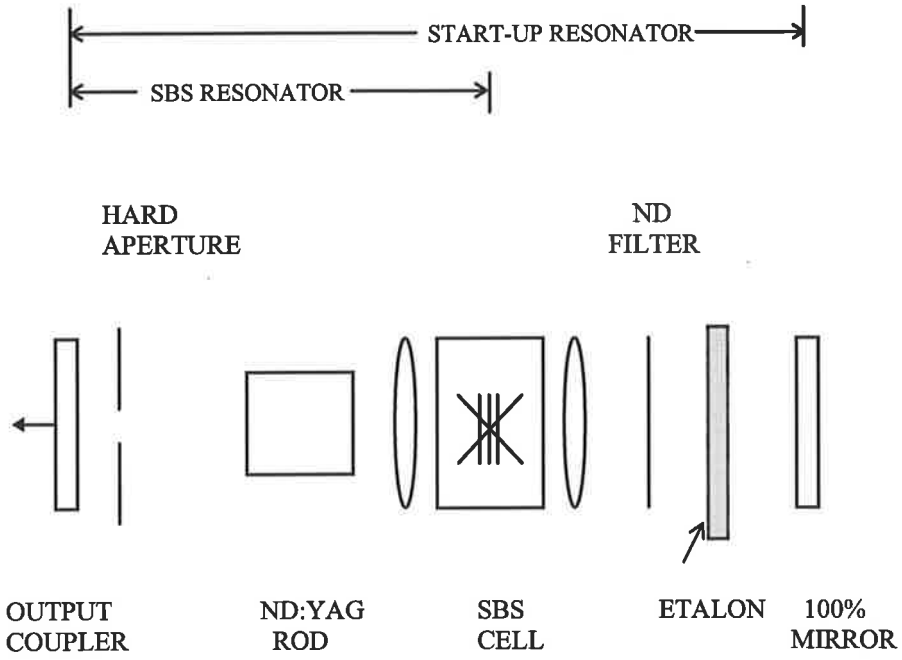

Figure 4.22 Schematic of SBS oscillator with longitudinal mode control.

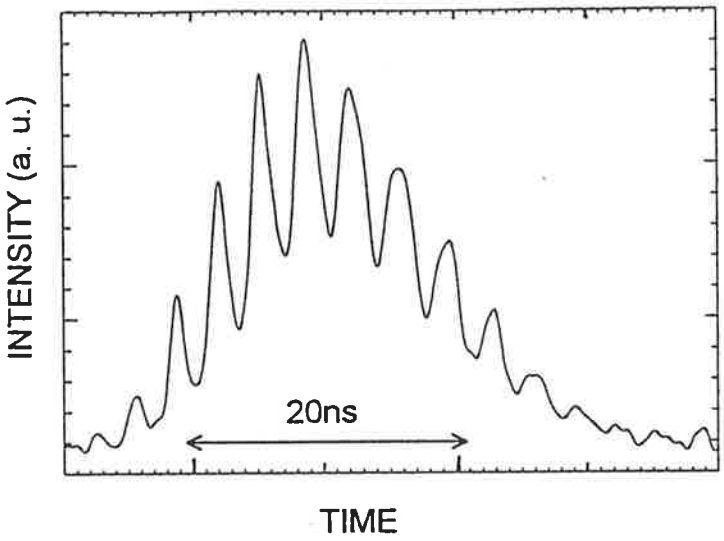

(a)

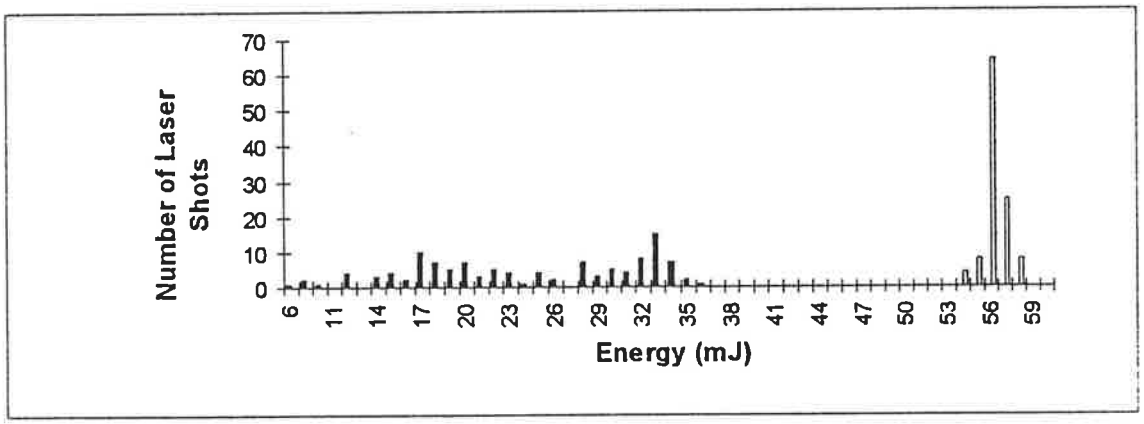

(b)

Figure 4.23 (a) Temporal profile of a typical pulse from the SBS oscillator with LMC, (b) Histogram plot of the Number of Laser Shots versus Energy for the SBS oscillator with (□) and without (■) LMC (at 1Hz PRF).

with a greater amplitude modulation. Also, no significant fluctuations were seen in the pulse energy of the laser output (see Figure 4.23(b)). The maximum output energy increased by a factor of ~1.7 compared with when no LMC was used, and was stable to less than 3%.

The alignment of the etalon was found to be critical. Any small misalignment between the etalon and the back mirror resulted in the recurrence of optical breakdown effects as well as large fluctuations in the temporal profile and energy of the output laser pulses.

When properly aligned, the laser operation and output energy of this SBS oscillator were limited only by the maximum pumping energy and PRF of the high-voltage power supply (E_{in}(max)~75J, PRF(max)~15Hz).

Figure 4.24 shows a comparison of the output energy from the SBS oscillator with the corresponding output energy from the start-up oscillator (N.B. the start-up oscillator configuration was identical to the SBS oscillator but without the Freon-113 in the SBS cell).

4.4.2.9 Coherence Length (with LMC)

It is difficult to predict the effect on the intracavity bandwidth when an intracavity etalon with low finesse is used to control the longitudinal modes. One way to do this is to measure the coherence length of the output pulse from shot-to-shot. Using the technique described in Section 3.2, the change in fringe visibility with path length difference was measured for a typical pulse from the SBS oscillator (with longitudinal mode control). Figure 4.25 displays the fringe visibility for output pulses from the SBS oscillator with and without longitudinal mode control. Using Michelson's definition for 'coherence length' it can be seen that the intracavity etalon increased the coherence length of the laser beam from ~2.5cm (without mode control) up to ~24cm (with mode

control). An increase in the coherence length indicates a corresponding decrease in laser bandwidth from ~12GHz (without mode control) to ~1.25GHz (with mode control).

4.4.2.10 Averaged and Time-resolved Intracavity SBS Reflectivity (with LMC)

In order to determine the reason for the improved oscillator performance, the SBS reflectivity of the SBS cell was measured both time-integrated and time-resolved. An effective reflectivity (R_{eff}) averaged over the pulse of 71±2% was observed. Using Equation 4.15 yields a corresponding SBS reflectivity (R_{SBS}) of ~68±2%. The time-resolved results are shown in Figure 4.26. The maximum temporal reflectivity recorded from this graph is ~80% (compared with ~68% when no LMC was used). From these results it can be seen that not only has the reflectivity of the intracavity SBS cell increased, it has also stabilized. The increased magnitude and stability of the SBS reflectivity is crucial for improved Q-switching performance (as described in Section 4.2), and has resulted in laser output characteristics that show no significant fluctuations.

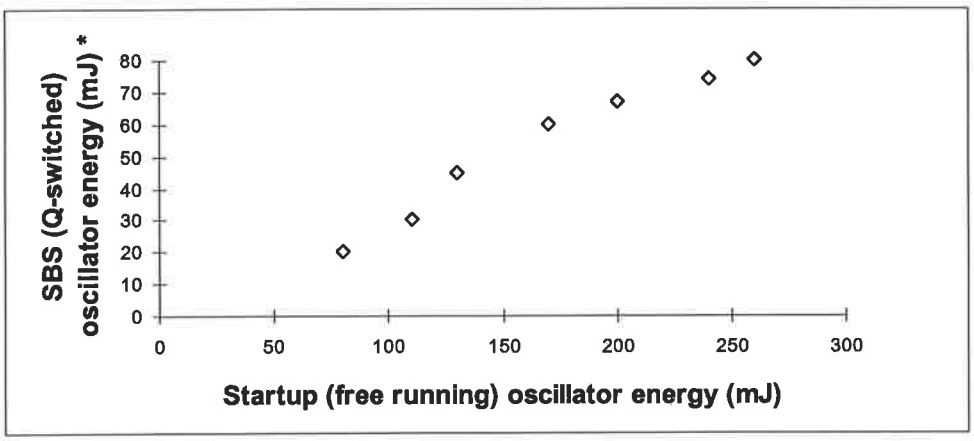

* energy plotted is the maximum value measured.

Figure 4.24 Startup oscillator Energy versus SBS oscillator Energy (Q-switched) with corresponding operating conditions.

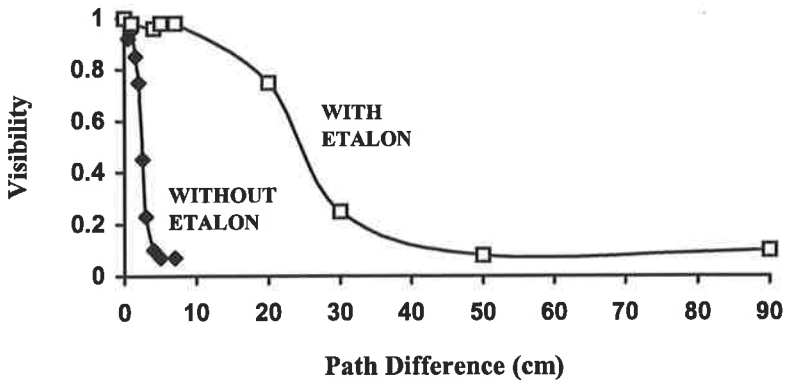

Figure 4.25 Visibility of Fringes versus Path Length Difference, for the SBS resonator with (□), and without (◆) LMC.

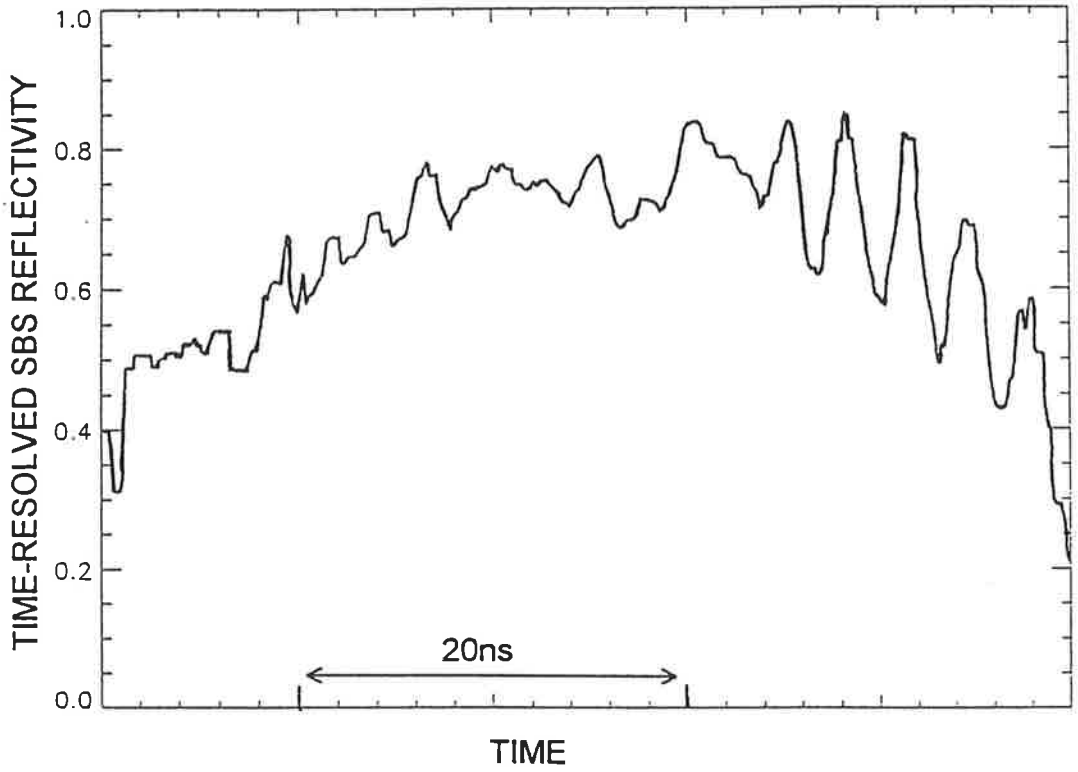

Figure 4.26 Time-resolved intra-cavity SBS Reflectivity vs Time (with LMC).

4.5 Summary

Experimental work and modelling of a laser oscillator incorporating an intracavity SBS mirror has been described.

A steady state analysis of the rate equations for Q-switching was used to model the passive Q-switching obtained using an SBS mirror with a non-linear intensity dependent reflectivity. The Q-switching behaviour was found to be highly sensitive to the Brillouin gain. Other parameters effecting the Q-switching time and magnitude (i.e. mirror reflectivity/start-up cavity losses) were modelled and compared with results found in other laser oscillators.

The initial experimental design resulted in significant shot-to-shot fluctuations in the temporal profile, output energy and near-field transversal mode pattern. These fluctuations were observed with the occurrence of optical breakdown (OBD) in the SBS cell. The coherence length of the output laser beam was measured, using a novel interferometer (described in Section 3.2.5 of this thesis), and found to be 25mm. It is believed that the extremely high electric fields present in the intracavity SBS cell, associated with laser radiation of high bandwidth, are sufficient to cause OBD effects in the purified Freon-113. The effect of the opaque plasma that is created is to restrict the laser radiation from propagating through the SBS interaction region.

The longitudinal mode structure of the start-up cavity was controlled using an intracavity etalon, in order to lower the bandwidth of the circulating laser radiation. By appropriate tuning of the etalon, stable laser output of coherence length ~25cm was achieved. The intracavity SBS reflectivity was found to increase and remain stable with the addition of the longitudinal mode control (LMC). No fluctuations in output characteristics and no optical breakdown effects were observed up to the maximum input operating conditions.

The efficiency of the Q-switching process was found to be poor, with one third the output energy of the corresponding free-running start-up cavity. This can be partly attributed to the early timing of the Q-switch. However, in these experiments, the timing of the Q-switch could not be delayed further by increasing the losses in the start-up cavity. As a result, a significant proportion of the pumping duration occurred after the Q-switch had taken place.

References

[1] O. Yu. Nosach, V. I. Popovichev, V. V. Ragul'shy, and F. S. Faizullov, '*Cancelation of phase distortions in an amplifying medium with a Brillouin mirror*' Sov. Phys. JETP Lett. **16**, 435 (1972).

[2] D. A. Rockwell, '*A review of phase conjugate lasers*', IEEE J. Quantum Electron. **24**, 1124 (1988).

[3] J-L. Ayral, J. Montel, and J-P. Huignard, '*Master oscillator-amplifier Nd:YAG laser with a SBS phase conjugate mirror*', SPIE **1500**, 81 (1991).

[4] D. A. Rockwell, M. S. Mangir, and J. J. Ottusch, '*Energy scaling of phase-conjugate lasers and Brillouin conjugators*', Int, J. Nonlin. Opt. Phys. **2**, No 1, 131 (1993).

[5] C. B. Dane, L. E. Zapata, W. A. Neuman, M. A. Norton, and L. A. Hackel, '*Design and operation of a 150W near diffraction-limited laser amplifier with SBS wavefront correction*', IEEE J. Quantum Electron. **31**, No 1, 148 (1995).

[6] H. J. Eichler, A. Haase, and R. Menzel, '*100-Watt average output power 1.2 diffraction limited beam from pulsed Neodymium single-rod amplifier with SBS phase conjugation*', IEEE J. Quantum Electron. **31**, No 8, 1265 (1995).

[7] J. AuYeung, D. Fekete, D. M. Pepper, and A. Yariv, '*A theoretical and experimental investigation of the modes of optical resonators with phase-conjugate mirrors*', IEEE J. Quantum Electron. **QE-15**, 1180 (1979).

[8] S. A. Lesnik, M. S. Soskin, and A. I. Khizhnyak, '*Laser with a stimulated-Brillouin-scattering complex-conjugate mirror*', Sov. Phys. Tech. Phys. **24**, No 10, 1249 (1979).

[9] I. M. Bel'dyugin, M. G. Galushkin, and E. M. Zemskov, '*Properties of resonators with wavefront reversing mirrors*', Sov. J. Quant. Electron. **9**, 20 (1979).

[10] P. A. Belanger, A. Hardy, and A. E. Seigman, '*Resonant modes of optical cavities with phase conjugate mirrors: Higher order modes*', Appl. Opt. **19**, 479 (1980).

[11] P. A. Belanger, A. Hardy, and A. E. Seigman, '*Resonant modes of optical cavities with phase conjugate mirrors*', Appl. Opt. **19**, 602 (1980).

[12] N. N. LL'ichev, A. A. Malyutin, and P. P. Pashinin, '*Laser with diffraction-limited divergence and Q-switching by stimulated Brillouin scattering*', Sov. J. Quant. Electron. **12**, No 9, 1161 (1982).

[13] G. Giuliani, M-M. Denariez -Roberge, and P. A. Belanger, '*Transverse modes of a stimulated scattering phase conjugate resonator*', Appl. Opt. **21**, 3719 (1982).

[14] I. M. Bel'dyugin, B. Ya. Zeldovich, M. V. Zolotarev, and V. V. Shkunov, '*Lasers with wavefront-reversing mirrors (review)*', Sov. J. Quant. Electron. **15**, No 12, 1583 (1985).

[15] V. S. Arakelyan, and G. E. Rylov, '*Laser with a wavefront-reversing mirror and Q-switching by stimulated Brillouin scattering*', Sov. J. Quant. Electron. **15**, No 3, 433 (1985).

[16] S. Chandra, R. C. Fukuda, R. Utano, '*Sidearm stimulated scattering phase-conjugated laser resonator*', Opt. Lett. **10**, No 7, 356 (1985).

[17] P. Yeh, '*Theory of phase-conjugate oscillators*', J. Opt. Soc. Am. A **2**, 727 (1985).

[18] P. P. Pashinin and E. I. Shklovsky, 'Solid state lasers stimulated Brillouin scattering mirrors operating in the repetitive pulse mode', J. Opt. Soc. Am. B **5**, No 9, 1957 (1988).

[19] A. A. Denisov, and O.L. Kulikov, '*Laser with a T-shaped resonator and a stimulated Brillouin scattering mirror*', Sov. J. Quant. Electron. **20**, No 6, 655 (1990).

[20] P. P. Pashinin, E. I. Shklovsky, and V. S. Sidorin, '*Characteristics of a SBS self-Injection locked laser*', Laser Physics **1**, No 2, 160 (1991).

[21] H. Meng, and H.J. Eichler, '*Nd:YAG laser with a phase-conjugating mirror based on stimulated Brillouin scattering in SF_6 gas*', Opt. Lett. **16**, No 8, 569 (1991).

[22] H.J. Eichler, R. Menzel, and D. Schumann, '*10-W single-rod Nd:YAG laser with stimulated Brillouin scattering Q-switching mirror*', Appl. Opt. **31**, No 24, 5038 (1992).

[23] A. Agnesi, and G. C. Reali, '*Passive and self-Q-switching of phase-conjugation Nd:YAG laser oscillators*', Opt. Comm. **89**, 41 (1992).

[24] C. Jun, L. Ying, and M. Yueru, '*Nd:YAG laser resonator with phase-conjugating mirror using Stimulated Brillouin Scattering based on SF_6 gas*', SPIE **1726**, 504 (1992).

[25] H. J. Eichler, A. Haase, S. Hermann, R. Menzel, D. Schumann, '*Beam quality improvement of pulsed Nd:YAG-lasers using Brillouin phase-conjugation*', SPIE **1834**, 176 (1992).

[26] H. J. Eichler, Chen, Jun, A. Kummrow, R. Menzel, and D. Schumann, '*Nd:YAG-Laser with SBS Q-switching mirror and repetition rate up to 50Hz*', Int. J. Nonlin. Opt. Phys. **2**, No 1, 187 (1993).

[27] R. A. Lamb, M. J. Damzen, '*Q-switching of a Nd:YAG phase conjugate laser using external stimulated Brillouin scattering*', AME1, 92 (1993).

[28] V. Bruckner, S. Heinemann and S. Ludwig, '*To the mechanism of Q-switching by phase conjugation using stimulated Brillouin scattering*', J. Mod. Opt. **40**, No 2, 187 (1993).

[29] S. Seidel, and G. Phillips, '*Pulse lengthening by intracavity stimulated Brillouin scattering in a Q-switched, phase conjugated Nd:YAG laser oscillator*', Appl. Opt. **32**, No 36, 7408 (1993).

[30] A. Kummrow, R. Menzel, D. Schumann, and H. J. Eichler, '*Length Tuning Effect in SBS-Lasers*', Int. J. Nonlinear Opt. Phy. **2**, No 2, 261 (1993).

[31] M. R. Perrone, and Y. B. Yao, '*Phase conjugated XeCl laser resonator*', Opt. Lett. **19**, No 14, 1052 (1994).

[32] P. J. Soan, M. J. Damzen, V. Aboites, and M. H. R. Hutchinson, '*Long-pulse self-starting stimulated-Brillouin -scattering resonator*', Opt. Lett. **19**, No 11, 783 (1994).

[33] K. D. Ridley, and A. M. Scott, '*Stimulated Brillouin scattering in a transverse resonator*' J. Opt. Soc. Am. B **11** No 8, 1361 (1994).

[34] P. Yeh, '*Two-wave mixing in Nonlinear media*', IEEE J. Quantun Electron. **QE-25**, No 3, 484 (1989).

[35] D. Pohl, '*A new laser Q-switch technique using stimulated Brillouin scattering*', Phys. Lett. **24A**, 239 (1967).

[36] A. E. Siegman, '*Lasers*', Ch 26, 1009 (1986).

[37] B. Ya. Zel'dovich, N. F. Pipiletsky, V. V. Shkunov, '*Principles of Phase Conjugation*', T. Tamir (ed.), Berlin:Springer, 25-45 (1985).

[38] R. A. Lamb, '*The Application of Phase Conjugation to high power lasers using stimulated Brillouin scattering*', Phd Thesis, University of London, (1994).

[39] R. A. Fisher (ed.), '*Optical Phase Conjugation*', New York: Academic Press, (1983).

[40] H. J. Eichler, S Heinrich and J. Schwartz, '*Self-starting Excimer laser SBS-oscillator without start resonator*', Proc. Intl. Conf. On Lasers'95, 487 (1996).

[41] W. Koechner, '*Solid-State Laser Engineering*', Springer-Verlag:New York, 3rd ed. (1992).

[42] M. J. Damzen, M. H. R. Hutchinson, W. A. Schroeder, '*Direct measurement of the acoustic decay times of hypersonic waves generated by SBS*', IEEE J. Quantum Electron. **23**, 328 (1987).

[43] A. A. Fillipo, M. R. Perrone, '*Stimulated Brillouin scattering in SF_6 with a free-running XeCl laser as pump*', Appl. Phys. B **57**, 103 (1993).

[44] P. J. Soan, M. J. Damzen, V. Aboites, M. H. R. Hutchinson, '*Long-pulse self-starting stimulated Brillouin scattering resonator*', Opt. Lett. **19**, No 11, 783 (1994).

Chapter 5

Conclusion

The main conclusions that can be drawn from the work in this thesis are highlighted and the possible areas for future research are considered.

In Chapter Three, a simple focussing SBS geometry was used to study the SBS performance under different operating regimes. Some previous studies have reported a degradation in phase fidelity at high energies whereas others have reported good phase fidelity. Using a long coherence length input pump, time-integrated results demonstrated >90% SBS reflectivity and ~90% phase fidelity for purified samples of Freon-113 at all input energies used.

Time-integrated measurements revealed a number of temporal fluctuations that did not occur in the input pump temporal profile. The first type of fluctuation always occurred on the leading edge of the Stokes return pulse. Its amplitude was found to become greater with increasing focusing depth, but to reduce at higher energies. No degradation in phase fidelity was observed when this fluctuation occurred. This temporal re-shaping of the Stokes return is attributed to the strong saturation of the pump beam by the leading edge of the counter-propagating Stokes wave, resulting in considerable amplification of the

acoustic grating. With appropriate choice of pulse length and SBS cell length, this technique has been widely used for pulse compression applications.

The second type of intensity fluctuation observed occurred at random times during the pulse and was associated with a phase fluctuation. This fluctuation was attributed to the spontaneous noise which initiates the SBS process in a simple focusing geometry. These phase jumps were correlated with a degradation in phase fidelity. Both types of intensity fluctuations were found to reduce at high input energies and with small interaction lengths. Under these conditions, high temporal phase fidelity was always observed.

The second part of Chapter Three described results obtained with short coherence length SBS pumping. Both the SBS reflectivity and phase fidelity of the Stokes return was found to degrade when the coherence length restricted the interaction length. Optical breakdown effects (i.e. plasma, bubbles) were also observed in the interaction region and were linked to a degradation in SBS performance. These effects were initiated by the high electric fields associated with the broadband input pump. In order to avoid the interaction length being restricted by the coherence length, it is advantageous to sharply focus the input laser beam to minimize the Rayleigh range. However, to avoid OBD, it is preferable to use a long focal length lens in order to reduce the peak intensities in the focal region.

From this work on short coherence length SBS pumping, a novel interferometric method for real-time measurement of the complete coherence function of a laser pulse was developed. This diagnostic tool was used to measure shot-to-shot variations in the coherence length of the input laser pump.

This study on SBS reflectivity and phase fidelity revealed fluctuations from the ideal, phase conjugate SBS process. This identifies operating regimes which should be avoided if optical phase conjugation is required. These regimes can be summarized as follows: firstly, that the SBS medium is clear of any suspended particles or dissolved impurities

which may reduce the optical breakdown threshold of the sample; secondly, the rise-time of the leading edge or any other part of the input pulse should not be shorter than the phonon lifetime; thirdly, the focusing depth should be minimized and the input energy maximized to avoid intensity fluctuations occurring on the leading edge of the Stokes pulse; fourthly, the ratio of the propagation time to the phonon lifetime should be minimized in order to reduce intensity fluctuations associated with phase jumps in the Stokes pulse; fifthly, the bandwidth of the input pump should not significantly exceed the SBS bandwidth of the medium. This condition is also closely related to ensuring that the input pump coherence length does not become shorter than the interaction length.

Chapter Four described a detailed experimental study of the application of an intracavity SBS mirror in a laser oscillator for phase conjugation and Q-switching. Steady-state modelling of the Q-switching performance was presented to highlight the important resonator parameters affecting the Q-switching time for an SBS, non-linear intensity dependent mirror.

The initial experimental design resulted in large shot-to-shot fluctuations in the temporal profile, output energy and near-field transversal profile. These fluctuations are attributed to high intracavity electric fields present inside the SBS cell. The opaque sparks produced in the interaction length have been reported, in other research studies, to be responsible for the degradation in laser performance. In this work, the bandwidth of the circulating radiation was controlled in order to reduce the peak intracavity intensities below the optical breakdown threshold. There are a number of experimental techniques to lower the peak intensities at the focus of the SBS lens, including longer focal length lenses and appropriate intracavity etalons. In this study, the tuning of an appropriate intracavity etalon was found to be successful. An indication of a reduction in bandwidth was observed from measurements, showing an increase in coherence length with longitudinal mode control. This was seen to have a positive effect on the intracavity SBS reflectivity which was observed to increase and stabilize from shot-to-shot. This, in turn, resulted in

higher output power with stable shot-to-shot performance, and the total elimination of optical breakdown up to the maximum operating conditions of the laser power supply used. It should be noted that this technique reduces the peak intensities at the focal region of the SBS lens. In order to scale these systems to higher energies, techniques such as longitudinal mode control as well as improved purification processes will be required to push back the threshold for competing phenomena such as optical breakdown.

Publications

M. O'Connor, V. Devrelis and J. Munch, '*Phase-conjugated Nd:YAG laser oscillator with stimulated Brillouin scattering*', Proc. Intl. Conf. on Lasers '95, p500, 1996.

V. Devrelis, M. O'Connor, J. Munch, S. Afsharvahid and C. Wei, '*Fidelity of optical phase conjugation using stimulated Brillouin scattering*', XX International Quantum Electronics Conference, Sydney, July 1996, *Technical Digest, Optical Society of America, WL59.*

M. O'Connor and J. Munch, '*Phase-conjugated Nd:YAG oscillator*', 10th AOS Proceedings, Brisbane, July 1995.

V. Devrelis, M. O'Connor and J. Munch, '*Coherence length of single laser pulses by CCD interferometry*', App. Opt. **34**, No 24, 5386, 1995.

J. Munch, V. Devrelis, A-M. Grisogono, M. O'Connor and C. Wei, *'Phase conjugation in solid-state lasers*', Australian Optical Soc. News **10**, 8-12, 1995.

V. Devrelis, M. O'Connor and J. Munch, '*Phase conjugation of solid state lasers*', ACOLS Proceedings, Melbourne, December 1993.

M. O'Connor, V. Devrelis, P. Foster, J. Munch, R. Weurker and A-M. Grisogono, '*Optical phase conjugate mirrors for solid-state lasers*', 8th AOS Proceedings, Sydney, February 1993.

Devrelis, V., O'Connor, M., and Munch, J., (1995) Coherence length of single laser pulses as measured by CCD interferometry.
Applied Optics, v. 34 (24), pp. 5386-5389.

O'Connor, M., Devrelis, V., and Munch, J., (1995) SBS phase conjugation of a Nd:YAG laser for high beam quality.
Proceedings of the International Conference on LASERS '95, pp. 500-504.